The Dynamics of Fine-Grain Sediment Dredged from Santa Cruz Harbor

By Curt D. Storlazzi, Christopher H. Conaway, M. Katherine Presto, Joshua B. Logan, Katherine Cronin, Maarten van Ormondt, Jamie Lescinski, E. Lynne Harden, Jessica R. Lacy, and Pieter K. Tonnon

Photo of Santa Cruz Harbor on 10/03/2009 by the California Coastal Record Project
http://www.californiacoastline.org/

Open-File Report 2011-1045

U.S. Department of the Interior
U.S. Geological Survey

U.S. Department of the Interior
KEN SALAZAR, Secretary

U.S. Geological Survey
Marcia K. McNutt, Director

U.S. Geological Survey, Reston, Virginia: 2011

For product and ordering information:
World Wide Web: http://www.usgs.gov/pubprod
Telephone: 1-888-ASK-USGS

For more information on the USGS—the Federal source for science about the Earth, its natural and living resources, natural hazards, and the environment:
World Wide Web: http://www.usgs.gov
Telephone: 1-888-ASK-USGS

Suggested citation:
Storlazzi, C.D., Conaway, C.H., Presto, M.K., Logan, J.B., Cronin, K., van Ormondt, M., Lescinski, J., Harden, E.L., Lacy, J.R., and Tonnon, P.K., 2011. The dynamics of fine-grain sediment dredged from Santa Cruz Harbor: USGS Open-File Report 2011-1045, 110 p. [http://pubs.usgs.gov/of/2011/1045/]

Contents

Figures

Tables

Appendixes

The Dynamics of Fine-Grain Sediment Dredged from Santa Cruz Harbor

By Curt D. Storlazzi[1], Christopher H. Conaway[1], M. Katherine Presto[1], Joshua B. Logan[1], Katherine Cronin[2], Maarten van Ormondt[2], Jamie Lescinski[2], E. Lynne Harden[3], Jessica R. Lacy[1], and Pieter K. Tonnon[2]

[1]U.S. Geological Survey, Pacific Coastal and Marine Science Center, 400 Natural Bridges Drive, Santa Cruz, CA 95060
[2]Deltares, P.O. Box 177, 2600MH Delft, the Netherlands
[3]University of California at Santa Cruz, Earth and Planetary Sciences Department, 1156 High Street, Santa Cruz, CA 95064

Abstract

In the fall and early winter of 2009, a demonstration project was done at Santa Cruz Harbor, California, to determine if 450 m^3/day of predominantly (71 percent) mud-sized sediment could be dredged from the inner portion of the harbor and discharged to the coastal ocean without significant impacts to the beach and inner shelf. During the project, more than 7600 m^3 of sediment (~5400 m^3 of fine-grain material) was dredged during 17 days and discharged approximately 60 m offshore of the harbor at a depth of 2 m on the inner shelf. The U.S. Geological Survey's Pacific Coastal and Marine Science Center was funded by the U.S. Army Corps of Engineers and the Santa Cruz Port District to do an integrated mapping and process study to investigate the fate of the mud-sized sediment dredged from the inner portion of Santa Cruz Harbor and to determine if any of the fine-grain material settled out on the shoreline and/or inner shelf during the fall and early winter of 2009. This was done by collecting high-resolution oceanographic and sediment geochemical measurements along the shoreline and on the continental shelf of northern Monterey Bay to monitor the fine-grain sediment dredged from Santa Cruz Harbor and discharged onto the inner shelf. These in place measurements, in conjunction with beach, water column, and seabed surveys, were used as boundary and calibration information for a three-dimensional numerical circulation and sediment dynamics model to better understand the fate of the fine-grain sediment dredged from Santa Cruz Harbor and the potential consequences of disposing this type of material on the beach and on the northern Monterey Bay continental shelf.

Introduction

Harbor depths and channels commonly are maintained through active dredging programs. The dredged material can be deposited in a variety of locations, including offshore and nearshore disposal sites. Because transporting material offshore for disposal can be costly, nearshore disposal can be a more cost effective alternative. However, due to the high percentage of fine-grain material often found in harbors (from terrestrial run-off and settlement processes), nearshore disposal is not necessarily an environmentally ideal solution. Nearshore dredge-material disposal is not currently a common practice in central California because of the potential negative impacts, caused by turbidity or fine-grain sedimentation, on the sensitive species and habitats managed by the National Marine Sanctuary Program. Currently, regulations prohibit the

discharge of sediment that is more than 20 percent mud (<0.063 mm) by mass into the coastal ocean. The 20 percent mud threshold currently is under consideration by a variety of management and research agencies to determine whether it is an appropriate guideline for all environments.

Background Information and Project Objectives

The area offshore of the City of Santa Cruz in northern Monterey Bay, California, is a complicated coastal setting of sea cliffs, pocket beaches, and low-relief bedrock reefs (Storlazzi and others, 2008) that is impacted by a variable wave climate due to its south-facing orientation (Storlazzi and others, 2007). Spatially- and temporally-variable wave conditions and the complex, shallow, rocky seabed in this area have restricted comprehensive field surveys in the past. Recent innovations in field techniques and equipment now make it possible to perform a detailed analysis of the sedimentological nature and physical processes operating on this type of complex coastline. Understanding the sedimentology and physical processes off Santa Cruz is important not only because it is part of the Monterey Bay National Marine Sanctuary (MBNMS) and encompasses rich coastal and marine ecosystems in the area, but also because these same environments are important areas for local economic and recreational activities. It is increasingly important to provide scientific data that allow government agencies involved with dredge-disposal operations to make the best informed management decisions.

The goal of the project described here was to determine the behavior of 5,400 m^3 of fine-grain sediment dredged from the inner portion of Santa Cruz Harbor and discharged at a depth of 2 m approximately 60 m offshore. This work follows a number of previous studies investigating the discharge of smaller volumes of fine-grain sediment from Santa Cruz Harbor on the inner shelf (Griggs, 1991; McLaren, 2000; Watt and Greene, 2002; Watt, 2003; Sea Engineering Inc., 2006), all of which suggested that fine-grain sediment dredged from the harbor would not deposit in observable quantities on the inner shelf. Similar to the previous projects, part of this project was designed to determine if the fine-grain material dredged from the inner part of Santa Cruz Harbor and disposed approximately 60 m offshore at a depth of 2 m would deposit in observable quantities along the shoreline and on the inner shelf. However, the bulk of this effort was intended to provide insight on the physical processes controlling the persistence (or lack thereof) of fine-grain dredge material on, and its advection off, the inner shelf to the mid-shelf (30-70 m depth) mud belt identified by Edwards (2002).

These measurements support the ongoing process studies being done as part of the U.S. Geological Survey's Pacific Coastal and Marine Science Center (USGS-PCMSC) Program's Benthic Habitats (Pacific) and Applied Sediment Transport Projects; the ultimate goal is to better understand the impact of sediment dynamics on benthic habitats along the U.S. west coast. The following report details the study location, the experimental set-up, in place observations, and a numerical modeling investigation to determine the transport pathways of the fine-grain dredged material.

Study Area

Spatial and temporal measurements of oceanographic and sedimentologic conditions were made during the fall and early winter of 2009 in northern Monterey Bay, California (fig. 1). The coast of central California lies along an active tectonic margin whose uplift has resulted in a rugged coastline with high sea cliffs cut into coastal mountains, narrow river valleys, and a relatively narrow continental shelf. The Monterey Bay area lies within a dextral strike-slip tectonic setting that comprises the transform boundary between the Pacific and North American tectonic plates. The shoreline is characterized by steep (up to 100 m high), actively eroding coastal bluffs that often are incised into uplifted marine terraces and are commonly

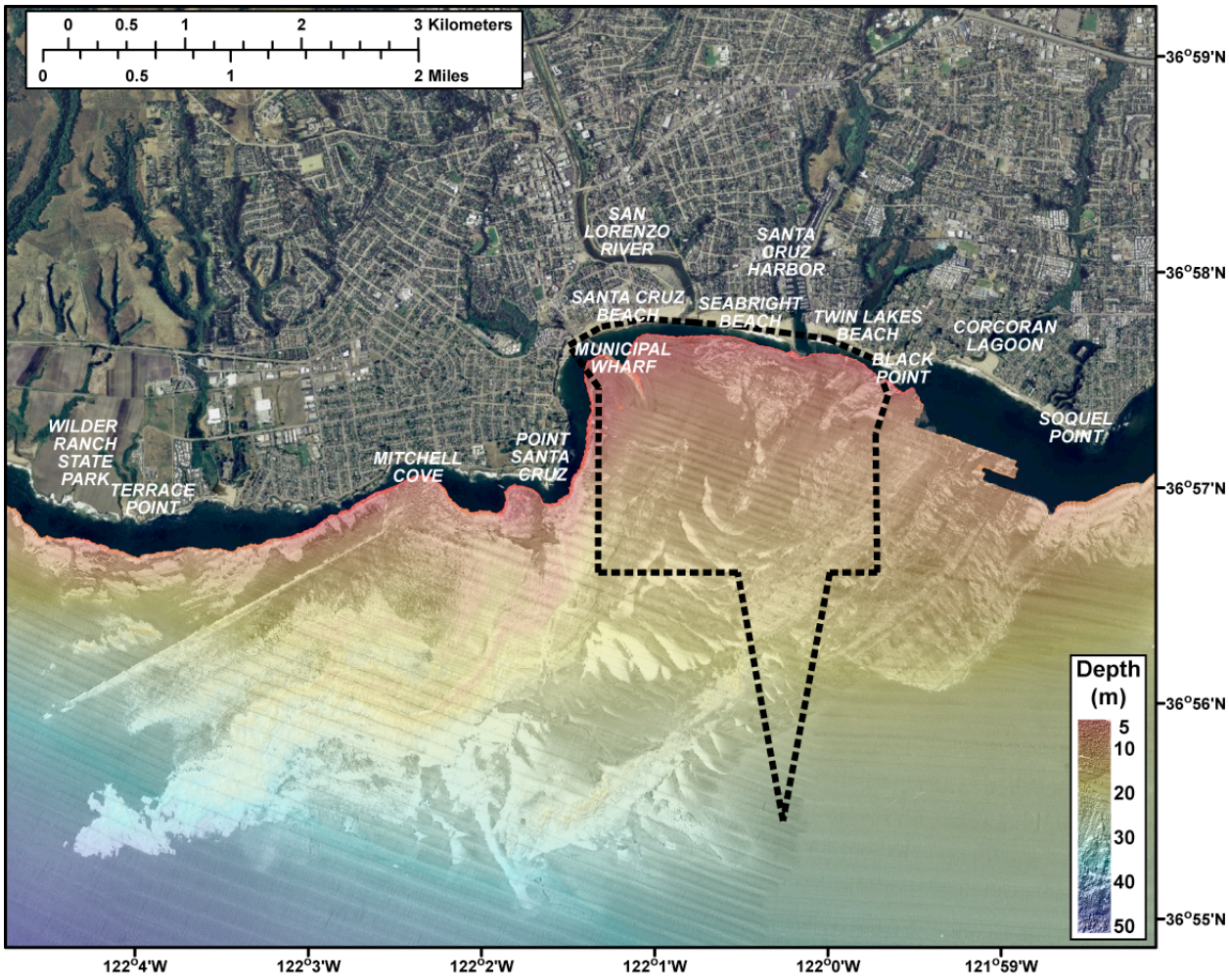

FIGURE 1. Map of the physiography of the study area in northern Monterey Bay, California; data from the U.S. Geological Survey's California Seafloor Mapping Program (http://walrus.wr.usgs.gov/mapping/csmp/). Darker, smooth areas represent sediment-covered seabed characterized by fine sand and mud; the lighter but smooth areas are sediment-covered seabed characterized by coarser sand; the lighter, rough areas are regions where bedrock is exposed on the seabed. The red and yellow shades denote shallower areas, and the blues and purples denote deep areas. The heavy dashed line defines the project study area.

fronted by low, wave-cut shore platforms, or pocket beaches. These seacliffs are dissected at irregular intervals by larger pocket beaches that form at the mouths of coastal streams and by infrequent continuous beaches in sheltered bays. The small, steep perennial streams and a few larger rivers in northern Monterey Bay are the primary sources of coarse-grained sediment to the littoral environment (Best and Griggs, 1991). During the last glacial maximum at 22 ka, streams flowed across the exposed continental shelf and cut channels through the bedrock (Anima and others, 2002); the mouths of many of these streams were inundated during the Holocene transgression, forming low-gradient floodplains, coastal lagoons, and marshes (Griggs and Savoy, 1985). The Santa Cruz Harbor was constructed by dredging Woods Lagoon in the 1960s, and it receives perennial fluvial input from Arana Creek. The inner shelf is characterized by intermittent rock outcrops that support dense kelp forests and it is covered predominantly by medium- to fine-grain sand to the 30 m isobath, where the sediment transitions predominantly to silts and clays, an area termed the "mud belt" by Edwards (2002). Seacliff erosion, with long-term rates ranging from zero to >30 cm/year, is episodic and locally variable (Griggs and Savoy,

1985), typically occurring during the infrequent combination of high tides and extreme storm waves.

The offshore wave climate along central California can be characterized by three dominant modes: the Northern Hemisphere swell, the Southern Hemisphere swell, and local wind-driven seas (Storlazzi and Wingfield, 2005). The Northern Hemisphere swell typically is generated by cyclones in the North Pacific Ocean off the Aleutian Islands during the winter months (November-March) and can attain deep-water wave heights exceeding 8 m. The Southern Hemisphere swell is generated by storms off New Zealand, Indonesia, or Central and South America during summer months and, although generally itproduces smaller waves than the Northern Hemisphere swell, this swell often has very long periods (15+ s). The local seas typically develop rapidly when low-pressure systems track near central California in the winter months or when strong sea breezes are generated during the spring and summer. Storms with deep-water wave heights in excess of 5 m occur five times a year on average.

Operations

This section provides an overview of the different aspects of the project and information about the personnel, equipment, and field operations used during the study. See table 1 for a list of personnel involved in the experiment and tables 2 through 6 for complete listings of instrument and deployment information.

An integrated study to characterize both the sedimentological nature of the coastline and inner shelf and the spatial and temporal variation in physical processes in northern Monterey Bay was done during the fall and early winter of 2009 (fig. 2). The data were collected by means of beach and inner shelf mapping, water-column surveys, geochemical analyses of suspended sediment, oceanographic instrumentation, and numerical modeling. All of the data will be collected according to USGS standards and, thus, be the foundation for any future comparisons. These surveys, initiated in October 2009 and running through December 2009, determined the impacts of the dredge-disposal demonstration project on the study area and provide insight into pathway(s) of the fine-grain sediment off the inner shelf.

Time-Series Physical Process and Turbidity Measurements

The USGS Sea Floor Observatory off the end of the Santa Cruz Wharf overlapped with the demonstration project. This system, the only one of its kind in the world, provided continuous measurements of the forcing physical mechanisms [tides, waves, currents, and/or internal waves (Storlazzi and Jaffe, 2002; Storlazzi and others, 2003)] that drive sediment dynamics and the resulting suspended-sediment concentrations and surficial seabed grain sizes. This real-time, cabled, observational platform system was supplemented by three additional self-contained seabed tripods from October 2009 through December 2009 to make similar physical measurements (tide, wave, current, and suspended-sediment concentration [turbidity]) close to the discharge site off the harbor and further offshore near the 30 m isobath, where the mid-shelf mud belt begins (fig. 2). The time series data from these four instrument packages were used to: (1) determine if the ambient oceanographic conditions that typify the northern part of the bay are quiescent enough for fine-grain dredge sediment discharged during the project to fall out of suspension and accumulate in observable quantities on the inner shelf, or if the conditions are energetic enough to keep the fine-grain sediment in suspension; (2) provide continuous time series measurements of suspended-sediment concentrations starting before and running through the course of the demonstration project to determine the magnitude and direction of sediment flux; and (3) provide the necessary boundary and calibration information for a numerical model of the dredge discharge plume (see below).

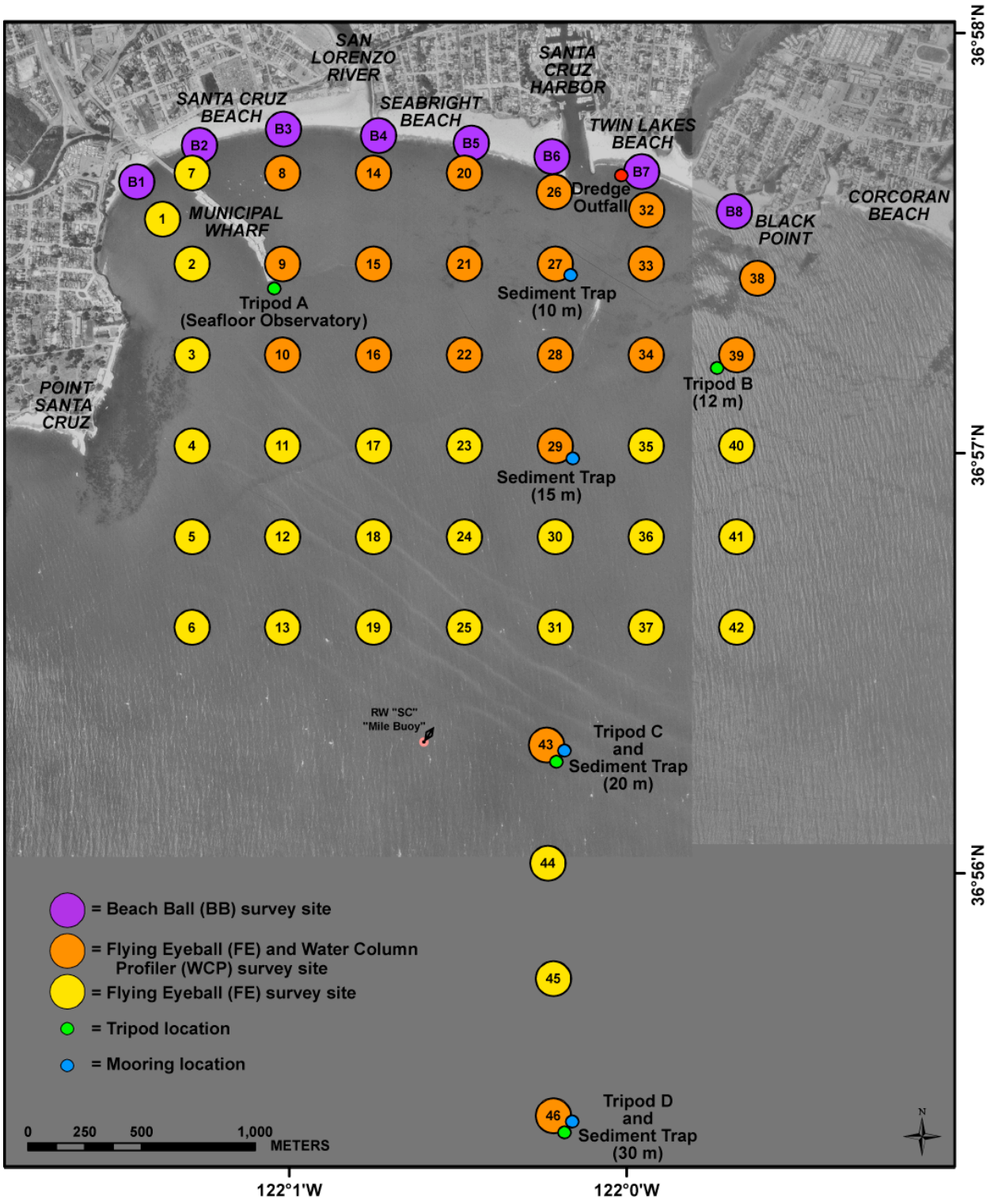

FIGURE 2. Map showing the location of the survey sites, moorings, and instrument packages. The instrument sites and survey area cover both the San Lorenzo River and the Santa Cruz Harbor, the two potential significant inputs of sediment to the study area, and extend offshore to the 30 m isobath where the mid-shelf “mud belt” begins.

Grain-Size and Turbidity Mapping

Seabed Grain-Size Mapping

The monthly USGS Flying Eyeball (Chezar and Rubin, 2004; Rubin and others, 2007) surveys were extended through the end of the demonstration project in the 2009-2010 winter. These surveys of surficial seabed-sediment grain size, taken at 42 locations off Santa Cruz in water depths between 5 m and 25 m (fig. 2), were carried out during the 2008-2009 winter to investigate the impact of river floods and winter storms on the sediment distribution in northern Monterey Bay. The Flying Eyeball (FE) system uses a magnified digital image of the seabed to measure grain size. Because the measurements are based only on the surface layer, these data are more accurate than grab samples that integrate both surface and subsurface grains. This makes the FE system uniquely suited to measure the active surface layer that would result from any dredge material settling on the seabed. FE surveys were focused on the dredge-disposal area of operations. The surveys were completed before, during, and following the demonstration project to determine if the dredge-disposal operations resulted in observable deposition of fine-grain material on the seabed in the study area. FE surveys during winter 2008-2009 provided a first-of-its-kind view of the heterogeneous nature, both in space and time, of seabed surficial grain-size variability on the inner shelf and provided invaluable background information that aided in the analysis of the data acquired during the demonstration project.

Beach Grain Size

The USGS Beach Ball (BB) uses similar technology to the FE but in a portable, hand-held package. BB surveys were done in the swash zone and at the wet/dry line between Cowell Beach and Black Point (fig. 2) to determine if fine-grain dredge material was being deposited onshore. These surveys were completed before, during, and after the demonstration project in concert with the offshore FE surveys to determine if the dredge-disposal operations resulted in significant deposition of fine-grain material along the shoreline in the study area.

Together, the BB and FE provided quantitative data on surficial sediment grain size from the wet/dry line on the subaerial beach, through the nearshore, and to the mud belt on the mid continental shelf.

Beach Monitoring

The quantitative data provided by the BB and FE systems were supplemented by visual observations made by Santa Cruz Port District personnel on the beaches adjacent to the disposal zone at all times during dredging operations. Personnel made observational sweeps and collected digital photography of the beaches peripheral to the disposal area between the San Lorenzo River mouth (to the west) and 20th Avenue (to the east). These sweeps were done to determine if fine-grain sediment (mud) from the dredge-disposal operations were impacting the beach and to halt dredge operations if impact occurred. The data from these surveys are not included in this report.

Nearshore Turbidity Mapping

Vertical profiles of water temperature, salinity, and turbidity were made using a conductivity-temperature-depth (CTD) profiler with an additional optical backscatter (OBS), transmissometer (Xmiss), PAR (photosynthetically-active radiation), and chlorophyll (chl) sensors. These surveys were done in concert with the Beach Ball and Flying Eyeball surveys before, during, and after the end of the demonstration project at 14 of the Flying Eyeball sampling stations on the inner shelf (fig. 2). These profiles were acquired to determine if the dredge-disposal operations resulted in significant changes in water-column properties (for

example, turbidity and light availability for photosynthetic organisms) in the study area. In addition to this, time-series imagery of the dredge-disposal outfall area was collected using the USGS Terrestrial Imaging System (TIS), which was deployed to provide visual records on the impact of storms, waves, and the dredge-disposal operations on sea surface-water properties in the study area.

Suspended Sediment Sampling and Geochemical Source Determinations

The USGS deployed four sediment traps on moorings across the inner shelf to collect material for geologic and geochemical analyses. Geochemical analyses were done on the collected material to try to determine if the sediment transiting the area was dredge material, relict shelf sediment, or material delivered by the San Lorenzo River during the course of the study. The geochemical data, in conjunction with the data from the tripods and Flying Eyeball, provided insight into the presence and quantity of dredge material on the inner shelf.

Numerical Wave, Circulation, and Sediment Transport Modeling

In place sensor data was combined with larger-scale wave models, NCEP-NAM wind model products (Gemmill and Peters, 1997), HF radar sea-surface currents (Paduan and Cook, 1997), TOPEX/POSIDEN tides (Egbert and Erofeeva, 2002), and HYCOM circulation model data (Halliwell, 1998) to provide boundary information and calibration data for a coupled wave-current-sediment transport numerical model for the project area. The Delft3D package was used to develop a model of the study area in order to extrapolate the limited Eulerian point measurements spatially. Due to the errors inherent to such modeling, the goal was not to model the dredge-disposal plume with extreme precision (which would be difficult), but rather to examine the effects of waves, winds, and tides on circulation and sediment transport through the study area to gain insight into the fate of the fine-grain dredge material.

Equipment and Data Review

Tripods

Four upward-looking acoustic Doppler current meters (ADCM) and three downward-looking ADCMs were mounted on four tripods between the 9 m and 30 m isobaths in northern Monterey Bay (Tripods A-D, fig. 2). The upward-looking ADCMs sampled from just above the tripods (2 m above the seabed) up to the sea surface to collect data for calculating tides (m) and profiles of mean current speeds (m/s) and mean current directions (°True). Directional wave data also were recorded by the ADCMs; these data included significant wave height (m), dominant wave period (s), mean wave direction (°True), and directional spread (°). The downward-looking ADCMs sampled 0.5-m above the seabed to allow calculation of near-bed mean current speeds (m/s) and mean current directions (°True). Acoustic backscatter data (dB) collected from the ADCMs for the current measurements also provided information on the amount of particulates in the water column and are used as a qualitative measurement of turbidity.

Four conductivity and temperature (CT) sensors measured water temperature (°C) and doivity (S/m), from which salinity (PSU) was calculated. Sensor types and locations are listed in tables 2 and 3. Six 880-μm optical backscatter sensors (OBS) recorded the amount of infrared light reflected off particles in the water column, which is a function of the particle size and density of particles. These OBSs provided turbidity data in either raw voltages or Nephelometric Turbidity Units (NTU). The OBSs were calibrated to suspended-sediment concentrations (SSC) in mg/l in the laboratory using suspended sediment collected from the tripods (appendix 1). The OBS on Tripod A was calibrated to NTUs via field cross-calibration with the water-column

profiler's (WCP) OBS. The OBSs on the tripods were mounted at or near the level of the ADCM sampling volumes in order for the OBS data to be correlated with the along- and cross-shore velocity data from the ADCMs to calculate suspended-sediment flux (appendix 2). All the sensor types and locations are listed in tables 2 and 3.

Flying Eyeball

Surveys of seabed grain size were made using FE digital imaging system (Chezar and Rubin, 2004; Rubin and others, 2007) to collect information on seabed surficial sediment grain size. At each survey location, a minimum of three images were acquired to account for within-site variability; the resulting three (at a minimum) grain sizes were then averaged to produce one statistically significant mean grain-size value for each location using the algorithms derived by Buscombe and Messelink (2009) and Buscombe and others (2010). The FE position information is listed in table 4. The FE surveys were completed before [09/23/2009 (2009 YD 266), 10/23/2009 (2009 YD 296)], during [10/29/2009 (2009 YD 302), 11/10/2009 (2009 YD 314)], and after [11/24/2009 (2009 YD 328)] the dredge disposal.

Beach Ball

Surveys of beach grain size were made using the BB digital imaging system to collect information on subaerial beach surficial sediment grain size. At each survey location, a minimum of three images were acquired in the swash zone and a minimum of three samples were taken at the wet/dry line to account for variability over the course of a tidal cycle and within the swash zone (for example, beach cusp horns and troughs); the resulting six (at a minimum) grain sizes were then averaged to produce one statistically significant mean grain size-value for each location using the algorithms derived by Buscombe and Messelink (2009) and Buscombe and others (2010). The BB position information is listed in table 5. The BB surveys were completed before [10/23/2009 (2009 YD 296)], during [10/29/2009 (2009 YD 302), 11/10/2009 (2009 YD 314)], and after [11/24/2009 (2009 YD 328)] the dredge disposal.

Water Column Profiler

Surveys of water-column properties were made using a CTD profiler with OBS, Xmiss, PAR, and chl sensors to collect vertical profiles of water temperature (°C), salinity (PSU), density (kg/m^3), turbidity (NTU), transmission (percent), PAR (mE), and chl (mg/m^3). The surveys were done to address both along- and cross-shore variability in water-column properties in northern Monterey Bay and to put the high temporal resolution but spatially limited measurements made by the CTs and SLOBSs on the tripods in the context of larger spatial patterns throughout the study area. The greater density of points near the coastline were established to identify areas where sediment might be entering the bay (San Lorenzo River or Santa Cruz Harbor dredging). The profiling extended offshore to the 30 m isobath to examine the extent of mixing with oceanic waters.

The OBS on the WCP was calibrated to suspended-sediment concentrations (SSC) in mg/l using suspended-sediment samples collected by using a Niskin sampler at multiple locations throughout the survey area during the profiling operations. The total mass of suspended sediment in the water column during a given survey was calculated by summing the SSCs (in mass per volume) throughout the water column for each profile to determine a mass per area, then interpolating between all of the profiles to produce a total mass for the study area. The profiler data position information is listed in table 6. The WCP surveys were completed before [10/16/2009 (2009 YD 289), 10/28/2009 (2009 YD 301)], during [11/12/2009 (2009 YD 316)], and after [11/25/2009 (2009 YD 329), 12/14/2009 (2009 YD 348)] the dredge disposal.

Terrestrial Imaging System (TIS)

Imagery of the dredge-disposal outfall was collected using the TIS, which consists of a Harbortronics time-series digital-imaging system. This system is comprised of a Pentax K200D 10-megapixel digital SLR camera, a control unit, and battery in a waterproof housing with an external solar panel. The TIS was mounted on the Santa Cruz Harbor lighthouse on the harbor entrance western jetty at an elevation of approximately 15 m. The TIS was oriented to provide an unobstructed view of the dredge-disposal outfall. This system collected a time series of hourly images to provide information on the natural frequency and duration of processes impacting the study area (sediment plumes, storms and waves). The TIS took images every hour throughout the deployment. The system's deployment and location information is listed in tables 2 and 3.

Sediment Collection and Grain-Size Analyses

Sediment traps were deployed during the experiment (October 2009 - December 2009) to collect suspended sediment from the water column. The sediment traps, which consisted of a 78-cm-long funnel, with an internal diameter of 26 cm at the top that tapered down to 4 cm, were deployed on moorings with their openings approximately 5 m above the seabed in a cross-shore array extending from the 10 m isobath to the 30 m isobath. A baffle was placed in the top of each tube trap to reduce turbulence and minimize disturbance by aquatic organisms (Bothner and others, 2006). Because of the energetics of the inner shelf environment, the traps did not measure net vertical sediment flux to the seabed. This is because material falling into the trap has a much lower potential for resuspension than the same material that settles on the adjacent seabed (Bothner and others, 2006). In addition, the traps may preferentially collect coarser particle sizes because of their higher settling velocity than finer particles. Particles with slow settling velocities relative to the circulation and exchange of water contained in the trap can be underrepresented in the collected samples (for example, Gardner and others, 1983; Baker and others, 1988). Sediment trap collection tubes were in place during 2009 Year Days 292–313, 313–336, and 336–349, representing two periods during dredging times (early and late) and after dredging times (including post-dredging storm and flood). It should be noted that these collection times somewhat overlap the various pre- and post-dredging categories described elsewhere in this document. The sediment traps' position and depth information is listed in table 7.

In addition, seabed sediment-grab samples were collected by divers at the main study sites. The bulk grain sizes of the sediment samples were analyzed using Beckman Coulter Counter (silt and clay fractions) and 2 m settling tubes (sand fraction), and within each grain size fraction the percent carbonate was determined with a UIC Coulometer. The critical shear stresses for the initiation of transport were calculated using the modified Shield parameter methodology of Madsen (1999); the values for coarse sand, fine sand, and coarse silt (mud) transport are 0.372 N/m^2, 0.185 N/m^2, and 0.131 N/m^2, respectively (table 8).

Sediment Geochemistry

Subsamples of suspended sediment collected in sediment traps and seabed sediment were processed for chemical analysis, including carbon and nitrogen isotopic and elemental composition, short-lived radioisotope activity, and trace-element composition in order to determine the sediment source (river, relect-shelf sediment, or dredge material). Efforts were taken to minimize contamination of samples for geochemical analysis by rinsing all parts of sampling equipment coming in contact with sediment with dilute HCl and with deionized water. The sediment traps were constructed avoiding contaminating materials wherever possible. During transport, sediment traps and collection tubes were protected in clean polyethylene bags, and handling of traps and sampling tools was done using clean polyethylene gloves whenever

possible. Immediately before deployment, traps and collection tubes were conditioned with local seawater.

In addition to suspended-sediment and seabed-sediment samples, samples of Santa Cruz Harbor material from the areas to be dredged (North Harbor areas A1, A2, A2A, A3, A4) were taken from sediment cores collected by Red Hills Environmental, Inc., in July 2009 using a Vibracore sampling system. Sampling was done using methods designed to minimize potential contamination, and subsamples were taken along the entire length of the sediment core. A technical report describing the Santa Cruz Harbor cores' locations and physical and chemical characteristics was completed by Red Hills Environmental, Inc. After collection, sediment samples were immediately frozen to prevent microbial degradation. Samples for geochemical analysis were then freeze dried, disaggregated, dry sieved with a nylon mesh to less than 100-μm, and then homogenized using a mortar and pestle.

Analyses for carbon and nitrogen isotopic and elemental composition were done at the USGS Menlo Park Stable Isotope Laboratory in California. Approximately 6 mg of sediment was weighed into a silver capsule and treated to remove carbonate material in a sealed chamber (desiccator) with HCl vapor. Samples were then dried in an oven for 3 hours at 50°C, sealed into a tin capsule, and stored in a desiccator until analysis. Instrumental analysis was performed with a Carlo Erba 1500 elemental analyzer attached to a Micromass Optima mass spectrometer.

Analyses for radionuclides were done at the USGS Santa Cruz Marine Geochemistry and Radiochemistry Laboratory. Samples were placed in 10 mL standard geometry plastic tubes and sealed. The samples were analyzed more than 14 days after sealing to allow time for secular equilibrium of ^{222}Rn and ^{226}Ra. Gamma counting was done for about 24 hours using a high-purity germanium well detector for ^{210}Pb (46 keV), ^{228}Ra (338 keV, 912 keV), ^{226}Ra (352 keV), ^{7}Be (476 keV), ^{226}Ra (609 keV), ^{137}Cs (662 keV), and ^{234}Th (63 keV). Excess ^{210}Pb ($^{210}Pb_{xs}$) was calculated as the difference between total ^{210}Pb activity and ^{226}Ra activity.

Analyses for trace metals were done at the USGS Denver Analytical Chemistry Laboratory. Trace-element composition of sediment samples was determined by using a multi-acid (low temperature mixture of hydrochloric, nitric, perchloric, and hydrofluoric) digestion and instrumental analysis by inductively coupled plasma-mass spectrometry (ICP-MS).

Numerical Circulation and Sediment-Transport Modeling

A Delft3D coupled wave-current-sediment transport numerical circulation model of northern Monterey Bay was constructed in order to extrapolate the limited Eulerian point measurements spatially and to examine the effects of waves, winds, and tides on circulation and sediment transport in the study area. The Delft3D Online Morphology system (Lesser, 2009; Delft user manual, 2006) was used to obtain estimates of sediment transport in the study area. The main components are the coupled Delft3D-WAVE and the Delft3D-FLOW modules. FLOW forms the core of the model system, simulating water motion due to tidal and meteorological forcing, by solving the unsteady shallow-water equations that consist of the continuity equation, the horizontal momentum equations, and the transport equation under the shallow water and Boussinesq assumptions. Vertical accelerations are assumed minor compared to gravitational acceleration (shallow-water assumption) reducing the vertical momentum equation to the hydrostatic-pressure relation. By specifying boundary conditions for bed (quadratic-friction law), free surface (wind stress), lateral boundaries (water level, currents, discharges), and closed boundaries with free-slip conditions at the coasts, the equations can be solved on a staggered grid using an Alternating Direction Implicit method (Stelling 1984; Leendertse, 1987; Delft, 2006).

Wave effects, such as enhanced bed shear stresses and wave current forcing due to breaking, are integrated in the flow simulation by running the third generation WAVE model. WAVE is based on discrete spectral action balance equations, computing the evolution of

random, short-crested waves through the SWAN wave processor (Holthuijsen and others, 1993; Booij and others, 1999; Ris and others, 1999). Physical processes include: generation of waves by wind, dissipation due to whitecapping, bottom friction and depth-induced breaking, and nonlinear quadruplet and triad wave-wave interactions. Wave propagation, growth, and decay are solved periodically on subsets of the flow grid. The results of the wave simulation, such as wave height, peak spectral period, and mass fluxes are stored on the computational flow grid and are included in the flow calculations through additional driving terms near surface and bed, enhanced bed shear stress, mass flux, and increased turbulence (Walstra and others, 2000).

In this study the Delft3D Online Morphology model (online approach) was used to resolve the sediment-transport patterns dynamically. Suspended sediment transport was computed by the advection-diffusion solver. To describe sediment characteristics, additional formulations are included to account for density effects of sediment in suspension, sediment settling velocity, vertical diffusion coefficient for sediment, suspended-sediment correction vector and sediment exchange with the bed (Van Rijn, 1993). The Partheniades-Krone transport formulation for cohesive sediment was used for the finer-grained dredge material. The elevation of the bed is updated dynamically at each computational time-step by calculating the change in mass of the bottom sediment resulting from the sediment gradients. One sediment fraction was applied to describe the dredge-disposal material. Real-time modeling was employed in this study. Complete overviews of the basics, testing, and validation of the Delft3D Online Morphology have been reported in Lesser (2009). See Walstra and others (2000), and Van Rijn (1993; 2007a,b,c) and Van Rijn and others (2007) for the transport formulations.

Surface currents in Monterey Bay have strong modes of variability (Paduan and Cook, 1997). At longer time scales, currents show patterns that evolve with major wind reversals and the proximity of mesoscale eddies. At the shorter time scales, current fluctuations are dominated by semidiurnal tidal forcing and diurnal wind (sea-breeze) forcing. Hydrodynamics along the Santa Cruz coastline are governed mostly by these large-scale current patterns. In order to model the fate of the dredge plume from Santa Cruz Harbor, it was important to predict these fluctuations, both on the short and longer timescales. For reasons of computational efficiency, the large-scale circulation in Monterey Bay (and further offshore) was computed with a cascade of hydrodynamic models with varying spatial resolution. The model used to investigate the dredge-disposal plume (Santa Cruz model) was nested within the smallest of these models through a one-way nesting procedure.

Miscellaneous Data Sources

Regional oceanographic and meteorological data were provided by the National Data Buoy Center's buoy #46042-Monterey Bay (NDBC, 2010) deployed approximately 40 km to the southwest of Santa Cruz in the central portion of the bay. The buoy provided averages of barometric pressure (mb), air temperature (°C), wind speed (m/s), wind direction (°True), wave height (m), wave period (s), and wave direction (°True) every hour. The buoy's location is listed in table 3. Discharge data (m^3/s) for the San Lorenzo River at Santa Cruz were provided by the USGS National Water Information System gage station #11161000-San Lorenzo River at Santa Cruz (NWIS, 2010); the gage station location is listed in table 3. The Santa Cruz Port District provided data on the volumes (m^3) of mud- and sand-sized fractions of material dredged each day. Navigation equipment for deployment, recovery, and survey operations included hand-held WAAS-equipped GPS units and a computer with positioning and mapping software. The positioning and mapping software enabled real-time GPS position data to be overlain on images of previously collected high-resolution swath bathymetry, shaded-relief bathymetry, 5 m isobaths, and aerial photographs of terrestrial portions of the maps.

Research Platform and Field Operations

The instrumentation tripod and sediment-trap mooring deployments and recoveries were done using the University of California at Santa Cruz's (UCSC) *R/V Paragon,* the USGS *R/V Parke Snavely,* and the *R/V Shana Rae.* The instruments were deployed by lowering them to the seabed and detaching them from the lowering line using a Pelican quick-release hook. The tripods along the 20 m and 30 m isobaths were recovered using an acoustic release, which, when triggered, released a float and recovery line that was used to winch the tripods back onboard the vessel. The tripod along the 14 m isobath and the sediment-trap mooring were recovered by scuba divers attaching a lifting line to the tripod or mooring weight, which was then winched onboard the recovery vessel. All of the tripods and sediment-trap mooring were situated on the sandy seabed in water depths ≤30 m. The FE and WCP surveys were done from the USGS *R/V Frontier*. The BB surveys were done on foot. Surficial seabed sediment samples at the sediment-trap mooring sites were collected by scuba divers.

Data Acquisition and Quality

Data were acquired for 55 days during the period between October 22, 2009, and December 15, 2009 (2009 Year Day [YD] 295-349). During the experiment, four periods were observed and quantified: late summer conditions before the dredge-disposal experiment (2009 YD 295-301), during the dredging (2009 YD 302-324), fall conditions following the dredge-disposal experiment (2009 YD 325-339), and the first large winter storm and flood after the end of the experiment (2009 YD 340-349). More than 400,000 data points were recorded by the ADCPs, CTs, and OBSs; more than 126 profiles were recorded by the WCP during 4 surveys. The TIS collected 1013 images, and the FE and BB collected 1747 and 392 images, respectively, during 5 surveys. The raw data were archived and copies of the data were post-processed for analysis.

The ADCM, CT, OBS, TIS, WCP, FE, and BB data generally were of high quality. Instrument controller issues on Tripod A (Sea Floor Observatory) caused intermittent power problems and, thus, resulted in long gaps in data. In order to obtain turbidity values higher in the water column, we computed suspended-sediment concentrations (in mg/L) for the OBS as addressed above. Calculated suspended-sediment concentrations were then correlated to colocated ADCM current velocity data to compute suspended-sediment fluxes.

The water-column profiler data were very high in quality; as typical, the data near the seabed often displayed spikes due to the sensors' interaction with the seabed. Electronic issues with the WCP's PAR sensor made the data unreliable, and therefore, these data are not presented in this report. The mooring along the 15 m isobath (Mooring-15 m) was struck and destroyed sometime after 2009 Year Day 313, and therefore, no suspended-sediment samples were collected from this mooring for grain size and geochemical analyses during the last two sampling periods (2009 YD 313-336 and 336-349). All errors are given as ± one standard deviation unless otherwise specified.

Results

This section reviews the data collected by the instruments during the deployments and addresses the significance of the findings to better understand the oceanographic conditions in the study area.

Inner Harbor Dredge Sediment Discharge

The dredging was done only during weekdays between October 29, 2009 (2009 YD 302) and November 20, 2009 (2009 YD 324). The total daily dredge discharge ranged from 76 to

1153 m^3/day, with a mean discharge of 450±237 m^3/day; overall, 7649 m^3 of sediment was dredged, 70.9 percent of which was mud-sized (<63 μm) material (fig. 3a, table 10). The total daily dredge discharge of mud-sized material ranged from 20 to 417 m^3/day, with a mean daily discharge of 319±133 m^3/day; the total daily discharge of sand-sized (>63 μm) material ranged from 31 to 772 m^3/day, with a mean daily discharge of 131±172 m^3/ day. Imagery from the TIS showed no apparent surface plume resulting from the dredge operations (fig. 3b-d), with the only turbidity visible in the imagery occurring on 2009 YD 311 (fig. 3e), which corresponded to a period of larger-than-normal wave heights and periods (see following section). Evidence of large waves can be observed by the presence of white bubbles in the water generated by waves breaking along the shoreline (wide surf zone along Twin Lakes Beach) and along the harbor breakwater (along the breakwater and tailing off to the east) can been seen in figure 3d.

Regional Oceanographic and Atmospheric Forcing

The study period from October 2009 through December 2009 covered the end of dry, low-energy summer conditions through the beginning of the wet, energetic winter season (fig. 4; table 10). The barometric pressure ranged from 1004.1 mb to 1024.4 mb, with a mean pressure of 1017±3.5 mb (fig. 4a). The water temperature ranged from 11.62ºC to 15.26ºC with a mean temperature of 12.77±0.79ºC (fig. 4b). The mean winds speeds offshore of Monterey Bay ranged from 0.34 m/s to 15.39 m/s, with a mean speed of 6.32±3.18 m/s; the mean wind direction was 264.1±109.9° (fig. 4c). The waves that impacted Monterey Bay during the course of the experiment had significant wave heights ranging from 0.95 m to 6.88 m, with a mean significant height of 2.72±1.03 m (fig. 4d). Dominant wave periods varied from 4.55 s to 23.53 s, with a mean dominant period of 13.22±3.08 s (fig. 4e). The mean wave direction was 299.5±18°. Northwesterly winds and relatively small waves dominated the period of study and were associated with dry, stable weather; this forcing characterized approximately 70 percent of the study period. Strong, south winds were associated with drops in barometric pressure from storms that usually coincided with the arrival of larger waves (for example, 2009 YD 308-312 and 343-348).

River Water Discharge

Daily discharge data provide a measure of the stream response to precipitation in the study area. Discharge ranged from 0.25 m^3/s to 5.47 m^3/s, with a mean discharge of 0.63±0.89 m^3/s (table 10). The greatest discharge during the period of study coincided with the heavy precipitation during 2009 YD 345-349 (fig. 4f). None of the small coastal lagoons (Schwann Lagoon at Twin Lakes State Beach, Blacks Beach, or Moran Lagoon) breached during the period of study.

Tides

The study period encompassed more than 4 complete spring-neap tidal cycles (fig. 5-8a). The tides in northern Monterey Bay are typical for California; mesotidal, mixed, semi-diurnal with two uneven high tides and two uneven low tides per day, thus the tidal period is slightly longer than 6 hours. The maximum spring tide range during the deployment was approximately 2.5 m, and the diurnal and mean tidal ranges were approximately 1.5 and 1.0 m, respectively.

Waves

The waves measured at the Tripod A site near the end of the Santa Cruz Municipal Wharf were consistently from the southwest due to refraction around Point Santa Cruz, with mean significant wave heights and dominant periods on the order of 0.35 m and 15 s; this site

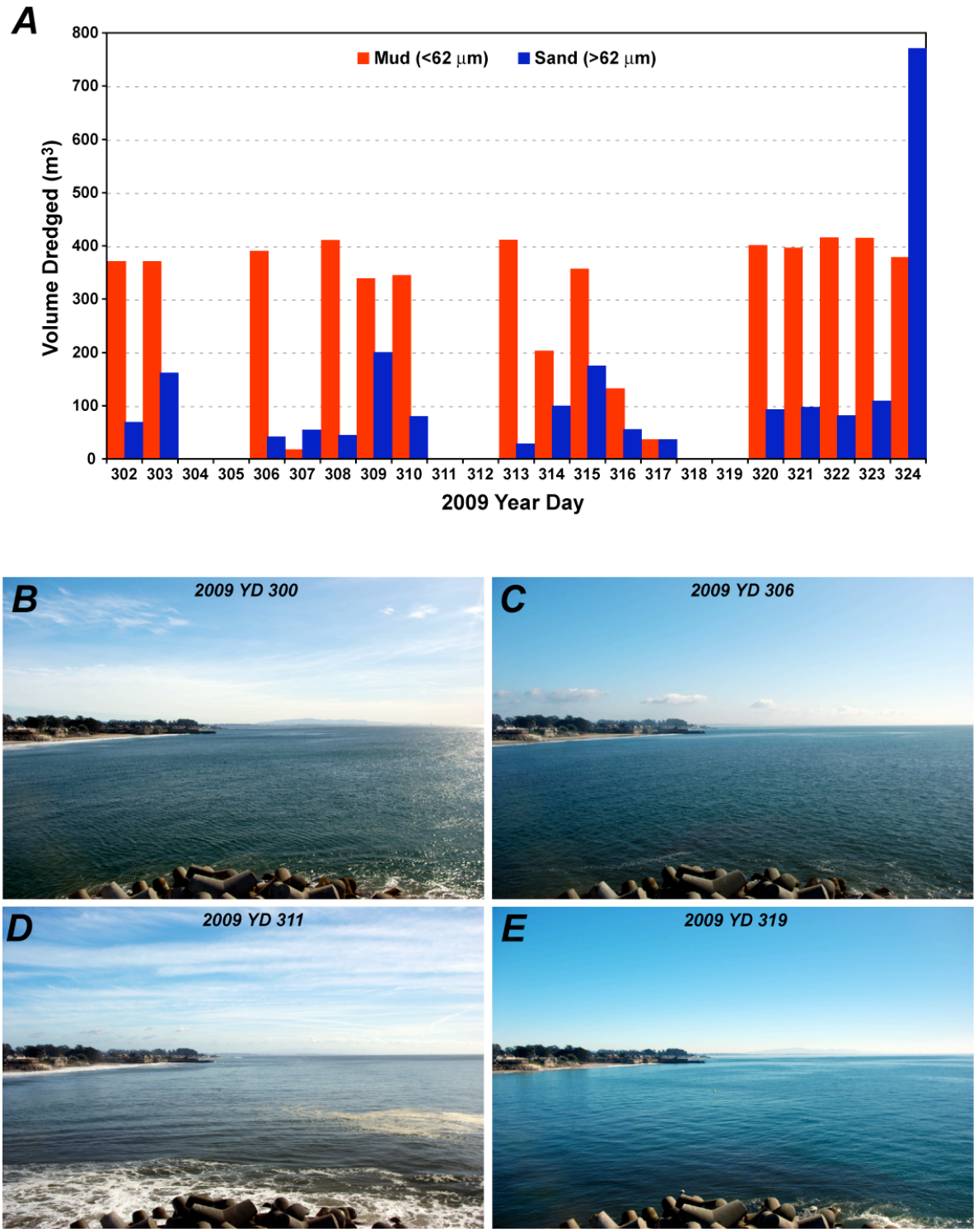

FIGURE 3. Plot of harbor dredging volumes and Terrestrial Imaging System (TIS) photographs. *A,* Volume of sediment dredged, in cubic meters, of both mud- (red) and sand-sized (blue) sediment. *B,* Image of dredge-disposal area on October 27, 2009, before dredging commenced. *C,* Image of dredge-disposal area during dredging on November 2, 2009. *D,* Image of dredge-disposal area during dredging on November 7, 2009, during large wave conditions. *E,* Image of dredge-disposal area during dredging on November 15, 2009.

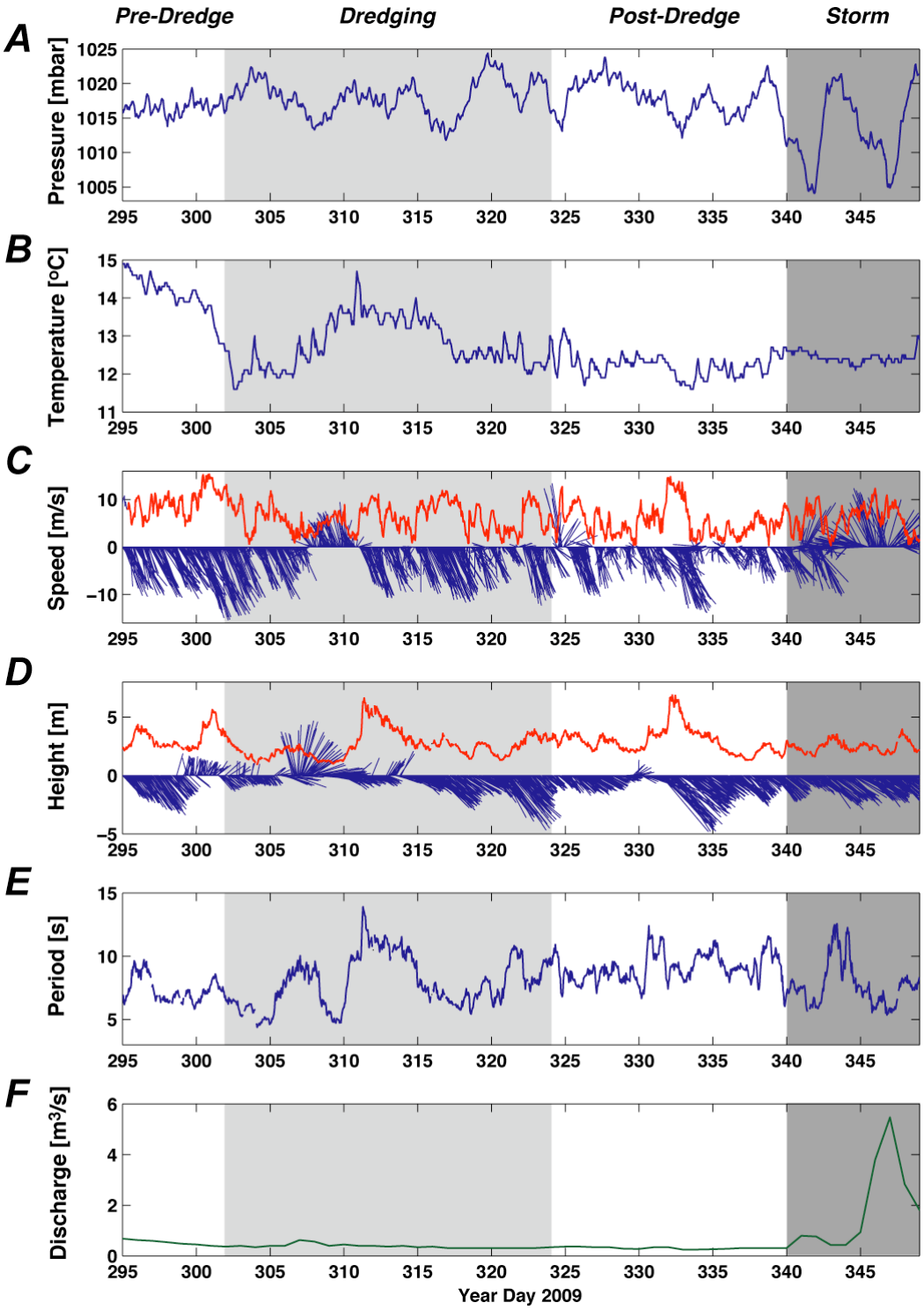

FIGURE 4. Time-series plots of regional meteorologic, oceanographic, and fluvial data during the study period. *A,* Barometric pressure, in millibars. *B,* Water temperature, in degrees Celsius. *C,* Red: wind speed, in meters per second; Blue: wind speed and direction, in meters per second from degrees true north. *D,* Red: wave height, in meters; Blue: wave height and direction, in meters from degrees true north. *E,* Wave period, in seconds. *F,* River discharge, in cubic meters per second. The period of dredge-disposal operations and the post-dredging storm and flood are denoted by the light grey (2009 Year Days 302-324) and dark grey boxes (2009 Year Days 340-349), respectively.

experienced the smallest waves in the study area due to refraction (table 11). The waves propagating over the sites farther to the east (Tripod B) and offshore (Tripods C and D) underwent less refraction and, thus, measured larger wave heights (0.85 m, 1.00 m, and 1.18 m for Tripods B, C, and D, respectively) and more westerly wave directions (218.5°, 230.7°, and 251.5° for Tripods B, C, and D, respectively) than Tripod A.

Currents

Similar to the wave heights, current speeds were greater to the east and offshore (fig. 5-8, table 12); the tidal currents flood to the north and ebb to the south. The mean current speed at Tripod A (depth ~9 m) was 0.02±0.02 m/s close to the seabed (fig. 5). The mean current speeds at Tripod B (depth ~12 m) were approximately twice the speeds measured at Tripod A, with a mean current speed of 0.05±0.03 m/s close to the surface and 0.05±0.02 m/s close to the seabed (fig. 6). The mean current speed at Tripod C (depth ~20 m) was greater (0.08±0.05 m/s) close to the surface than at Tripod B, but slower (0.03±0.02 m/s) close to the seabed (fig. 7), possibly due to greater influence of wind-driven surface currents and thermal stratification. The currents at Tripod D (depth ~30 m) were the fastest, with the mean current speeds of 0.09±0.05 m/s close to the surface and 0.05±0.03 m/s close to the seabed (fig. 8).

Overall, the mean currents offshore along the 20 m and 30 m isobaths were much stronger and more uniform than those closer to shore, where the mean currents were weaker and more variable (fig. 9). Close to the seabed, the currents primarily were oriented cross-shore (north-south) closer to shore, but alongshore (east-west) to the west at Tripod D along the 30 m isobath. Currents near the surface primarily were oriented alongshore. Surface currents close to shore (sites A and B) typically were to the east, while surface currents at the offshore sites (C and D) typically were to the west.

Turbidity

The turbidity in the northern part of the bay ranged between 0 NTU and 693 NTU (fig. 5-8), with a mean turbidity of 19±23 NTU (table 13). The near-bed turbidity at Tripod A, off the wharf (depth ~9 m), was between 0 NTU and 311 NTU, with a mean turbidity of 29±35 NTU. The near-bed turbidity at Tripod B (depth ~12 m) was between 0 NTU and 311 NTU, with a mean turbidity of 29±35 NTU. The turbidity at Tripod C (depth ~20 m), in the lower water column at a height of 2 m above the seabed, was between 1 NTU and 61 NTU, with a mean turbidity of 6±6 NTU, while the near-bed turbidity was between 0 NTU and 490 NTU, with a mean turbidity of 22±36 NTU. The near-bed turbidity at Tripod D was between 2 NTU and 693 NTU, with a mean turbidity of 23±32 NTU. Near-bed turbidity was, in general, higher during and after the dredging than before the dredging, and was greatest during the storm and flood following the dredge-disposal experiment.

Temperature

The near-bed water temperature at Tripod B ranged between 10.89°C and 14.31°C, with a mean temperature of 12.12±0.79°C (fig. 10a; table 15). The near-bed water temperature at Tripod C was between 10.82°C and 13.79°C, with a mean temperature of 11.85±0.66°C. The near-bed water temperature at Tripod D was between 10.56°C and 13.59°C, with a mean temperature of 11.58±0.56°C. The inshore and offshore sites showed similar seasonal patterns in decreasing temperature during the deployment. The daily near-bed temperature variations did not appear to be coherent between instrument sites. At times the offshore sites showed greater daily variation than the inshore sites, while at other times the inshore sites showed greater daily

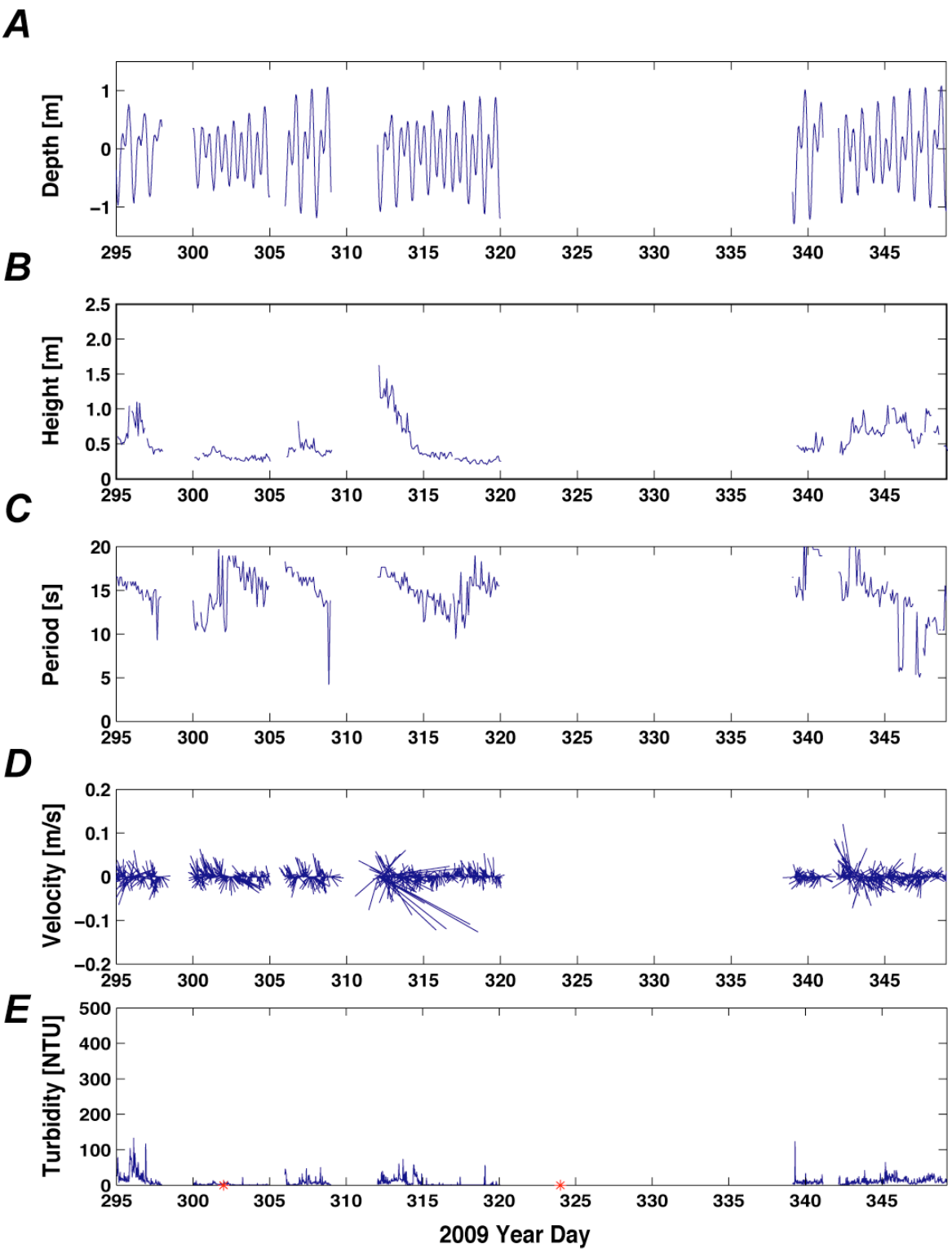

FIGURE 5. Time-series plots of tides, waves, currents, and turbidity at Tripod A (Sea Floor Observatory at 9 m depth). *A,* Tide, in meters. *B,* Wave height, in meters. *C,* Wave period, in seconds. *D,* Current speed and direction, in meters per second from degrees true north close to the seabed (depth is 8.5 m). *E,* Turbidity, in National Turbidity Units (NTU).

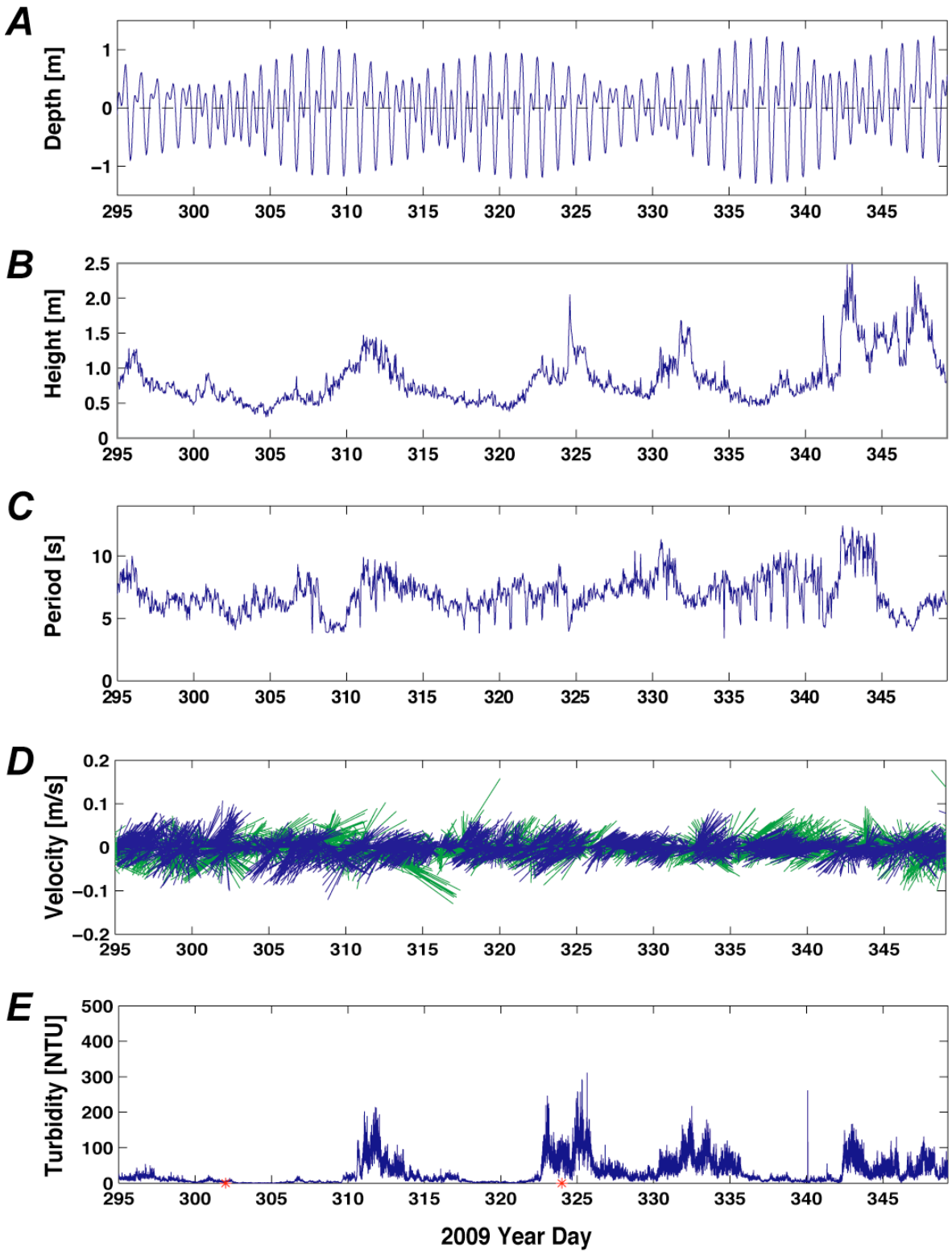

FIGURE 6. Time-series plots of tides, waves, currents, and turbidity at Tripod B (12 m depth). *A,* Tide, in meters. *B,* Wave height, in meters. *C,* Wave period, in seconds. *D,* Current speed and direction, in meters per second from degrees true north close to the surface (depth is 2 m, in green) and lower in the water column (depth is 6 m, in blue). *E,* Turbidity, in National Turbidity Units (NTU).

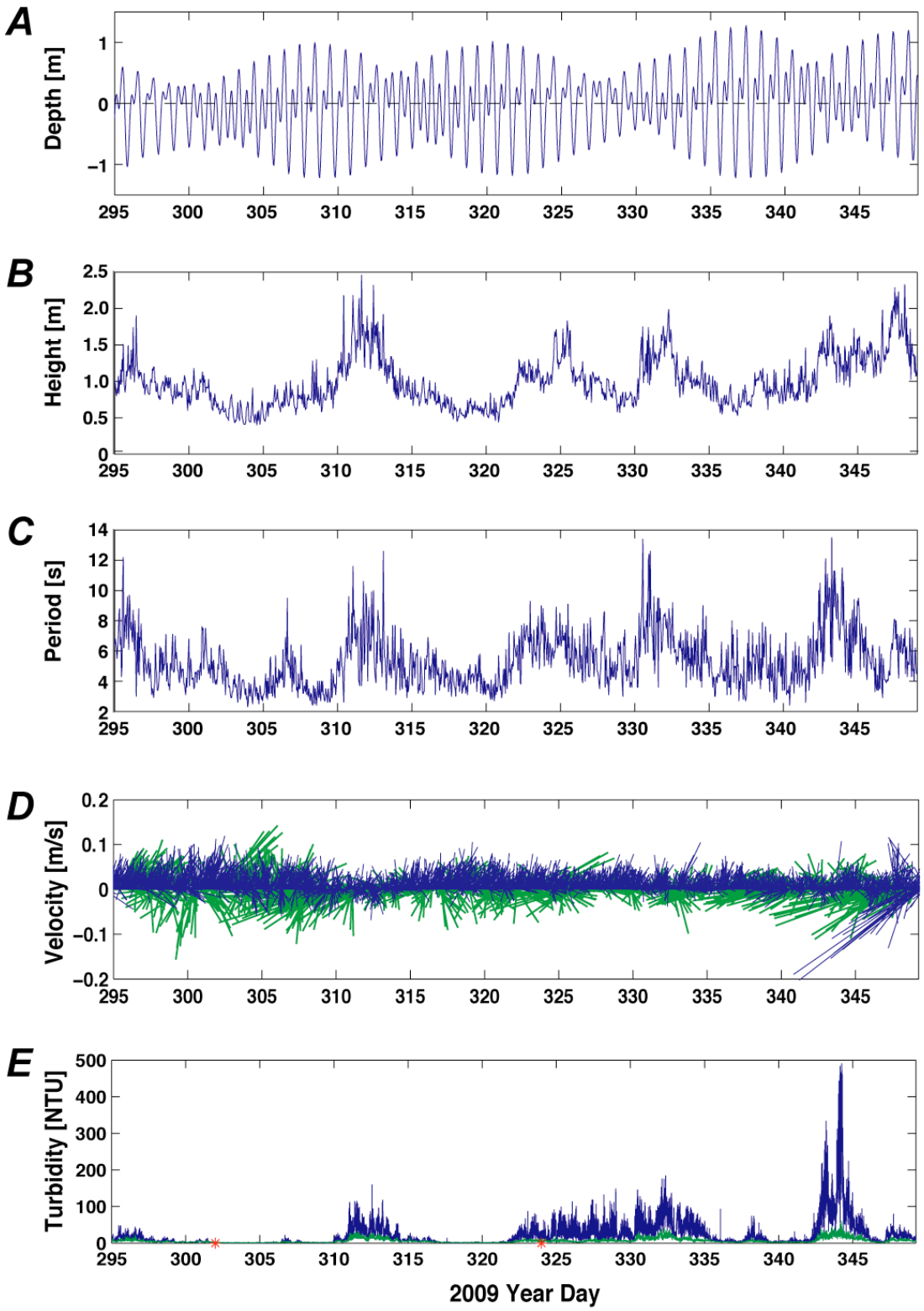

FIGURE 7. Time-series plots of tides, waves, currents, and turbidity at Tripod C (20 m depth). *A,* Tide, in meters. *B,* Wave height, in meters. *C,* Wave period, in seconds. *D,* Current speed and direction, in meters per second from degrees true north close to the surface (depth is 2 m, in green and lower in the water column (depth is 18 m, in blue). *E,* Turbidity, in National Turbidity Units (NTU).

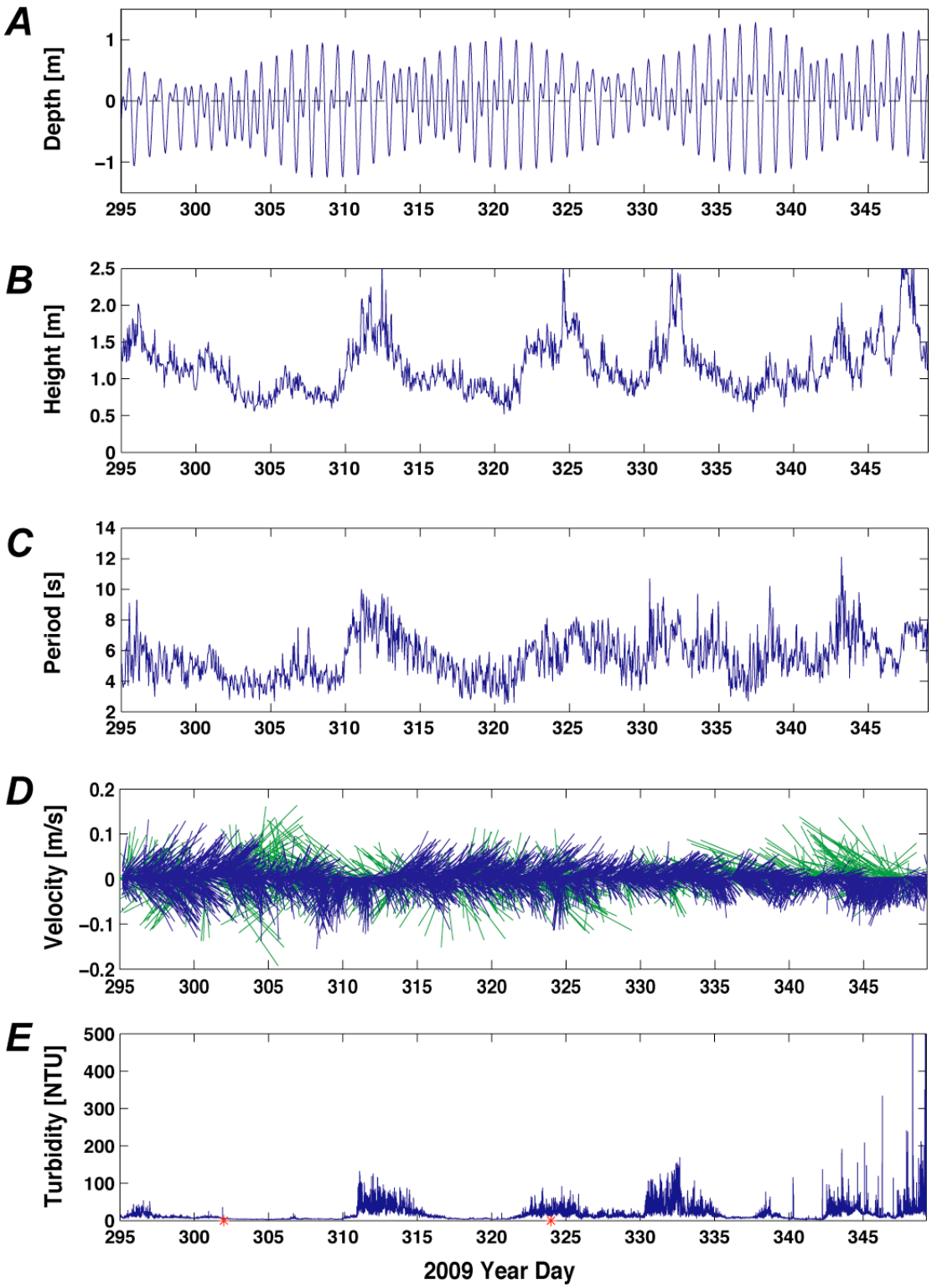

FIGURE 8. Time-series plots of tides, waves, currents, and turbidity at Tripod D (30 m depth). *A,* Tide, in meters. *B,* Wave height, in meters. *C,* Wave period, in seconds. *D,* Current speed and direction, in meters per second from degrees true north close to the surface (depth is 2 m, in green) and lower in the water column (depth is 28 m, in blue). *E,* Turbidity, in National Turbidity Units (NTU).

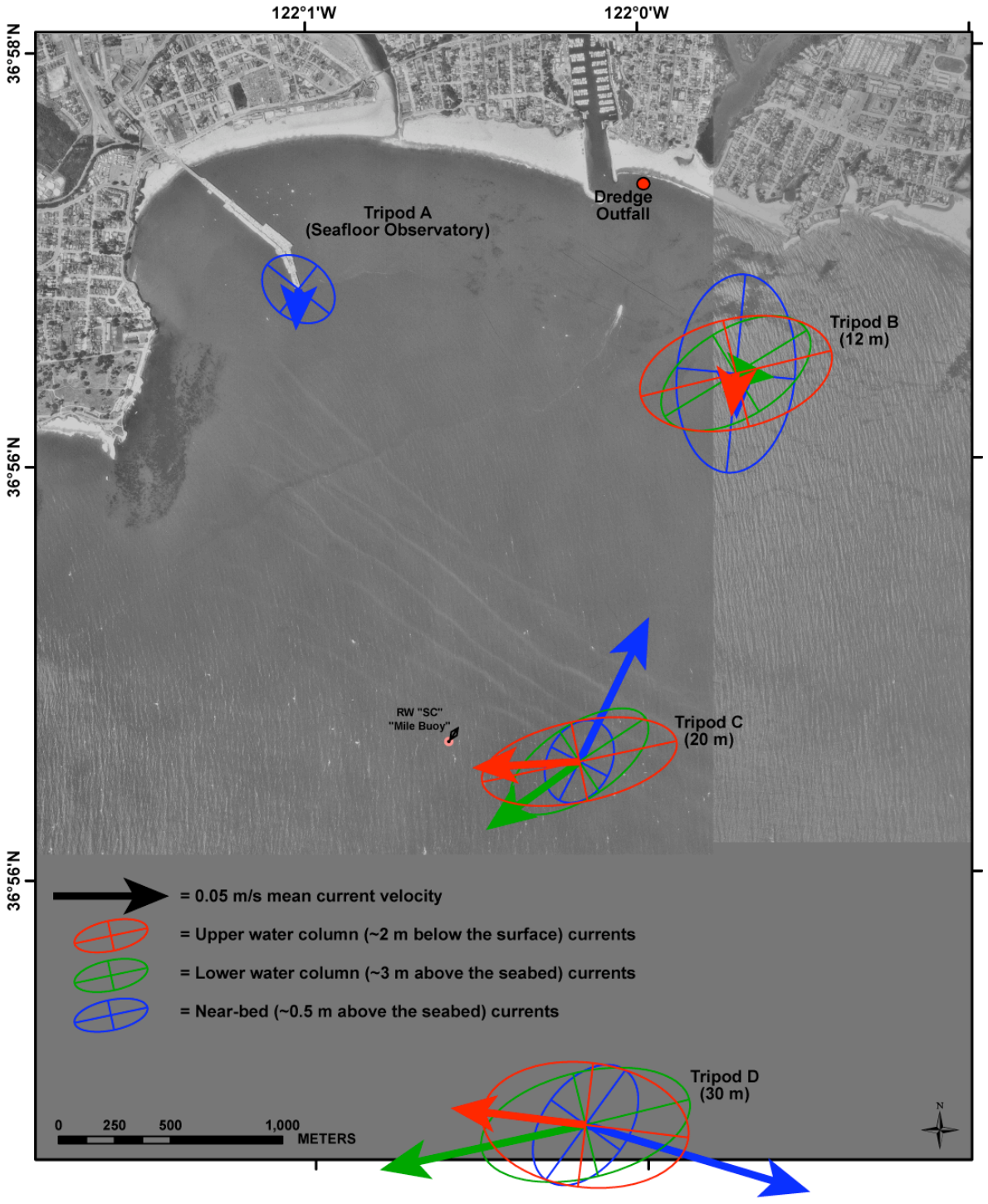

FIGURE 9. Map showing principal axis ellipses and mean current speeds and directions, in meters per second from degrees true north, at the main study sites for the entire period of study. Data from close to the seabed, the lower water column, and close to the surface are shown in blue, green, and red, respectively.

variability and the offshore sites showed less variation. This variability may be caused by variations in the propagation of deeper, cooler oceanic water replacing warmer nearshore waters driven by the tidal cycle.

Salinity

Near-bed salinity in the study area was between 19.64 PSU and 35.21 PSU, with a mean salinity of 34.83±0.31 PSU (fig. 10b; table 16). The near-bed salinity at Tripod B was between 23.41 PSU and 33.23 PSU, with a mean salinity of 31.06±1.87 PSU. The near-bed salinity at Tripod C was between 33.14 PSU and 33.59 PSU, with a mean salinity of 33.43±0.06 PSU. The near-bed salinity at Tripod D was between 33.10 PSU and 33.61 PSU, with a mean salinity of 33.35±0.11 PSU. The brief, low salinity levels that quickly returned to pre-event levels likely are spurious data that were caused by wave-driven sediment blocking the conductivity sensor.

Spatial Variations in Water-Column Properties

The OBS on the WCP provided turbidity values in NTUs, which are useful for comparing to U.S. Environmental Protection Agency guidelines for water clarity. The turbidity before dredge-disposal operations generally was low except for the nearshore region off the Santa Cruz Harbor's west jetty and extending east (down-coast in terms of wave direction) from that point (fig. 11; appendix 3). It appeared that wave-breaking on the west jetty resulted in increased sediment resuspension, and this plume was advected eastward past the harbor mouth, Twin Lakes Beach, and Black Point. The total mass of sediment suspended in the water column across the study area calculated from the OBS during the pre-dredge survey was 58.1±9.9 metric tons. During dredge operations, turbidity increased approximately 40 NTUs offshore and to the east of the harbor mouth; while elevated, these turbidity values were less than those observed during a red tide that occurred before the beginning of dredge-disposal operations as identified in the chl data (appendix 5). The total mass of sediment suspended in the water column across the study area calculated from the OBS during dredging was 43.8±11.1 metric tons. Following the dredge-disposal operations, most of the offshore turbidity values returned to their pre-dredging levels, except at survey sites #16 and #33, which were approximately 1000 m and 300 m offshore Seabright Beach and Twin Lakes Beach, respectively. The total mass of sediment suspended in the water column across the study area calculated from the OBS following the dredging was 52.1±11.9 metric tons.

Similar to the turbidity, the light transmission from the Xmiss on the WCP before dredge disposal operation generally was low except for the nearshore region off Seabright Beach and Black Point (fig. 12; appendix 4). It appeared that wave-breaking on the harbor's western breakwater resulted in increased sediment suspension. During dredge operations, transmission decreased approximately 15 percent offshore and to the east of the harbor mouth; although lower, these transmission values were less than what was observed during a red tide that occurred before the beginning of the dredge-disposal operations as identified in the chl data (appendix 5). Following dredge-disposal operations, most of the offshore transmission values returned to their pre-dredging levels, except at survey sites #32 and #33, which were approximately 150 m and 300 m offshore Twin Lakes Beach.

Spatial Variations in Beach and Seabed Surficial Grain Size

There were no statistically significant differences in surficial sediment size observed by the BB system along the shoreline during the period of investigation (fig. 13). While there was variability at each location (determined from the multiple samples taken at each location (appendix 6), there was no observed change in grain-size class over time along the shoreline. Offshore, there were no statistically significant differences in surficial sediment size observed by

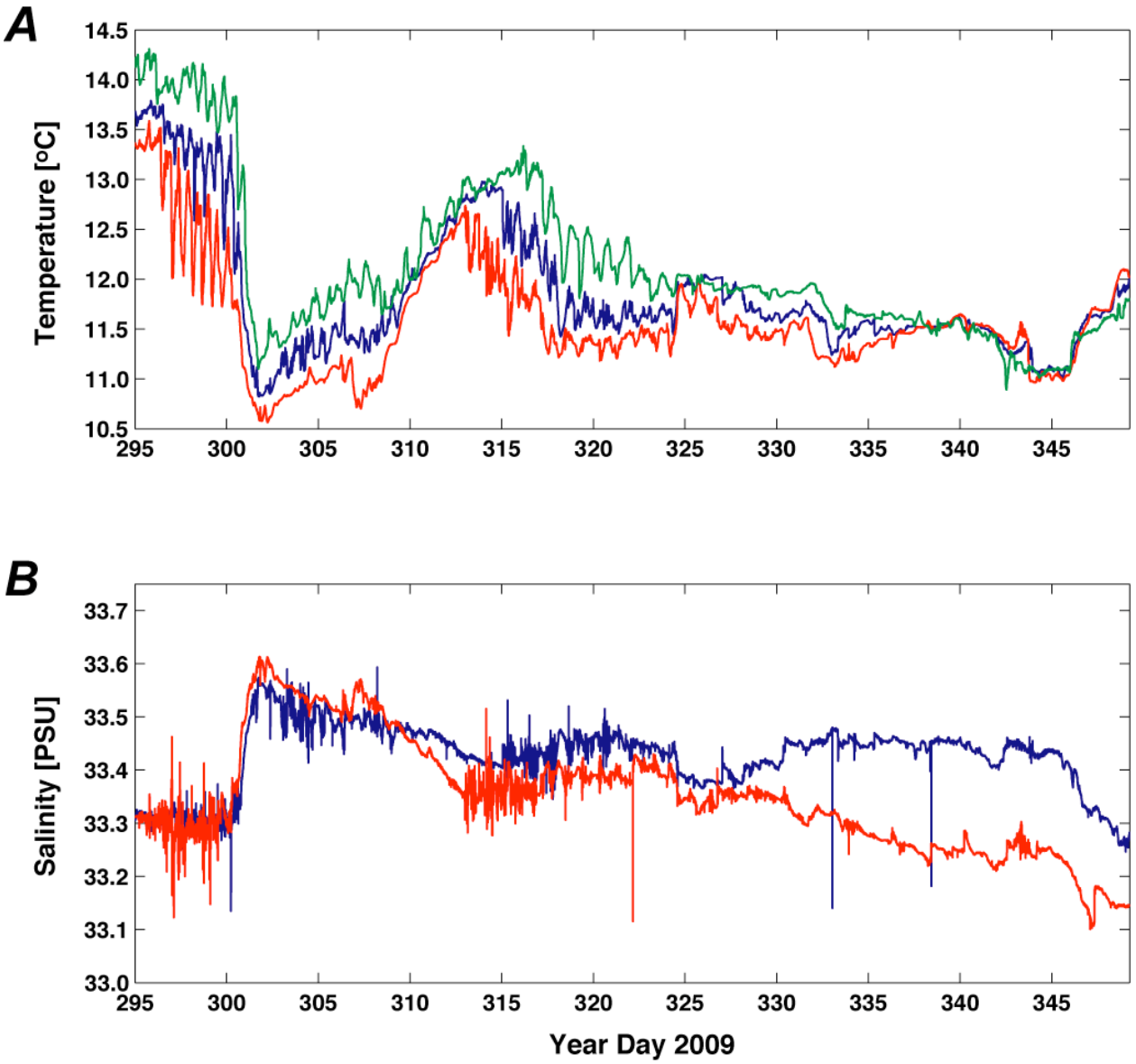

FIGURE 10. Time-series plots of temperature and salinity data during the study period. *A,* Water temperature, in degrees Celsius. *B,* Salinity, in practical salinity units (PSU). Data from Tripod B (12 m depth), Tripod C (20 m depth), and Tripod D (30 m depth) are shown in red, green, and blue, respectively. No salinity data are presented for Tripod B because sediment clogged the doivity cell and resulted in spurious salinity values.

the FE system on the seabed during the demonstration project (fig. 13). The same number of sites experienced a fining of grain size by one grain-size class as experienced a coarsening of grain-size class (two each) during the dredge operations. Following the cessation of dredging, three sites fined by one grain-size class, and four sites coarsened by one grain-size class. The variability in surficial grain size at each seabed site was, in general, greater farther offshore than close to shore (appendix 6).

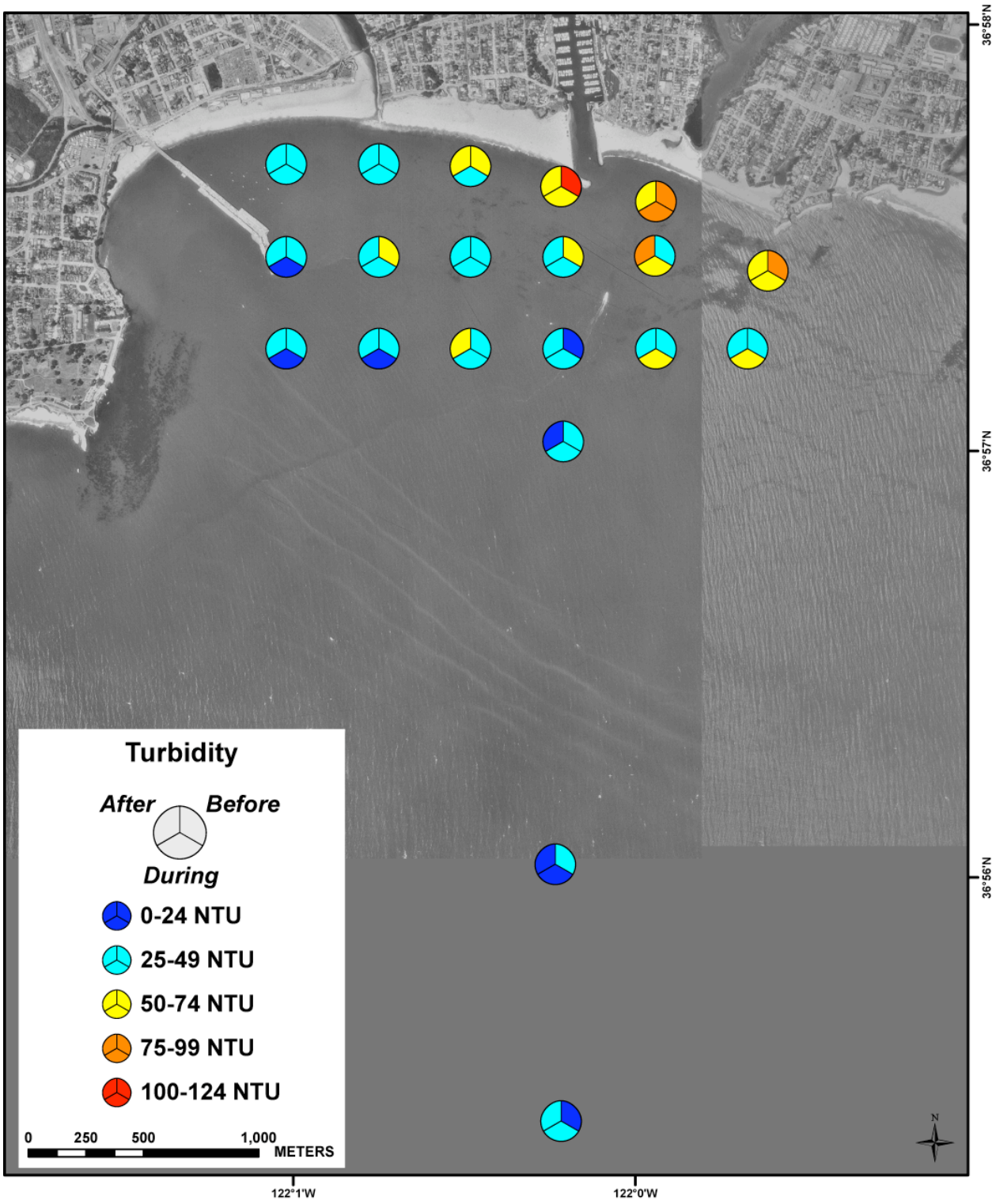

FIGURE 11. Map showing spatial variability in optical backscatter, in National Turbidity Units (NTU), during the surveys. Data from before, during, and after the dredge-disposal operations are shown in the upper right, lower, and upper left sectors of the circles, respectively.

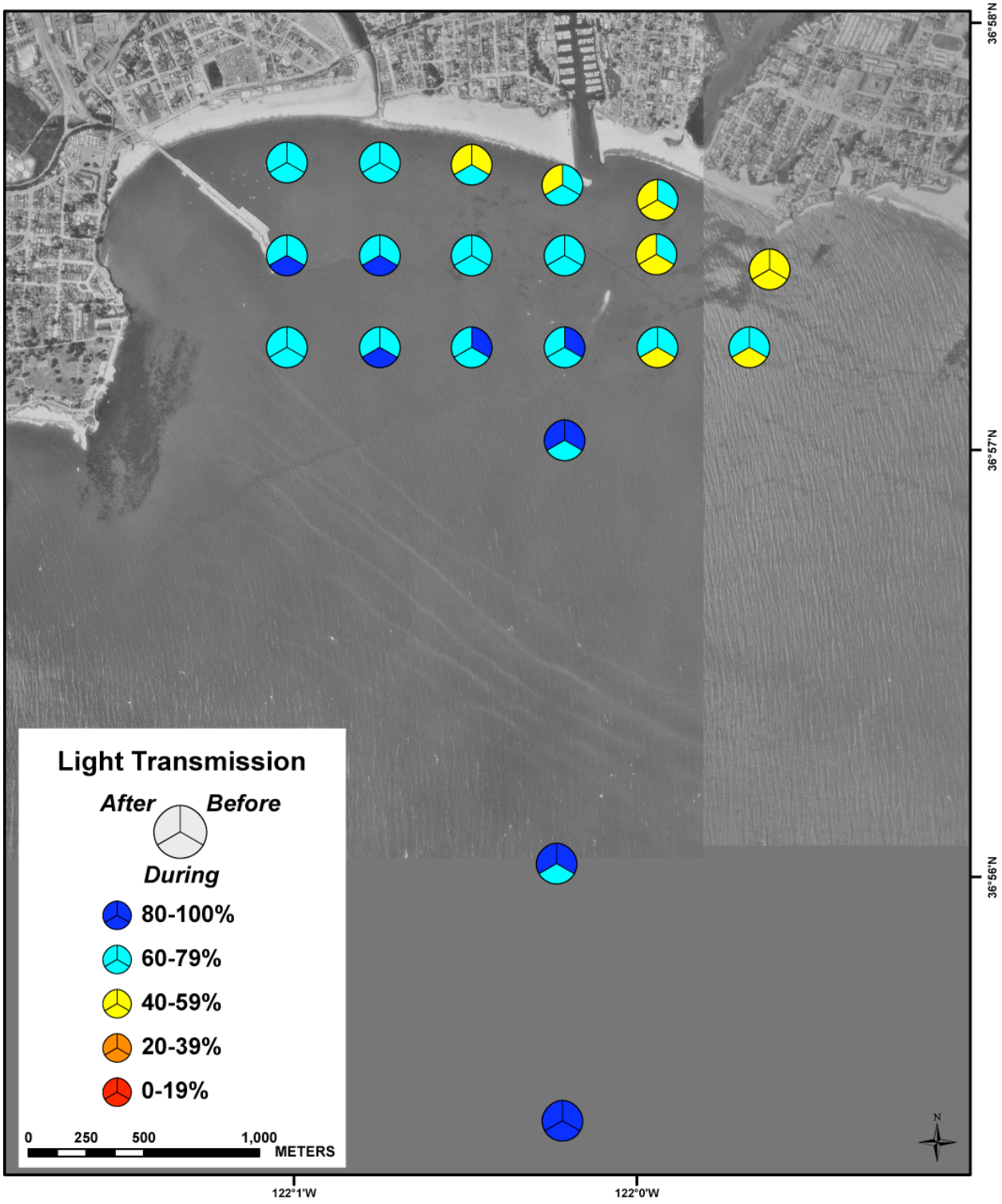

FIGURE 12. Map showing spatial variability in light transmission, in precent, during the surveys. Data from before, during, and after the dredge-disposal operations are shown in the upper right, lower, and upper left sectors of the circles, respectively.

Burial or exhumation of bedrock occurred at 7 sites; two sites became buried and two sites were exhumed during the dredge operations, and two sites were buried and one site was exhumed after the end of the dredging. These burials and exhumations did not occur at sites immediately adjacent to the dredge-disposal sites, and there is no evidence to suggest that they were caused by the dredge-disposal operations. All rocky sites that were buried were covered by medium- to fine-grain sand; none of the sampling sites were characterized by very fine sand or mud before, during, or after the dredge operations.

Trapped Sediment Accumulation and Grain Size

The grain size of the sediment collected in the traps shows a very different distribution than the seabed samples. The seabed at sediment trap mooring sites was predominantly (mean was 82.9 percent) a poorly sorted fine sand (mean size of 0.1758±0.1312 mm) with lesser percentages of silt, clay, and gravel (mean was 12.5 percent, 3.5 percent, and 1.1 percent, respectively; fig.14). The material collected in sediment traps was primarily (mean was 65.1 percent) very poorly sorted medium silt (mean size of 0.0251±0.0018 mm) with lesser percentages of clay and sand (mean was 20.9 percent and 14.0 percent, respectively) with no gravel. This difference in grain size between the seabed and what accumulates in sediment traps is not uncommon; finer-grained, lighter particles can be more easily resuspended and carried higher up into the water column and thus to the height of the trap's opening than coarser particles. Once these fine-grain particles settle into the trap, they cannot be resuspended and advected away as could the same-sized material on the adjacent seabed. Furthermore, as discussed above, the sediment traps collect coarser particle sizes preferentially because of their higher settling velocity. Overall, the trap sediment accumulation rates varied between 0.676 and 0.827 mg/cm^2/day, with a mean accumulation rate of 0.770±0.071 mg/cm^2/day and showed no general cross-shore trend (table 16).

Sediment Geochemistry

Sediment Carbon and Nitrogen Contents and Isotopic Compositions

Carbon and nitrogen isotopic and elemental compositions of sediment (table 17) show statistically significant differences in sediment chemistry between Santa Cruz Harbor material and suspended sediment collected in sediment traps. There were significant differences in percent C (p=0.03, Student's t-test), ^{15}N (p=0.02, Student's t-test), ^{13}C (p=10^{-8}, Student's t-test), and the molar ratio of carbon to nitrogen (p=10^{-5}, Student's t-test). In addition, there were statistically significant differences in the chemistry of suspended sediment collected during dredging and post-dredging periods. The elemental carbon data (percent C) showed a significant difference in the means between the early-, late-, and post-dredging collection periods (p=0.008, ANOVA), with the percent C in the post-dredging collection period being lower than the two dredging collection periods. Similarly, there was a significant difference in the elemental nitrogen (percent N) in suspended sediment during the different collection times (p=0.042, ANOVA), with the percent N being lowest in the post-dredging period. There was, however, no significant difference in the mean molar ratio of carbon to nitrogen (C/N) among the three periods (p=0.39, ANOVA), and no significant difference in suspended-sediment accumulation rate in the traps (p=0.08, ANOVA).

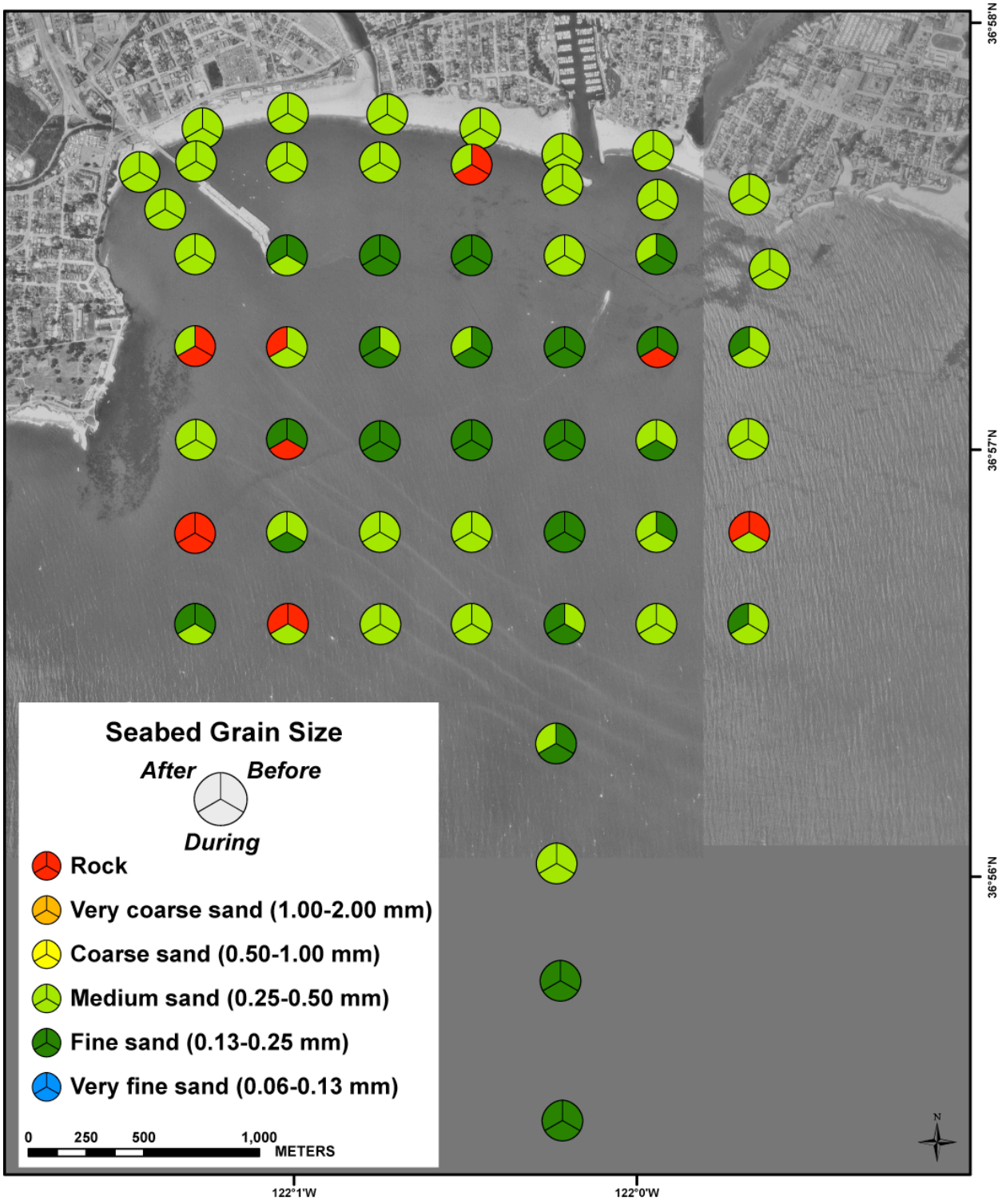

FIGURE 13. Map showing spatial variability in beach and seabed surficial grain size, by grain-size class, during the surveys. Data from before, during, and after the dredge-disposal operations are shown in the upper right, lower, and upper left sectors of the circles, respectively.

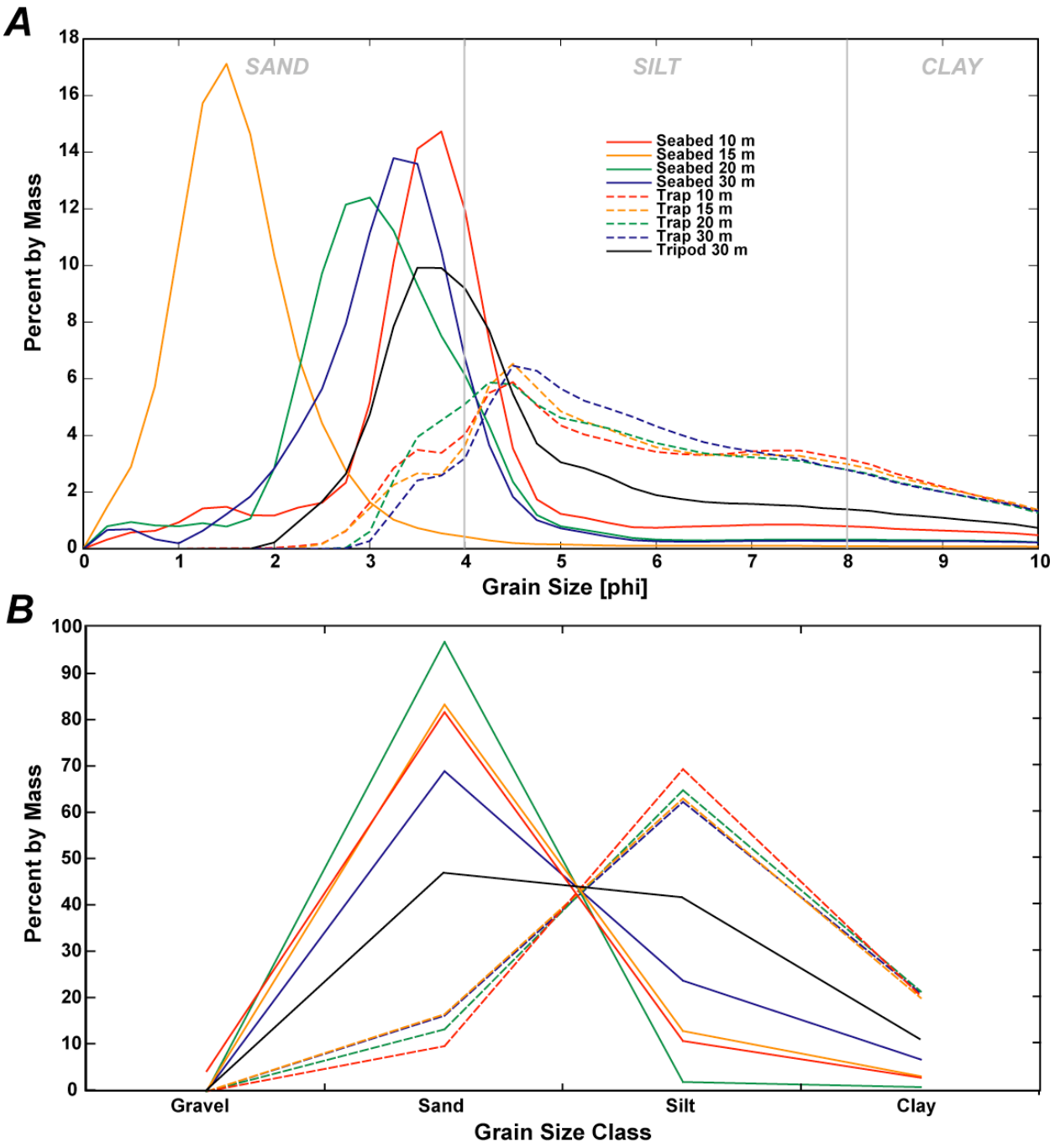

FIGURE 14. Plot showing grain-size distribution of sediment on the seabed and collected in sediment traps. *A,* Distribution, in quarter-phi intervals. *B,* Distribution, by grain-size class. Data from the 10 m, 15 m, 20 m, and 30 m mooring sites are shown in red, orange, green, and blue, respectively. The data from the seabed samples are shown by solid lines, the sediment-trap samples (height above bottom, 5 m) are shown by dashed lines, and the black solid line denotes the data from 2 m above the bottom at the Tripod D (30 m depth) site.

Short-lived Radionuclides

Results for short-lived radioisotope analyses are shown in table 18. In trap-collected suspended sediment, ^{7}Be activity was less than 1.2 dpm/g during dredging activity. In suspended sediment, ^{7}Be activity was relatively higher (0.92–1.88 dpm/g) in post-dredging compared with

activity levels during dredging (0.0–1.14 dpm/g). It is difficult to compare most of the short-lived radioisotopes in sediment-trap material directly with the sediment collected from Santa Cruz Harbor because the harbor sediment was analyzed a substantial length of time (about 250 days) after their collection date [07/15/2009-07/17/2009 (2009 Year Days 196-198)], and there was a substantial amount of time between harbor sediment sampling and dredging. Nevertheless, $^{210}Pb_{xs}$ (half life=22.3 years) was significantly lower in harbor sediment compared to suspended sediment collected in traps (p=0.0001, 0.0002; Student's t-test).

Elemental Concentrations

The sedimentary contents of 35 elements (Ag, Al, As, Ba, Be, Ca, Ce, Co, Cr, Cs, Cu, Fe, Ga, K, La, Li, Mg, Mn, Mo, Na, Nb, Ni, P, Pb, Rb, Sb, Sc, Sr, Th, Ti, Tl, U, V, Y, Zn) for dry weight elemental concentrations in sediment determined by ICP-MS are shown in tables 19-23. With the exception of silver (Ag), which was always below the limit of detection (1 ppm), all elements were above the limits of detection reported by the USGS CR Mineral Resources Team Analytical Chemistry Laboratory. A subset of 16 of these elements (Al, As, Ba, Co, Cr, Cu, Fe, K, Mg, Mn, Mo, Ni, P, Pb, Ti, Zn) was selected for closer examination.

Among the trap-collected sediment, there was a significant positive correlation (p<0.05, linear regression) between the fraction of fine-grain material present (either as a percentage of silt or as a pecerntage of silt+clay) and the concentration of Co, Cr, Fe, and Ni. A single value (1 out of 10) for grain size (Trap-20 m, 2009 Year Day 336–349 collection), which was farthest from the rest, prevented the inclusion of Mg, Mn, and Ti with elements showing a significant correlation. However that single grain-size value was not a significant outlier in the grain-size data for either percent silt or percent mud (p>0.01, Grubb's test). Other elements show a significant positive [As, Cu, Mo, Pb, Zn (and percent C)] or negative (Ba, K) correlation with percentage clay (p<0.05, linear regression). Of the subset of 16 elements reviewed in detail, none show a significant correlation with both percentage clay and percentage silt or percentage mud (silt+clay). When considering all 35 elements analyzed, however, Cs, Li, and V are exceptions to this lack of significant correlation. Looking at the correlation coefficient for these elements, Cs correlates slightly better with percentage clay than percentage silt (R=0.88 vs. 0.77), Li shows little difference (R=0.81 versus 0.83), and V correlates slightly poorer with percentage clay than percentage silt (R=0.64 versus 0.70). Percentage C was significantly and positively correlated (p<0.05, linear regression) to a number of elements in both Santa Cruz Harbor (As, Cu, Fe, Mg, P, Pb, Zn) and trap-collected sediment samples (As, Cu, Mo, P, Pb, Zn). Similarly, percentage C showed a significant negative correlation (p<0.05, linear regression) to Ba in harbor sediment, and to Al and K in trap-collected sediment.

Significant changes in the mean values of percentage C and percentage clay are associated with the different collection periods for the sediment traps. The percentage clay was significantly higher in the late dredging period (Year Days 313–336) compared to early or post-dredging time periods (p<0.05, Students' t-test), with enrichments in mean values of 1.2 and 1.6 times, respectively. In addition there was a significant decrease in percentage C between the late- and post-dredging periods (p<0.05, Students' t-test). The mean percentage C in the trap-collected sediment from the late-dredging period is 1.3 to 1.9 times higher than the percentage C in sediment collected in early- and post-dredging periods, respectively. Similar changes are seen in elements significantly correlated with percentage clay or percentage C (As, Cu, Mo, Pb, Zn). There was no significant change in percentage silt over the collection periods (p>0.05, ANOVA), and elements showing significant correlations with percentage silt (Co, Cr, Fe, Ni) also showed no significant change over the collection periods (p>0.05, ANOVA).

The concentration of Co, Cr, Mg, Mn, Ni, and Ti in trap-collected sediment showed a significant positive correlation (p<0.05, linear regression) with distance from shore as measured

south from the mouth of Santa Cruz Harbor (mooring distances were about 0.4, 1.2, 2.5, and 4 km from shore for the 10, 15, 20, and 30 m traps, respectively). One element, Pb, showed a significant negative correlation with distance. Percentage silt, clay, and C showed no significant correlation with distance offshore ($p>0.05$, linear regression). To account for changes in elemental concentration unrelated to changes in grain size, elements showing a significant correlation to a grain-size fraction (percentage silt or percent clay) were normalized to that fraction. After normalization to percentage silt, Co, Cr, and Ni still showed a significant positive correlation to distance offshore. After normalization to percent clay, Cu and Mo but not Pb showed a significant negative correlation to distance offshore.

The concentrations of 10 elements (Al, Co, Cr, Cu, Fe, Mn, Mo, Pb, Ti, Zn) were significantly higher in Santa Cruz Harbor sediment than in trap-collected sediment ($p<0.05$, Student's t-test), and the concentrations of one element (K) was significantly lower. Elements showing the greatest average concentration enrichment in harbor sediment compared to trap-collected sediment were Cu and Zn, at 4.3 and 2.3 times, respectively. When using percentage C corrected data for elements that show a significant linear correlation with percentage C (harbor and mooring considered separately), two elements (Cu, Zn) were significantly higher in Santa Cruz Harbor sediment than in trap-collected sediment samples ($p<0.05$, Student's *t*-test). Cu was 2.5 times and Zn was 1.3 times in Santa Cruz Harbor sediment than in trap-collected sediment samples, and two elements significantly lower (As, P), with As was 1.3 times and P was 2.1 times higher in the sediment traps. Normalizing to percentage clay would be ideal for this enrichment calculation, but percentage clay data were not generated by the USGS for harbor sediment. Nevertheless, percentage C is a reasonable proxy for percentage clay in systems where percentage C represents fine, organic material, which is likely the case in Santa Cruz Harbor.

Numerical Wave, Circulation, and Sediment Transport Modeling

Circulation Model Boundary Forcing

Open boundary conditions for the Santa Cruz model (SC01) were obtained from a larger FLOW model of Monterey Bay (MBY). This model, in turn, was nested in a FLOW model of Central California (CCA). Figure 15 shows the three FLOW model grids applied in this study. The models included the effects of:(1) spatially and time-varying wind and atmospheric pressure, (2) salinity and temperature stratification, (3) heat exchange with the atmosphere through solar radiation and evaporation, and (4) Coriolis forcing.

The CCA and MBY models both contained 44 vertical (z) layers, ranging in thickness from 1 m at the surface to several hundreds of meters near the ocean floor. The horizontal grid spacing of the CCA model ranged from ~5000 m along the offshore boundary to ~1500 m inside Monterey Bay. The grid-cell sizes in the MBY model ranged from ~2000 m offshore to 500 m along the boundaries of the SC01 model. Bathymetry data for the MBY and CCA models were obtained from the National Geophysical Data Center's Coastal Relief Model (2010).

The CCA and MBY models were forced along their open boundaries by weakly reflective Riemann conditions (Verboom and Slob, 1984). The Riemann invariant time series $f(t)$ for each z-layer is given by:

$$f(t) = U \pm \zeta \sqrt{\frac{g}{d}},$$

where U is the normal velocity per layer, ζ is the water level, g is the gravitational constant, and d is the local water depth.

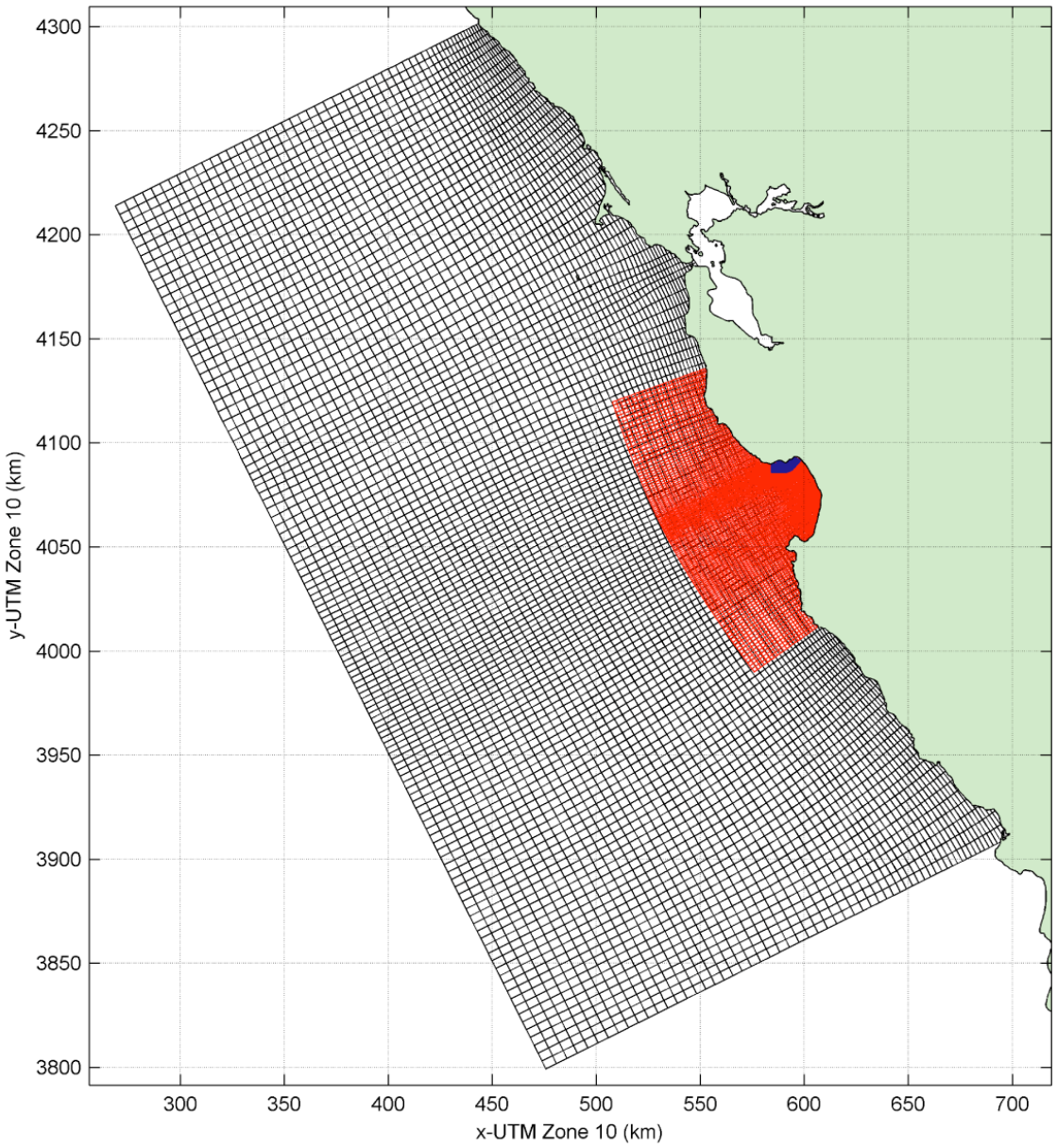

FIGURE 15. Map showing the FLOW model computational grids CCA (black), MBY (red), and SC01 (green).

Open boundary forcing data for the CCA model was obtained from a combination of the TOPEX/POSEIDON global tide data (Egbert and Erofeeva, 2002) and the global HYCOM flow model output (Halliwell, 1998) that does not include tides. The normal velocity (U) was taken as the sum of the baroclinic currents from the HYCOM model and the tidal currents obtained from the TOPEX/POSEIDON model. The water level, ζ, was computed as the sum of the sea surface height from the HYCOM model and tide levels from the TOPEX/POSEIDON model. Salinity and temperature boundary conditions for the CCA model also were taken from the HYCOM model. Furthermore, both the CCA and MBY models were initialized with currents, salinity and temperatures from the HYCOM model (fig. 16). Spatially and time-varying wind and

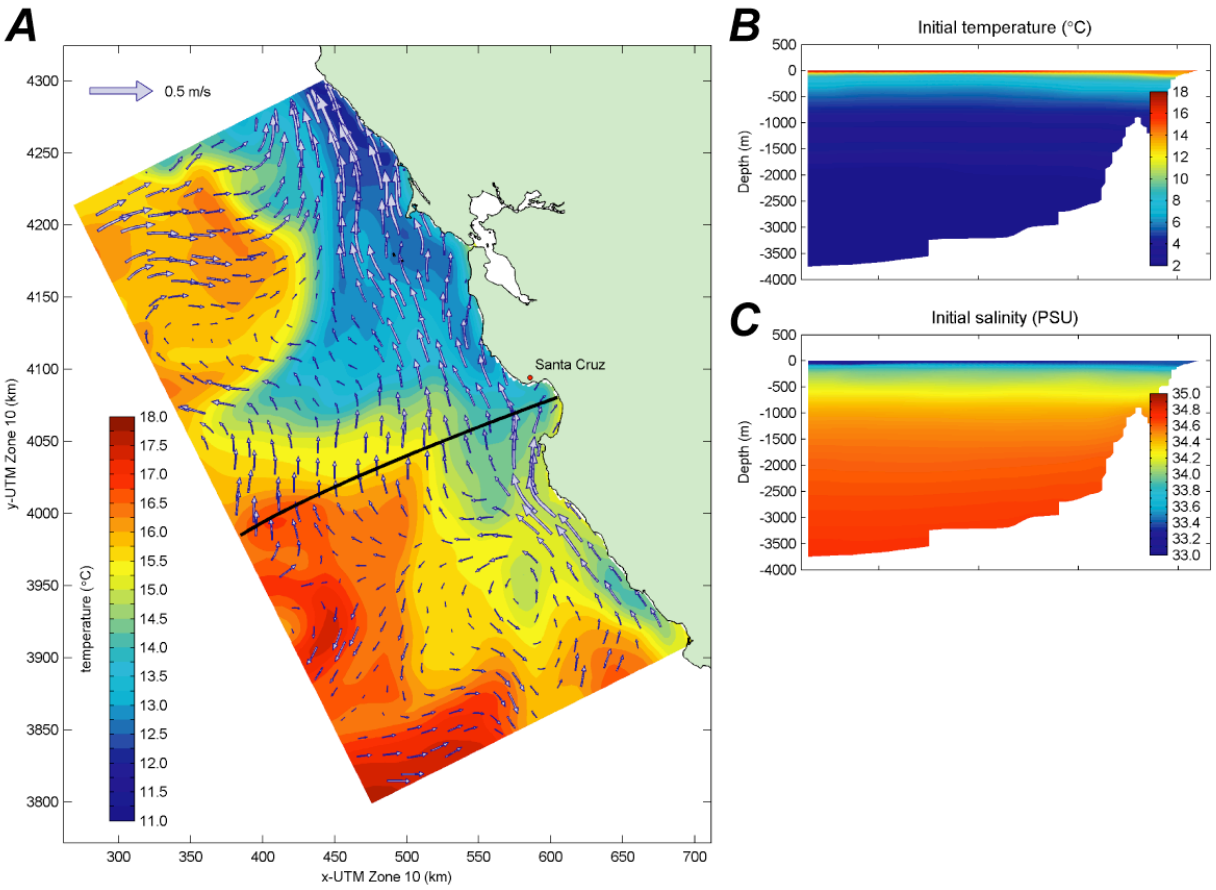

FIGURE 16. Map and cross-sections showing the Initial conditions in the CCA FLOW model. *A,* Surface temperature, in degrees Celsius, and surfacecurrent speeds and directions, in meters per second from degrees true north. *B,* Cross-section of temperature, in degrees Celsius. *C,* Cross-section of salinity, in practical salinity units (PSU). The location of the cross-section is shown as a black line in *A*.

atmospheric pressure fields applied in the CCA, MBY, and SC01 models were obtained from the NCEP-NAM model (Gemmill and Peters, 1997).

The results of the MBY model were assessed by comparing them against in place observations at five sites (fig. 17). The focus of this comparison was for surface currents and surface temperatures during the 2-month period of the dredge experiment. Observed current speeds at these locations were obtained from HF radar data (Paduan and Cook, 1997). It must be noted that the accuracy of the HF radar data, especially for the distant locations 46042 and 46239, is poor. The MBY model was able to reproduce the diurnal wind-driven fluctuations reasonably well at all five sites (appendix 7). The residual currents in both the MBY model and the observations compared well for the nearshore sites (in particular MBM1, and to a lesser extent MBM0 and Tripod D at 30 m), but generally were poorer at the more distant NDBC buoys 46042 and 46239. It is interesting to note that, whereas the modeled meridional (north-south) residual currents at Tripod D along the 30 m isobath closely resembled the observations, the zonal (east-west) currents in the model did not match the observations at all.

The MBY model was capable of hindcasting the temperature fluctuations during the 2 month period (appendix 7). In particular, the sudden decrease in temperatures around October 30, 2009 (2009 Year Day 303), was reproduced well. This strong upwelling event appeared to be

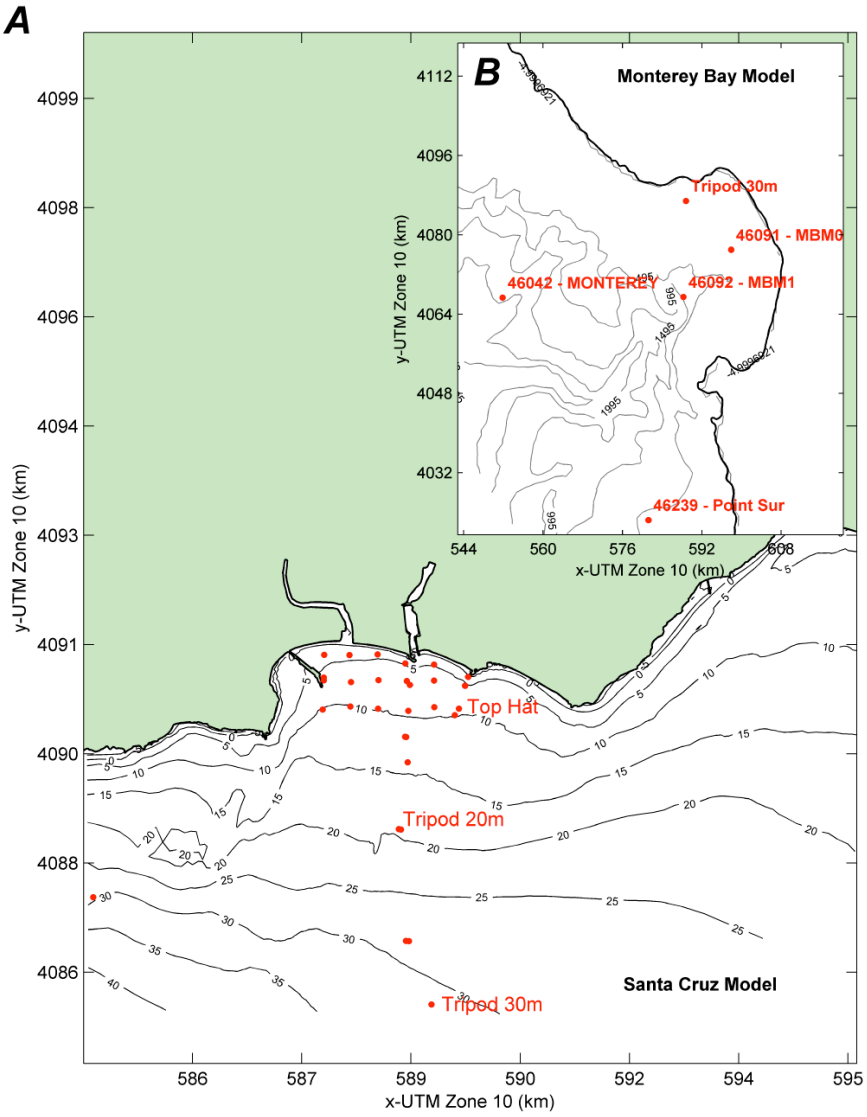

FIGURE 17. Map showing the observation points in the MBY FLOW model used for validation and calibration.

related to the peak in winds out of the north that drove strong southward-directed surface currents.

A number of experiments (not presented here) with the CCA and MBY models revealed the sensitivity of the model output to wind forcing, indicating the need for accurate wind input in the model. A comparison between the model wind input obtained from the NCEP-NAM model and local observation was therefore carried out to assess the quality of the wind product that was used (appendix 7). At the most offshore site (NDBC buoy 46042), the wind predictions closely matched the observations. However, closer to the shore, the model predictions appeared to deteriorate (see stations MBM0 and MBM1). It appears that the NCEP-NAM model significantly under-predicted the diurnal sea-breeze, as well as the wind speeds during some of the high-velocity wind events.

Wave Model Boundary Forcing

Wave effects, such as enhanced bed shear stresses and wave current forcing due to breaking, are integrated in the flow simulation by running the WAVE model on a grid (WAV1) surrounding Monterey Bay (fig. 18). The bathymetry for the wave grid was provided by the USGS based on the NGDC Coastal Relief Model (2010). Time-varying boundary conditions for the wave model for the period of study were derived from the NDBC buoy 46042 (2010) situated at the western edge of the WAV1 grid. The significant wave height (m), peak period of the energy spectrum (s), mean wave direction (degrees), directional standard deviation (-), wind speed (m/s), and wind direction (degrees) were prescribed.

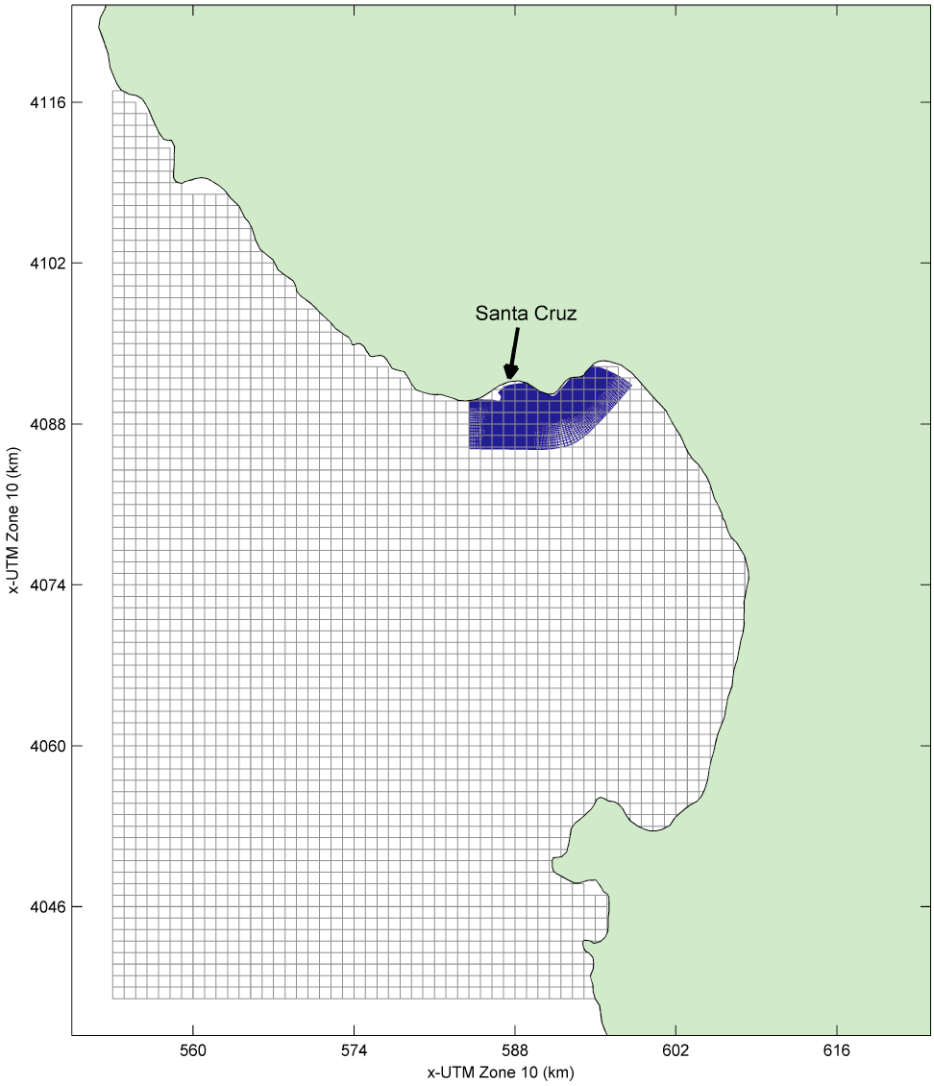

FIGURE 18. Map showing the WAVE model computational grids WAV1 (black) and SC01 (blue).

Fine-Scale Hydrodynamics and Sediment Transport

The results of the WAV1 simulations, such as wave height, peak spectral period, and mass fluxes, were stored on the computational SC01 grid and included in the flow calculations through additional driving terms near surface and bed, enhanced bed shear stress, mass flux, and

increased turbulence (Walstra and others, 2000). In this study, wave effects, flow, and the resulting sediment-transport patterns were computed on the detailed SC01 grid off Santa Cruz Harbor. The curvilinear (land-boundary fitting) SC01 model grid consisted of 10 layers in the vertical. The maximum horizontal grid spacing at the outer edge of the domain was approximately 300 m, becoming progressively finer towards the area of interest to a minimum grid spacing of 16 m (fig. 19). The San Lorenzo River water discharge for the simulated period also was included in this model.

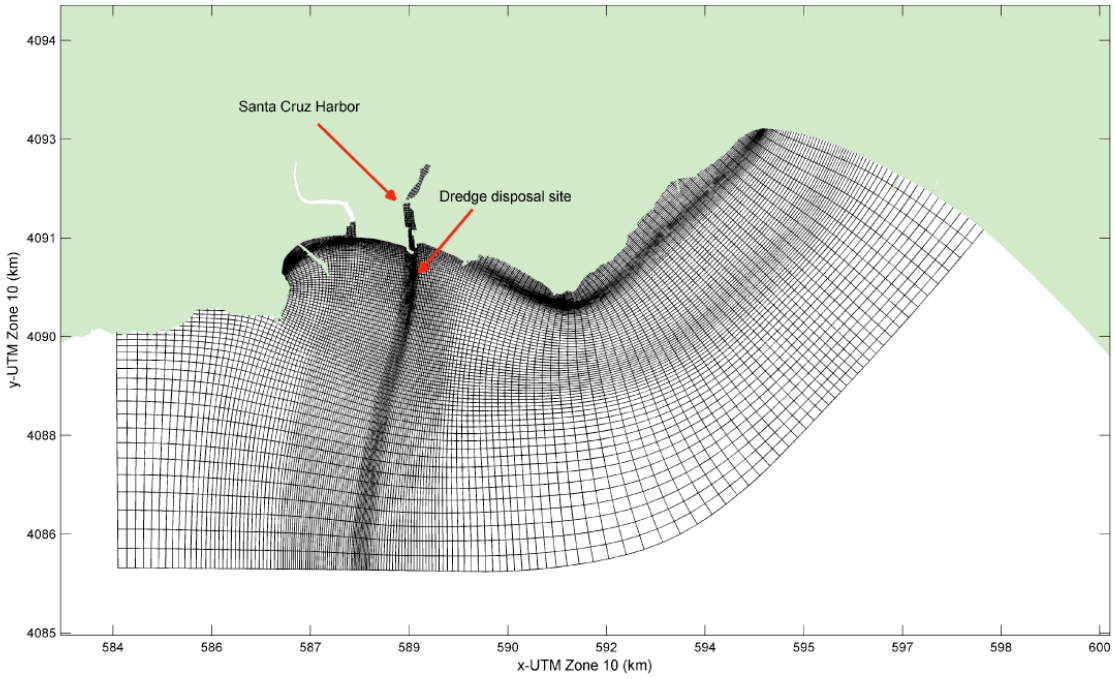

FIGURE 19. Map showing the details of FLOW and WAVE models' computational grid SC01.

Simulated water levels in the SC01 model compared well with predicted water levels (appendix 7). The WAVE model performed well in the SC01 domain, with root-mean squared errors between the model and the observations averaging 0.31 m in this bathymetrically-complex and, thus, refractive environment (appendix 7); the locations where large waves break along the bedrock reefs off Point Santa Cruz and Soquel Point were well-reproduced, as were the quiescent locations of Cowell's Beach and the Santa Cruz Municipal Wharf (fig. 20). Modeled surface- and bottom-current speeds were compared with observation data from the ADCMs at three locations within the SC01 domain. Results at Tripod D along the 30 m isobath showed that the near-bed current velocities, the important forcing for sediment transport, were reproduced well, with root-mean squared errors between the model and the observations averaging 0.062 m/s; the errors between the near-surface measured and modeled current velocities was slightly greater, averaging 0.083 m/s (appendix 7). Note the significant shear in the water column (fig. 21-22), with the near-surface currents often heading at different speeds and in different directions than the near-bed currents, similar to that observed at the tripod locations (fig. 9). During large wave conditions (fig. 22), wave shoaling and breaking generated strong eastward-directed currents

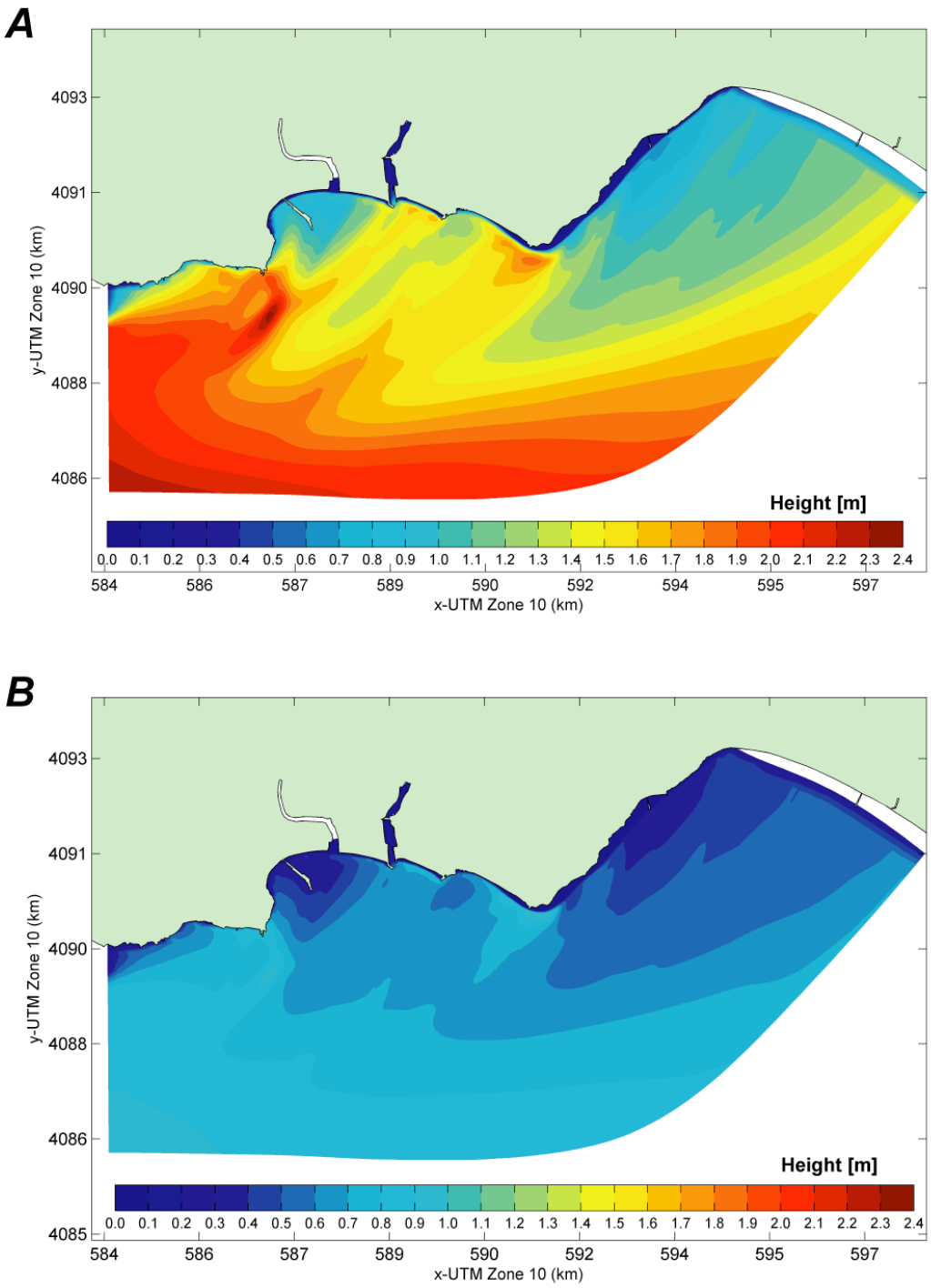

FIGURE 20. Map of modeled wave heights, in meters, in the study area. *A*, During large (deep-water height is 4.3 m at 15.2 s from 302°) wave conditions. *B*, During small (deep-water height is 1.2 m at 12.7 s from 270°) wave conditions. Note how the locations where large waves break along the bedrock reefs off Point Santa Cruz and Soquel Point were well-reproduced, as were the quiescent locations of Cowell's Beach and the Wharf (fig. 1).

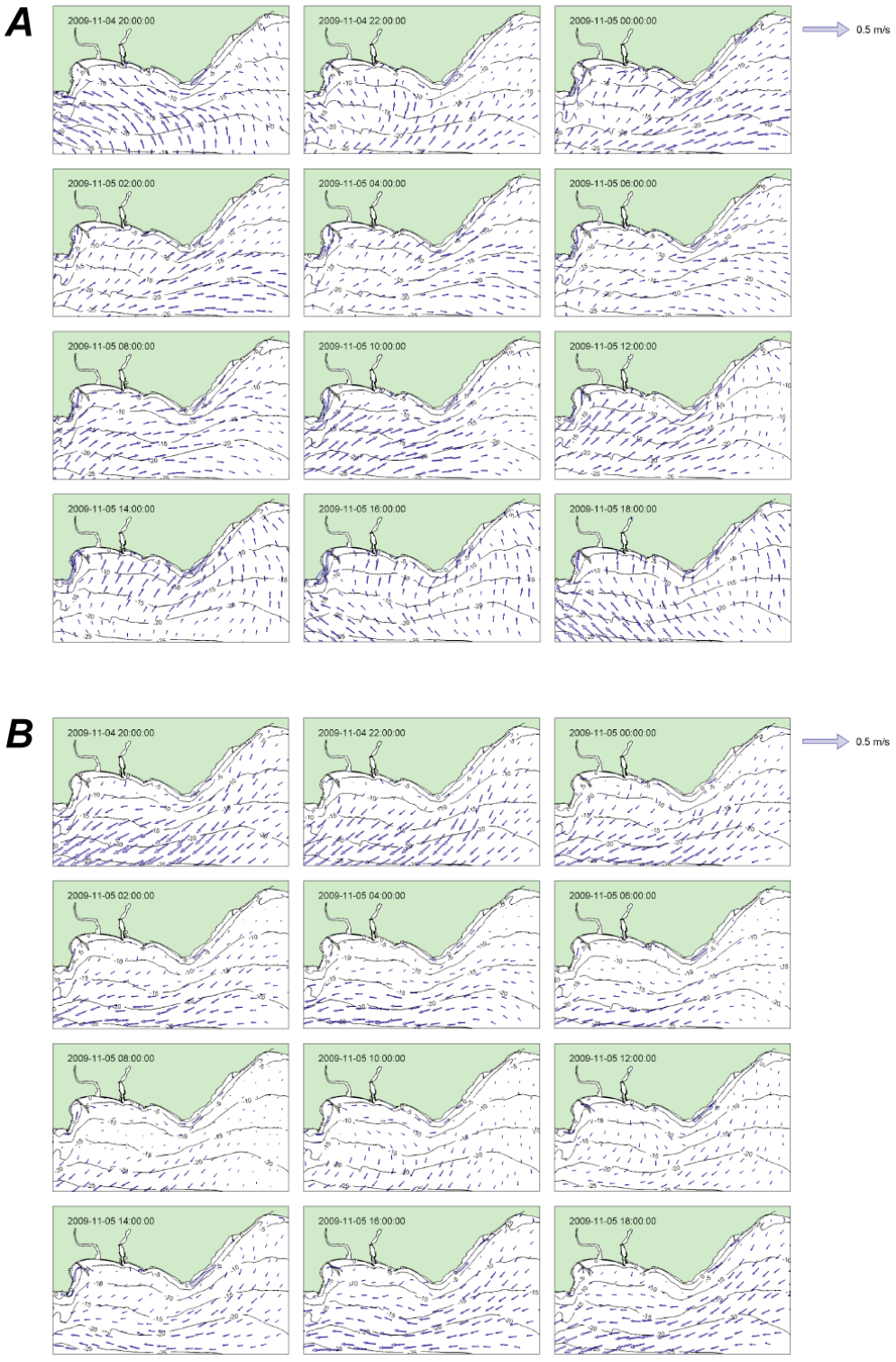

FIGURE 21. Map of modeled current speeds and directions, in meters per second from degrees true north, over a 24-hour tidal cycle during small wave conditions (fig. 20*A*). *A*, Near-surface currents. *B*, Near-bed currents.

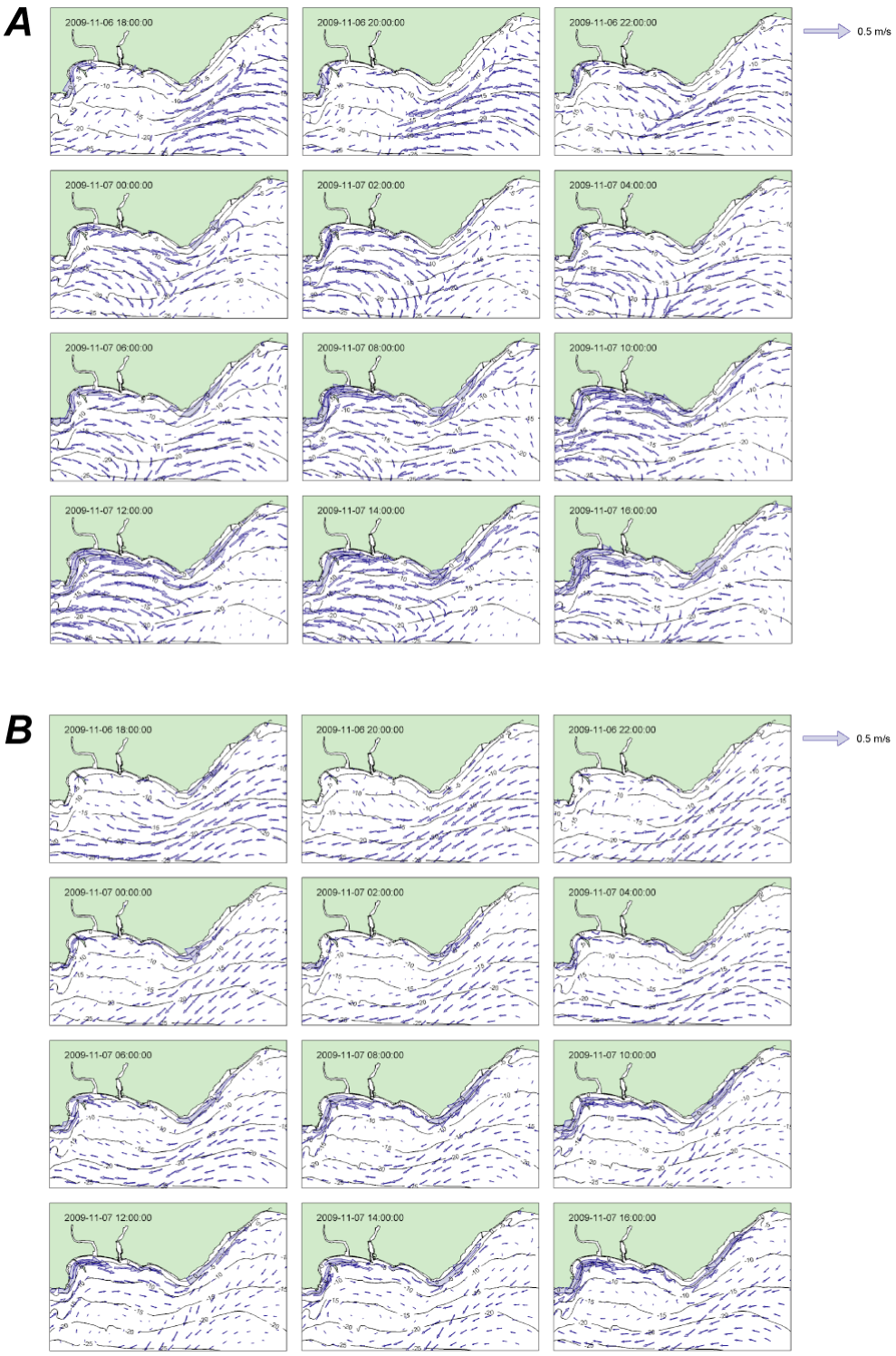

FIGURE 22. Map of modeled current speeds and directions, in meters per second from degrees true north, over a 24-hour tidal cycle during large wave conditions (fig. 20*B*). *A*, Near-surface currents. *B*, Near-bed currents.

close to shore that are virtually nonexistent during lower wave-energy conditions (fig. 21); the strong eastward-directed alongshore current dissipated near Capitola due to wave energy divergence (fig. 20a).

A single cohesive sediment fraction was included to represent the dredge-disposal outfall. The disposal of the dredge material was simulated as a discharge of fine sediment at the location of the end of the dredge discharge pipe in the model domain. The dredge start and stop times were adjusted to represent the 60.9 hours of pumping that took place. The dispersal of sediment in the water column from the dredge plume was compared with measurements of suspended sediment from the WCP casts. Several time-series plots of bottom and surface concentrations were made, but the temporally-limited measurements made it difficult to come to any concrete conclusions about the behavior of the model.

The movement of the simulated plume also was compared with a higher resolution time-series of OBS measurements at three tripod locations. Those measurements also contained background concentrations of the coarser seabed-sediment fractions, not included in the model, and the large peaks coincided with large wave events that resuspended large volumes of seabed sediment not related to the dredge plume, even after 2009 Year Day 324 when the dredging had been completed. A settling velocity of 0.0005 m/s was required to simulate the distribution of fine sediment in the water column correctly. A number of sensitivity tests (not shown) indicated that with a smaller setting velocity, the dredge plume peaks in suspended-sediment concentration were overestimated.

The importance of the outer boundary forcing conditions, such as waves, for the simulation of the sediment plume can be seen in figure 23. During low wave-energy conditions (deep-water height=1.2 m at 12.7 s from 270°), the plume was advected offshore to the southwest by subtidal flows. During larger wave-energy conditions (deep-water height=4.3 m at 15.2 s from 302°), however, the plume bifurcated, with some of the plume heading offshore to the southwest as during lower wave-energy conditions and some entrained in the strong eastward-directed alongshore flow and transported to the east, similar to the modeling done by Sea Engineering, Inc. (2006). As wave energy decreased off Capitola (fig. 20a), the strong eastward-directed alongshore currents weakened (fig. 22), and the suspended sediment became entrained in the southwestward-directed subtidal flow, and was driven to the southwest, where it dissipated. Initially, these waves and flow patterns resulted an initial deposit on the order of 3.5 cm thick just offshore of the end of the discharge pipe that was eroded within 3 days. The sediment was advected eastward and resulted in a thin (thickness~0.1 cm) modeled deposit of fine-grain sediment on the seabed offshore of Capitola for approximately 20 days (fig. 24); this thin deposit subsequently was eroded again and advected offshore to the southwest out of the study area in the direction of the mid-shelf mud belt by the beginning of December. Due to the small errors in modeled wave and current patterns, and relatively low suspended-sediment concentrations, the thin, temporary accumulation patterns produced by the model off Capitola are well within the error of the model and may not be real. The modeled sediment-accumulation patterns are a mix of the transport patterns for low wave-energy conditions (fig. 21) at the beginning of the study and transition into higher wave-energy conditions (fig. 22) towards the end of the dredge-disposal experiment.

The model also was run in two simulations to evaluate the potential sedimentation that could occur if fine-grain sediment was discharged at two times (650 m^3/day; fig. 25) and four times (925 m^3/day; fig. 26) the rate of the 2009 dredge disposal project (450 m^3/day of 71 percent fine-grain sediment~325 m^3/day of fine sediment). Both simulations show similar patterns to the predicted transport and deposition during the 2009 dredge-disposal experiment (fig. 24), with initial thick deposition just offshore of the end of the dredge discharge pipe (~35 cm and ~80 cm for the 650 m^3/day and 925 m^3/day daily dredge volumes, respectively). These initial deposits off

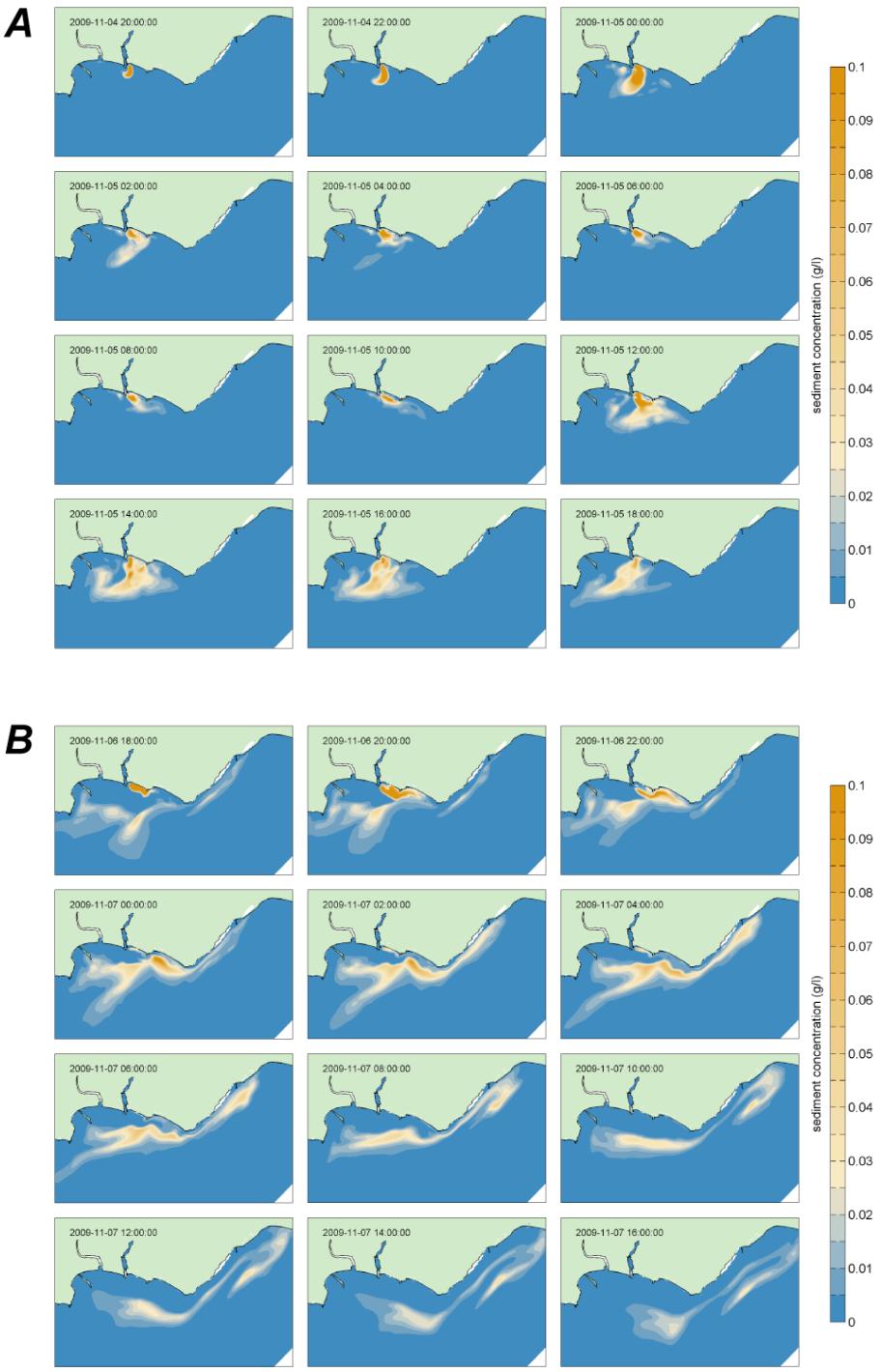

FIGURE 23. Map of modeled suspended-sediment concentrations, in grams per liter, over a 24-hour tidal cycle. *A*, During small large wave conditions (fig. 20*A*). *B*, During large wave conditions (fig. 20*B*).

the end of the dredge discharge pipe persisted for longer (~20-25 days) than were modeled for the 2009 experiment when 325 m^3/day of fine sediment were dredged. Similar to the 2009 experiment, these initial deposits off the dredge discharge pipe were eroded, advected eastward, and formed a thin (thickness~1-2 cm) temporary deposition deposit off Capitola for approximately 30 days, then were subsequently eroded and advected offshore to the southwest

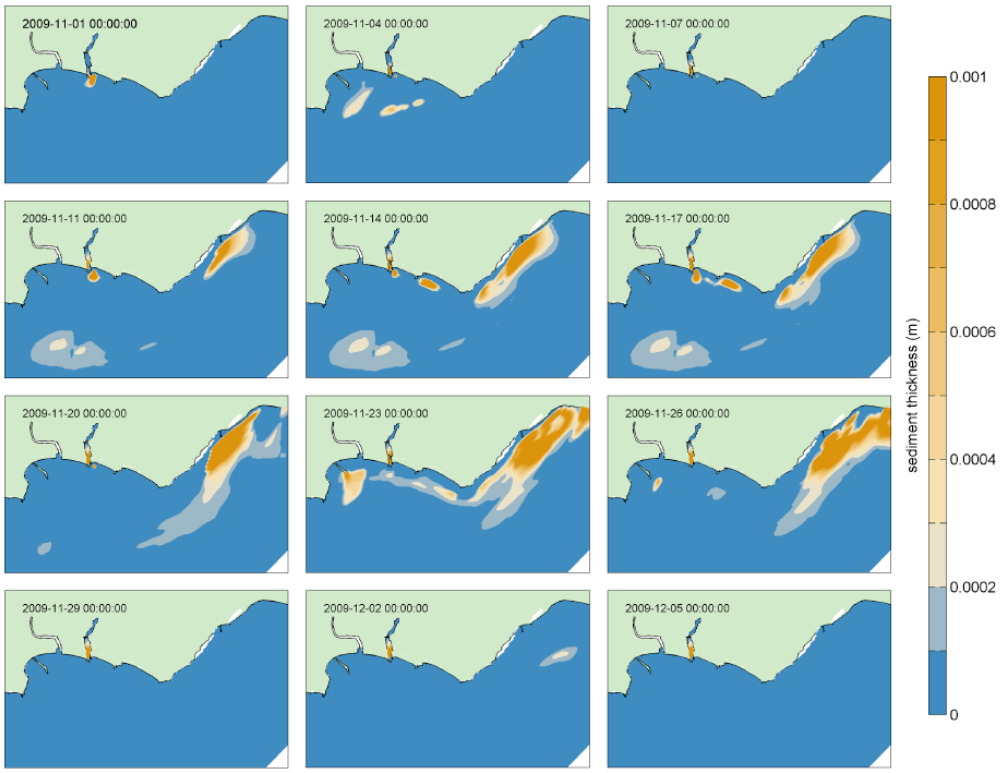

FIGURE 24. Map of modeled sediment accumulation, in millimeters, in the study area during the dredge-disposal project. The resulting sediment accumulation is thin (thickness is approximately 0.1 cm) and temporary in nature (residence time on the seabed is on the order of 20 days).

out of the study area in the direction of the mid-shelf mud belt by the beginning of December. While the sediment accumulation patterns produced by the model for these higher discharge rates are greater than the patterns for the 2009 dredge-disposal experiment, due to the small errors in modeled wave and current patterns, and relatively low suspended-sediment concentrations, the projected sediment accumulations off Capitola may not be real.

Lastly, the model suggests that during both low and high wave-energy conditions as were observed during the study, combined wave and current shear stresses were sufficient to inhibit the substantial deposition of mud throughout the model domain (fig. 27). Note how under large wave conditions, the regions where shear stress are low enough to allow for the deposition of mud (critical shear stress for mud ~0.14 N/m^2) are so far offshore that they are not in the SC01 model domain shown.

Discussion

Distribution of Forcing Conditions

The surveys and instrument deployments in northern Monterey Bay described here took place during the months of October-December, at the transition from summer conditions through the beginning of winter (fig. 4). During the experiment four periods were observed and quantified: late summer conditions before the dredge-disposal experiment (2009 YD 295-301), during the dredging (2009 YD 302-324), fall conditions following the dredge-disposal

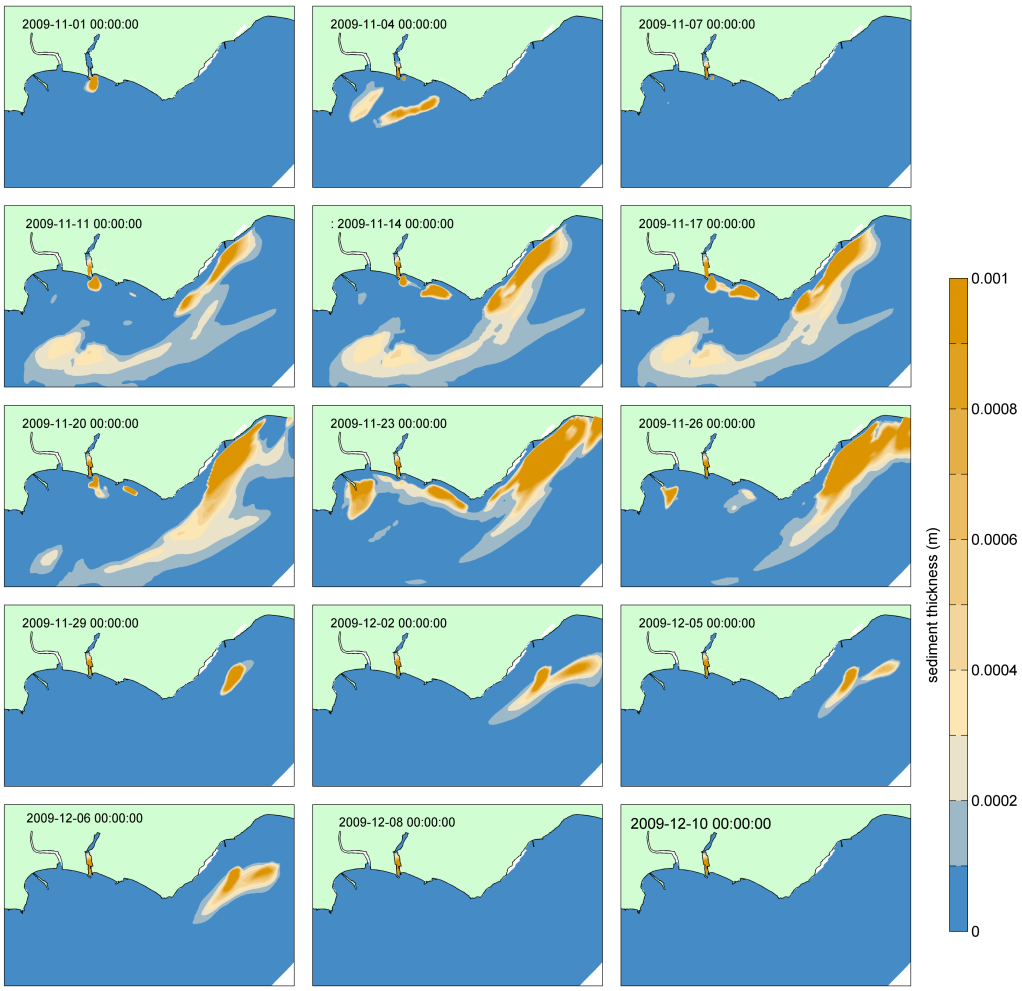

FIGURE 25. Map of modeled sediment accumulation, in millimeters, in the study area at two times the daily rate of fine-grain sediment discharge (650 m^3/day) of the 2009 dredge-disposal project. The resulting sediment accumulation is thin (thickness is approximately 1.0 cm) and temporary in nature (residence time on the seabed is on the order of 30 days).

experiment (2009 YD 325-339), and the first large winter storm and flood after the end of the experiment (2009 YD 340-349).

Spatial and Temporal Variability in Circulation Patterns and Water-Column Properties

The circulation patterns are described below for each of the sets of oceanographic conditions and their implications for the transport of sediment in northern Monterey Bay.

Before Dredging

The period preceeding the harbor dredge-disposal experiment (2009 YD 295-301) was characterized by consistent strong daily winds out of the northwest (fig. 4c) and deep-water waves out of the northwest (fig. 4d). These strong northwest winds and northwest waves, which are reduced significantly in the northern part of Monterey Bay due to refraction, resulted in little mixing and strong stratification in the water column. This stratification is evident in the large

daily swings in temperature (fig. 10a) that are indicative of internal tidal bores and high cross-shore and vertical temperature variability, declining water temperatures, and increasing salinity values that generally result from strong upwelling (Storlazzi and others, 2003). The strong winds and stratification resulted in relatively high current speeds, and thus, relatively high current shear stresses (fig. 28a). These stresses were sufficient to keep coarse silt and even fine sand in motion, preventing mud deposition in the study area except at the protected Tripod A location.

The period before dredging followed the San Lorenzo River's first significant flood (discharge=48.7 m^3/s) of the season on 2009 YD 286; river discharge was approaching base flow levels (order~0.5 m^3/s) by the start of the study on 2009 YD 290 (fig. 4f). Elevated turbidity levels at all of the tripods generally coincided with the larger-than-normal wave heights during 2009 YD 296-299 (figs. 5-8). The comparisons between combined (wave+current) shear stresses and the resulting suspended-sediment fluxes near the bed (fig. 29), however, suggest that some of the elevated suspended-sediment fluxes near the seabed were due to the advection of material (high suspended-sediment concentrations at low shear stresses), and not only the resuspension of

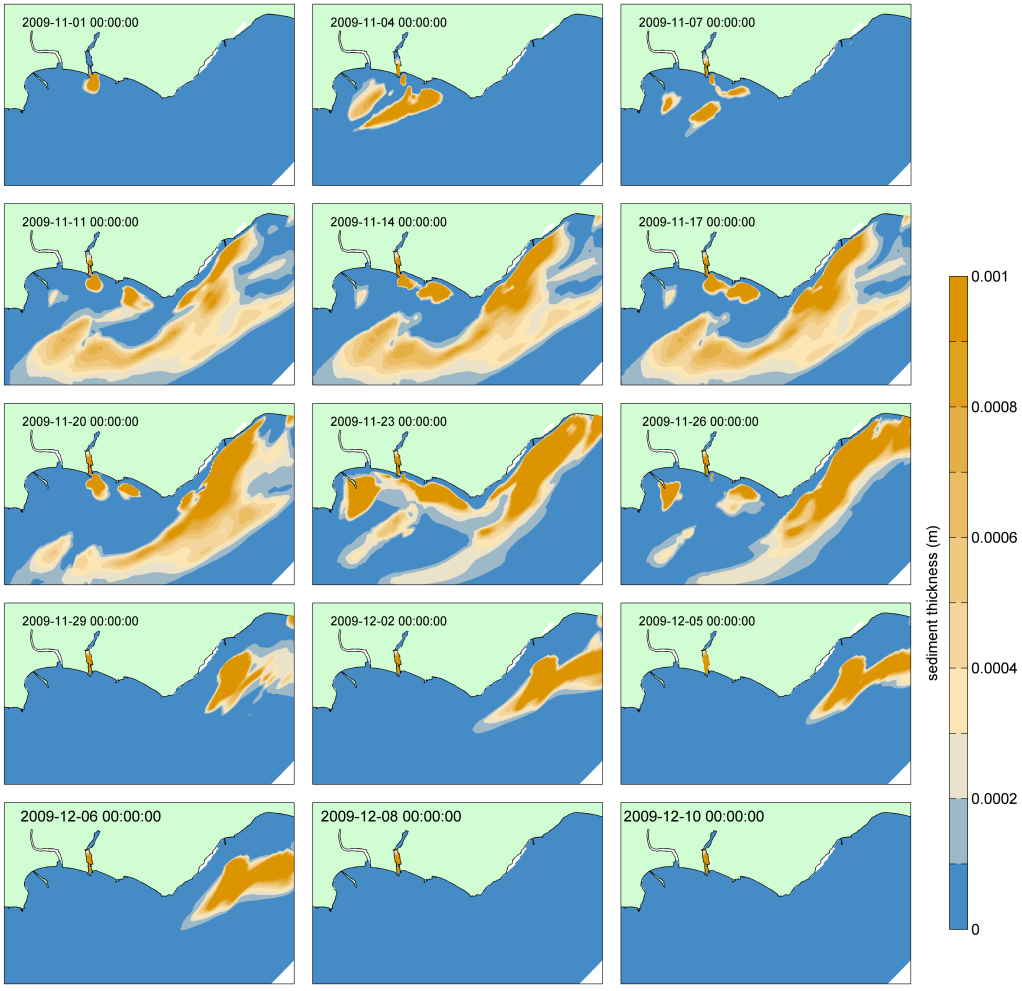

FIGURE 26. Map of modeled sediment accumulation, in millimeters, in the study area at four times the daily rate of fine-grain sediment discharge (925 m^3/day) of the 2009 dredge-disposal project. The resulting sediment accumulation is thin (thickness is approximately 2.0 cm) and temporary in nature (residence time on the seabed is on the order of 30 days).

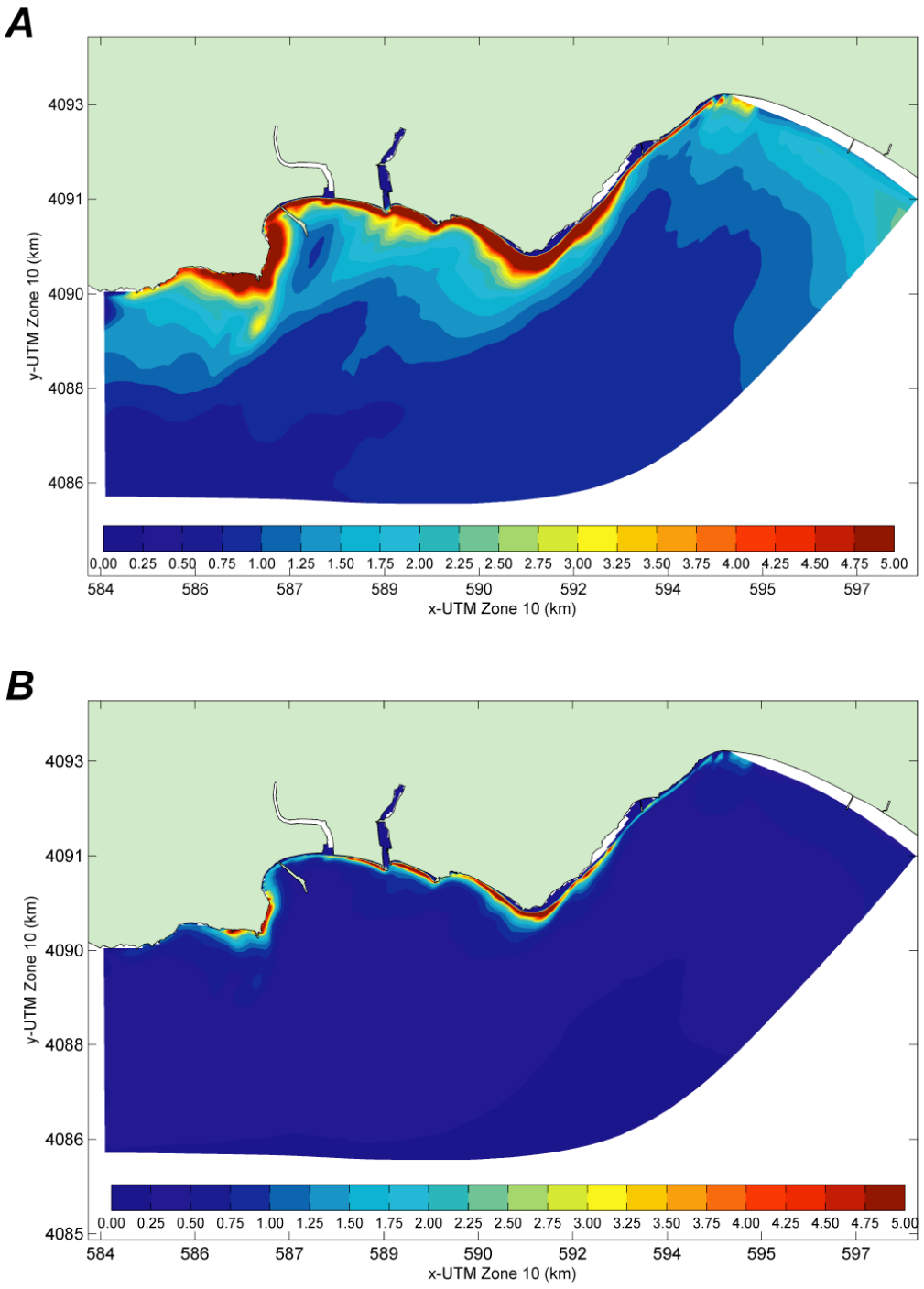

FIGURE 27. Map of modeled combined maximum bed shear stress, in Newtons per square meter, in the study area. *A*, During large (deep-water height is 4.3 m at 15.2 s from 302°) wave conditions. *B*, During small (deep-water height is 1.2 m at 12.7 s from 270°) wave conditions.

material on the seabed (higher suspended-sediment concentrations at higher shear stresses). These higher suspended-sediment concentrations at low shear stresses possibly are due to the advection of sediment from the 2009 YD 286 flood over the seabed near the tripods. Although the beach and seabed sampling were not done during the larger-than normal wave event during 2009 YD 296-299, the beach and seabed surveys surrounding this event display a primarily medium- to fine-grain beach and seabed (fig. 13), suggesting that if any fine-grain flood sediment settled out, it was resuspended rapidly by the combined shear stresses and advected out of the study area. The data from the water-column surveys show a clear water column, except off Twin Lakes Beach and Black Point (figs. 11-12).

During Dredging

The period during the harbor dredge-disposal experiment (2009 YD 302-324) generally was characterized by weaker daily winds out of the northwest than those observed before the start of dredging (fig. 4c) and deep-water waves out of the northwest (fig. 4d). This general trend was punctuated by a period of waves out of the southwest and southerly winds (2009 YD 307-310) followed by larger-than-normal waves with long periods out of the northwest (2009 YD 310-314). Due to the breakdown in northwest wind forcing between 2009 YD 307-310, the water column became mixed and warmed as upwelling shut down (fig. 10a). The weaker, less consistent winds and stratification resulted in lower current speeds, and thus current shear stresses were weaker than observed before the start of dredge-disposal operations (fig. 28a). The current shear stresses were high enough to keep coarse silt in motion intermittently except at Tripod A off the wharf, where the current shear stresses were not sufficient to keep coarse silt in motion. The combined (wave+current) shear stresses were sufficient to inhibit the deposition of coarse silt and even to keep fine sand often in motion, except at the location of Tripod A. Elevated turbidity levels at all of the tripods generally coincided with larger-than-normal waves during the period of dredging (figs. 5-8). The long-period waves out of the southwest caused slightly higher turbidity on 2009 YD 307; the larger waves out of the northwest on 2009 YD 310-314 resulted in turbidity levels exceeding 100 NTUs at all of the tripod sites. The strong correlation between combined (wave+current) shear stresses and the resulting suspended-sediment fluxes (fig. 29) suggests that resuspension of material from the seabed (higher suspended-sediment concentrations at higher shear stresses) was the driving factor behind the high turbidity levels and suspended-sediment concentrations near the seabed during the dredge-disposal operations.

While not sampled concurrently with the larger-than normal wave event on 2009 YD 310-314, the beach and seabed surveys during this time period display no consistent change from a primarily medium- to fine-grain beach and seabed (fig. 13), suggesting that if deposition of fine-grain dredge sediment occurred in the study area, it was not great enough to cause a large-scale shift in either the beach or seabed sediment to finer grain sizes. Similar to the data collected before the dredge-disposal operations, the data from the water-column surveys during the dredge operations show a clear water column, except off the dredge disposal site and Black Point where turbidity levels were higher than before the start of dredging (figs. 11-12), suggesting that the plume of fine-grain sediment discharged by the dredge-disposal operations was advected offshore to the southwest. The turbidity levels apparently caused by the dredge operations, however, were not significantly greater than those observed in the study area before the commencement of dredging.

After Dredging

The period just after the harbor dredge-disposal experiment (2009 YD 325-339) generally was characterized by weaker daily winds and larger deep-water waves out of the northwest than

those observed before the start of dredging (fig. 4c-d); this general trend was punctuated by a minor storm with some rain and small southwesterly waves, followed by large northwesterly waves (2009 YD 330-332). The weak northwest wind forcing and larger waves resulted in little to no water column stratification due to a lack of wind-driven upwelling (fig. 10a). The weaker and less consistent winds and stratification resulted in lower current speeds, and thus, lower current shear stresses than observed before the start of the dredge-disposal operations (fig. 28a).

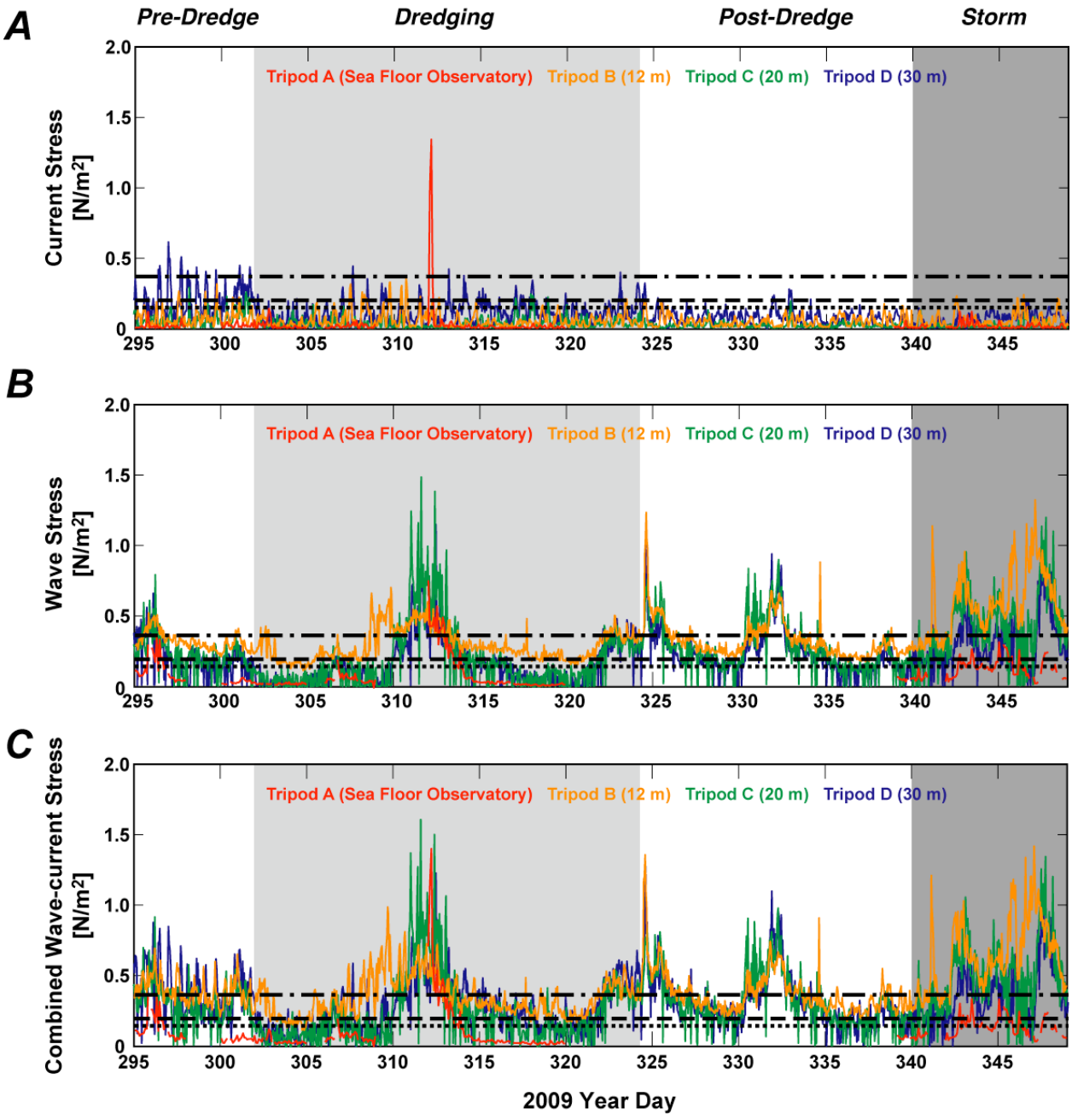

FIGURE 28. Time-series plot of wave, current, and combined shear stresses, in Newtons per square meter, at the main study sites. Data for Tripod A (Sea Floor Observatory), Tripod B (12 m), Tripod C (20 m), and Tripod D (30 m) are shown in red, orange, green, and blue, respectively. The horizontal dotted, dashed, and dot-dashed black lines denote the critical shear stresses for coarse silt (mud), fine sand, and coarse sand transport, respectively.

The current shear stresses were high enough to keep coarse silt in motion only intermittently at Tripod D's location along the 30 m isobath. The combined (wave+current) shear stresses were great enough to inhibit the deposition of coarse silt and to keep fine sand often in motion in the study area, except at the location of Tripod A off the wharf.

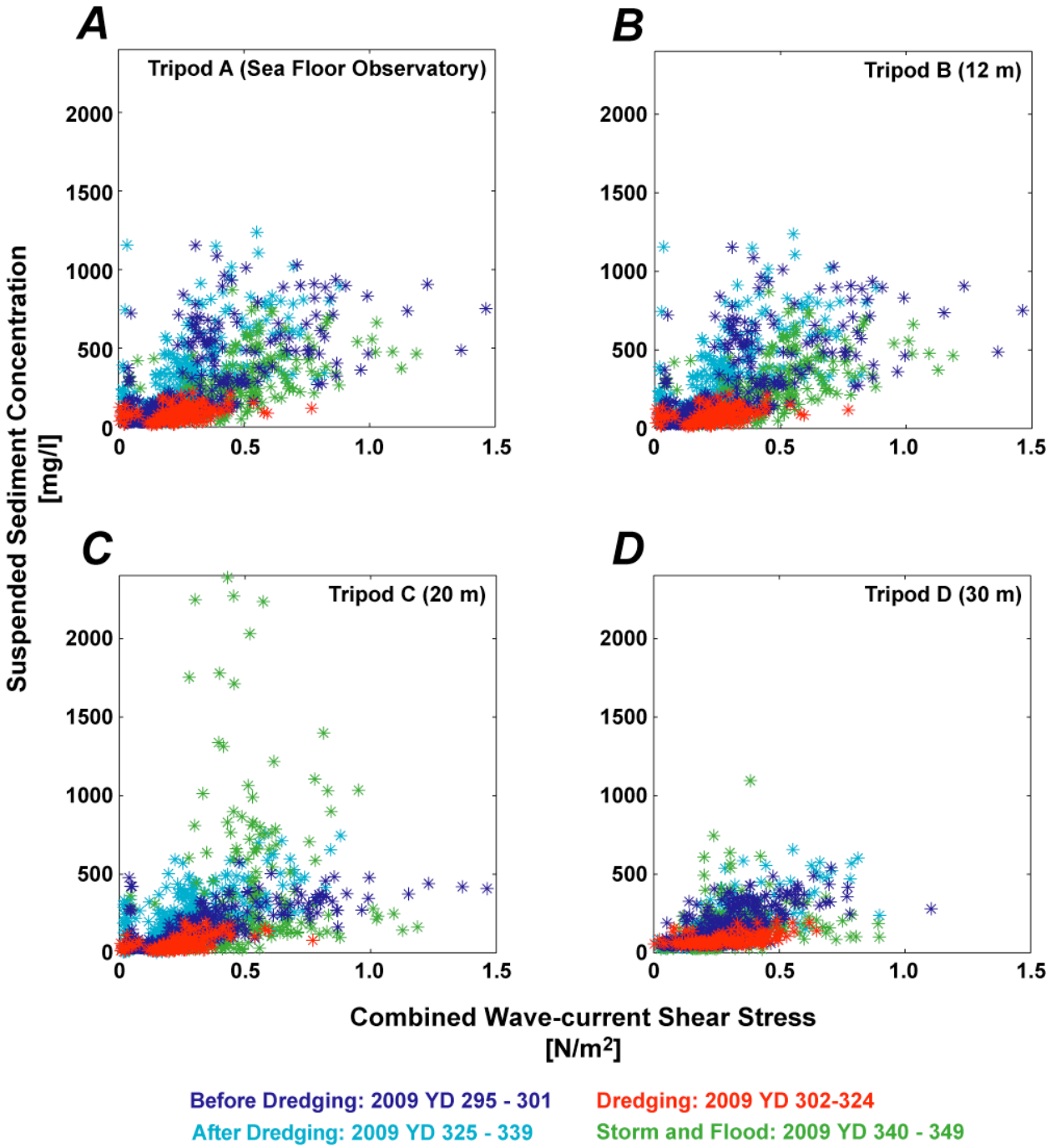

FIGURE 29. Scatter plots of near-bed suspended-sediment concentrations (SSC), in milligrams per liter, as a function of combined shear stress, in Newtons per square meter, at the main study sites. Data from before the start of dredging, during the dredging, after the dredging, and during the post-dredging storm and flood are shown in blue, red, green, and orange, respectively.

Elevated turbidity levels at all of the tripods generally coincided with larger-than-normal waves following the period of dredging (figs. 5-8). The large waves out of the northwest caused turbidity levels exceeding 100 NTUs at all of the tripod sites. The strong correlation between combined (wave+current) shear stresses and the resulting suspended-sediment fluxes (fig. 29) suggests that resuspension of material from the seabed (higher suspended-sediment concentrations at higher shear stresses) was the driving factor behind the high turbidity levels and suspended-sediment concentrations near the seabed during most of the period following the end of dredge-disposal operations. However, during the few days following the end of dredge operations (2009 YD 324-327), turbidity levels were elevated, while the shear stresses were low (fig. 28), suggesting that the advection of material, possibly from the dredge-disposal operations, past the study sites.

While not sampled concurrently with the larger-than normal wave event on 2009 YD 330-332, the beach and seabed surveys during this time period display no consistent change from a primarily medium- to fine-grain beach and seabed (fig. 13), suggesting that if deposition of fine-grain dredge sediment occurred in the study area, it was not great enough to cause a large-scale shift in either the beach or seabed sediment to finer grain sizes. Similar to the data collected before dredge-disposal operations, the data from the water-column surveys after dredge operations show a clear water column, except directly off the dredge disposal site and Black Point where turbidity levels continued to be higher than they were before the start of dredging (figs. 11-12). This suggests that some of the fine-grain sediment discharged by the dredge-disposal operations may have been resuspeded inshore of the tripods and advected offshore to the south. Farther offshore, however, the turbidity levels decreased to their pre-dredging levels.

Post-Dredging Storm and Flood

The final portion of the study period (2009 YD 340-349) was characterized by the San Lorenzo River's second significant flood (daily mean discharge=4.6 m^3/s) of the season on 2009 YD 345 (fig. 4f); this flood was an order of magnitude smaller than the first flood of the season that preceded the dredge-disposal operations. The storm started on 2009 YD 340 with rainfall (not shown) and the winds slowly changing from the northwest to southwest (fig. 4c) as the region of low pressure passed over central California. By 2009 YD 345, the winds were blowing strongly from out of the south, the river was discharging water at a rate of more than 4 m^3/s (fig. 4f), and the wave period decreased (fig. 4e) as locally generated wind waves became more pronounced. These strong south (downwelling-favorable) winds and waves resulted in intense mixing, a break-down in stratification, and the advection of warmer offshore water into the bay, as evident in the increase in temperature (fig. 10a). Such temperature increases are indicative of downwelling (Storlazzi and others, 2003). While the inner shelf water temperatures increased due to downwelling, the influx of freshwater from the San Lorenzo River resulted in decreases in salinity along the 20 m and 30 m isobaths (fig. 10b). The southerly winds did not generate high current speeds or current shear stresses high enough to keep coarse silt in motion at the shallower tripod locations (fig. 28a). However, when combined with the short-period storm waves, the combined (wave+current) shear stresses were great enough to inhibit the deposition of coarse silt and fine sand throughout all of the study area; coarse sand was kept in motion at all but the location of Tripod A off the wharf. The current-induced shear stresses typically were not sufficient to resuspend the material on the seabed inshore of the 30 m isobath. The wave-induced stresses, however, generally were sufficient to inhibit the deposition of mud at all of the four instrument sites. Under the combination of waves and currents, even fine-grain sand was generally in motion; during large wave events, even coarse sand is mobilized at all of the four instrument sites.

Elevated turbidity levels at all of the tripods generally coincided with discharge from the San Lorenzo River and storm waves, which resulted in levels exceeding 100 NTUs at all of the tripod sites (figs. 5-8). Although there was some correlation between combined (wave+current) shear stresses and the resulting suspended-sediment fluxes (fig. 29) that suggested near-bed turbidity was due to the resuspension of seabed material, often the turbidity levels were elevated while the shear stresses were low (fig. 28), suggesting that the sediment causing the elevated turbidity levels resulted from the advection of material, possibly from the dredge-disposal operations but likely due to discharge from the San Lorenzo River, past the study sites. Due to the rough atmospheric and oceanographic conditions, no beach, seabed, or water-column surveys were done during this time period.

Sediment Geochemistry

The observed differences in percent C, ^{15}N, ^{13}C, and C/N between Santa Cruz Harbor sediment and trap-collected suspended sediment suggest that the material collected in the sediment traps did not originate from the material dredged from the harbor (specifically the north harbor areas). Although percent C and percent N contents of trap-collected sediment changed between the early-, late-, and post-dredging collection periods, the lack of change in C/N with time suggests a change in the fraction of organic material accumulating, but not a change in the predominant source of organic material. Carbon isotopic compositions of both harbor sediment and suspended sediment collected in traps are distinct from that of San Lorenzo River suspended sediment (^{13}C~ -28‰, Conaway, unpublished data). Because of the differences in ^{13}C between the harbor, trap-collected suspended sediment, and San Lorenzo River suspended sediment, it is unlikely that recent or contemporaneous material from the San Lorenzo River or dredge disposal from the north harbor are a substantial part of the organic fraction of material collected in sediment traps. Carbon and nitrogen isotopic and elemental composition data provide insight into the nature and origin of material accumulating in the harbor and the suspended sediment collected offshore. Compared to typical average compositional values of major particulate organic matter sources (Kendall and others, 2001), the ^{15}N, ^{13}C, and C/N values of harbor sediment samples are consistent with aquatic macrophytes, C3 terrestrial plants, or a mixture of the two. Similarly, carbon and nitrogen isotopic composition and C/N molar ratios of suspended sediment collected in traps are consistent with a mixture of plankton and particles derived from aquatic macrophytes.

The short-lived radionuclide data show the lack of a substantial contribution of recent sediment from the San Lorenzo River to suspended sediment collected in the sediment traps during the dredging period. Suspended sediment collected from the San Lorenzo River during a high-flow event on 10/17/2009 (2009 Year Day 290) had ^{7}Be activity of 6.9–23 dpm/g and a $^{7}Be/^{210}Pb_{xs}$ ratio of 1.4–2.4 (Conaway, unpublished data). Although ^{7}Be has a short half life of 53 days, the values for San Lorenzo River sediment would not be expected to change much over the 23 day period of the first trap deployment (2009 Year Day 313) and the last suspended sediment collection date (2009 Year Day 349) occurred only slightly more than one half-life of ^{7}Be after the flood event. These values are substantially higher than the ^{7}Be values observed in trap collected suspended sediment (<1.2 dpm/g) during dredging activity, indicating that suspended sediment collected was not predominantly (re)suspended material from the recent San Lorenzo River storm event. The relatively high activity of ^{7}Be in trap-collected suspended sediment post-dredging compared to trap-collected suspended sediment during dredging may reflect the resuspension or input of some recent San Lorenzo River material in the post-dredging storm and flood period (2009 Year Days 340–349), or alternatively direct wet deposition (through rainwater) of ^{7}Be to the ocean, and sorption to suspended sediment. Because ^{210}Pb is scavenged rapidly from the water column to suspended sediment, it is difficult to make any comparison

between $^{210}Pb_{xs}$ activities in harbor sediment and trap-collected sediment. This suggests that the fine-grain sediment dredged from the harbor was either not transported to these locations or was diluted to such a degree compared to resuspended seabed sediment that it was difficult to identify in the trap samples.

Elements associated with fine-grain material or organic matter, such as particle-reactive contaminants, are expected to show a positive correlation with percent clay or percent C. Conversely, elements associated with discrete mineral grains may show a positive correlation with the abundance of coarser grain-size fractions or percent silt. Note that all samples were sieved to 100 micron (very fine sand) before geochemical analysis, and therefore we consider percent silt to be representative of the silt and very fine sand fractions. The observed correlation of Cu, Pb, and Zn with percent clay and organic C suggests that these elements behave as particle-reactive, organic-associated elements. The correlation of Co, Cr, Fe, and Ni with percent silt suggests that these elements are associated with (natural) mineral grains, presumably ferromagnesian minerals.

Spatial and temporal trends of the contents of elements in the sediment trap-collected material are related predominantly to grain size and organic matter. The observed early-, late-, and post-dredging trend in percent C, and associated changes in elements As, Cu, Mo, Pb, Zn, are interpreted to mean that an increase in fine-grain, organic-rich (high percent C) material collected in the sediment traps at mooring sites close to the end of the dredging period resulted in an increase in particle-reactive, organic-associated, and redox-sensitive elements compared to other collection periods. The positive correlation of Co, Cr, and Ni in the sediment traps with increasing distance from shore reflects a changing lithology as marine sediment predominates. The observed offshore decrease in Cu and Mo is interpreted to mean that Cu and Mo are derived from land, whereas Pb, which showed no change after grain-size normalization, may be more pervasive in the shore-shelf system. The up to 2-fold enrichment of Cu and Zn in north harbor sediment relative to sediment collected at the moorings shows that sediment collected at the mooring locations was not predominantly from the harbor, although geochemical changes in sediment during dredging or transport are a possibility.

Sediment Dynamics

The calculated suspended-sediment fluxes from the four tripods (figs. 30-33) for the four periods (before, during and after dredge operations and during the following storm and flood) show two consistent trends. First, the near-bed suspended-sediment fluxes were always an order of magnitude greater (~100 tons/m^2/day) than those observed higher (>2 m above the seabed) in the water column (~10 tons/m^2/day). Since coarser grain sizes have faster settling velocities (table 8) and are not resuspended to great heights above the seabed, it can be assumed that these higher near-bed suspended-sediment fluxes generally represent coarser-grained material. Conversely, the suspended-sediment fluxes higher in the water column likely are slower-settling fine-grain material, presumably including the mud-sized material dredged during the demonstration project. Second, there was vertical shear in suspended-sediment flux at each tripod site, meaning that the direction of suspended-sediment flux always varied vertically through the water column at a given location. These two observations, combined, suggest that large quantities of primarily coarse-grained sediment moved through the study area near the bed and smaller quantities of finer-grained sediment generally headed in a different direction higher in the water column. The lack of sufficient quantities of material in the sediment traps that could be geochemically linked to the harbor dredge disposal or deposition of fine-grain material on the seabed, in conjunction with the low suspended-sediment concentrations measured by the tripods, suggests that the fine-grain dredge-disposal outfall was diluted significantly and advected

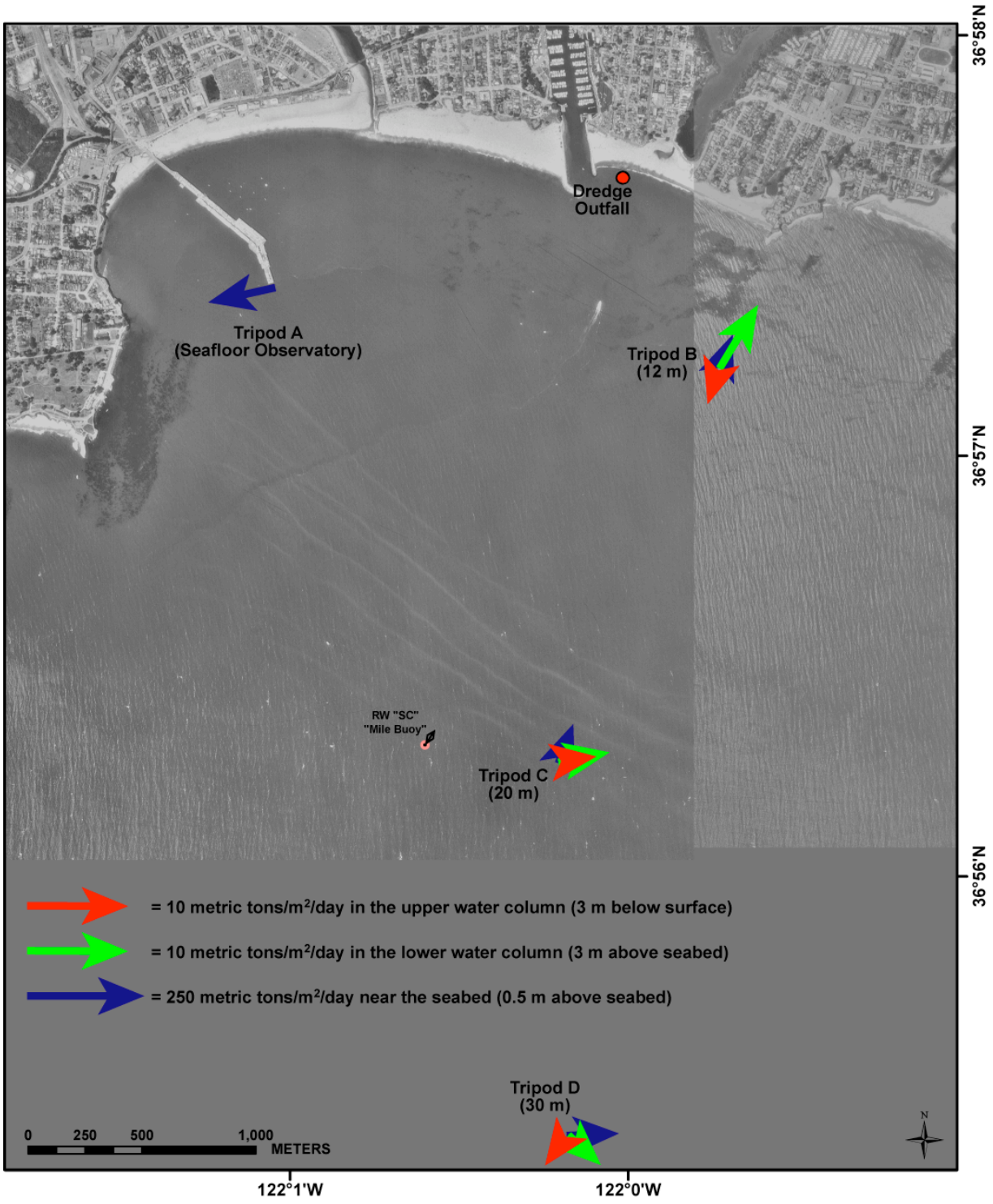

Before Dredging

FIGURE 30. Map showing the daily mean suspended-sediment fluxes, in metric tons per square meter per day, before the start of dredging (2009 YD 295-301). Data from close to the seabed, the lower water column, and close to the surface are shown in blue, green, and red, respectively. Note the difference in scale of the vectors.

through the study area such that net deposition on the seabed did not occur and the flux of material at the height and location of the traps was minimal.

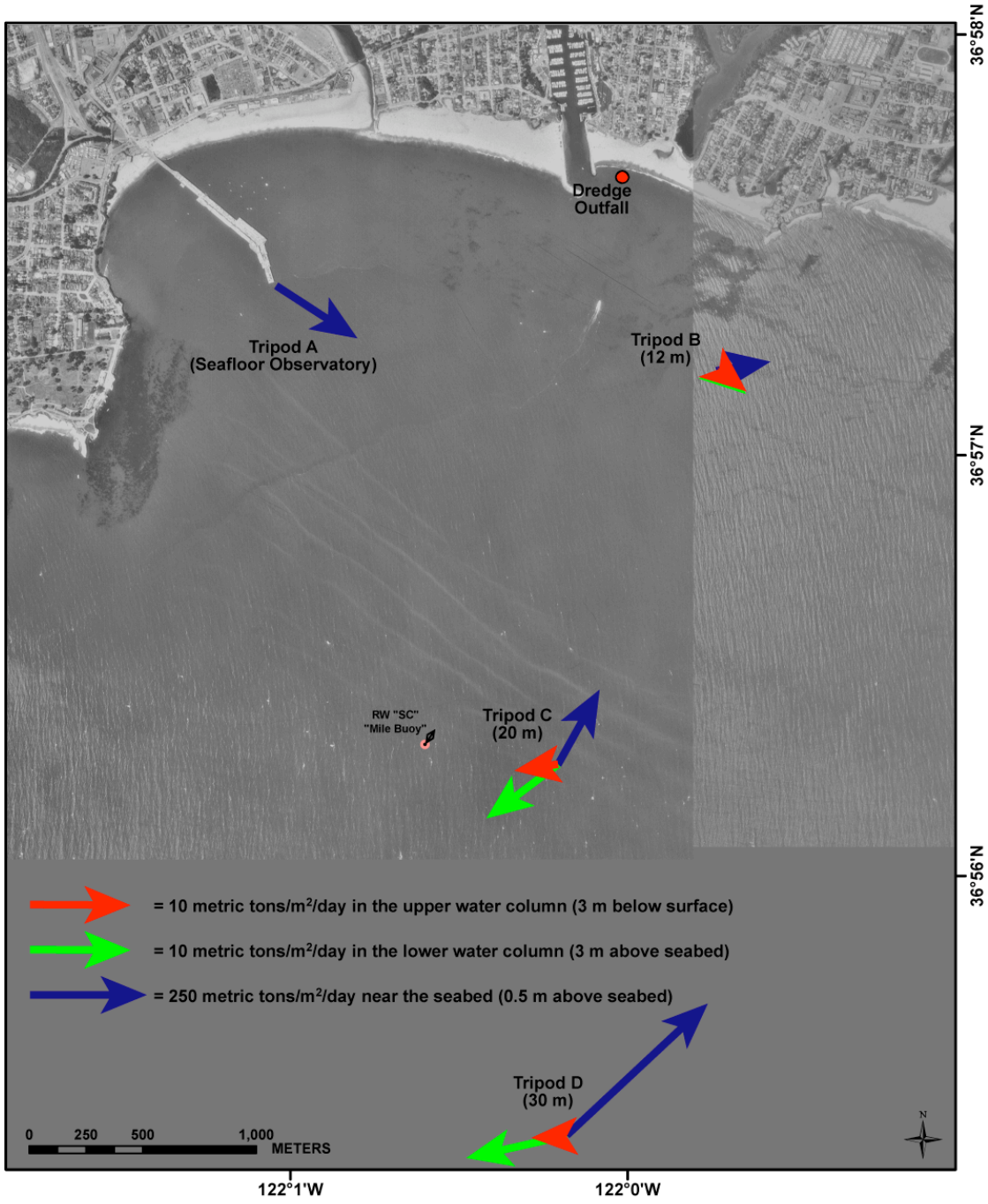

FIGURE 31. Map showing the daily mean suspended-sediment fluxes, in metric tons per square meter per day, during the dredging (2009 YD 302-324). Data from close to the seabed, the lower water column, and close to the surface are shown in blue, green, and red, respectively. Note the difference in scale of the vectors.

Before the start of dredging (2009 YD 295-301; fig. 30), sediment flux near the seabed and in the lower water column was obliquely onshore to the northeast; the sediment flux near the

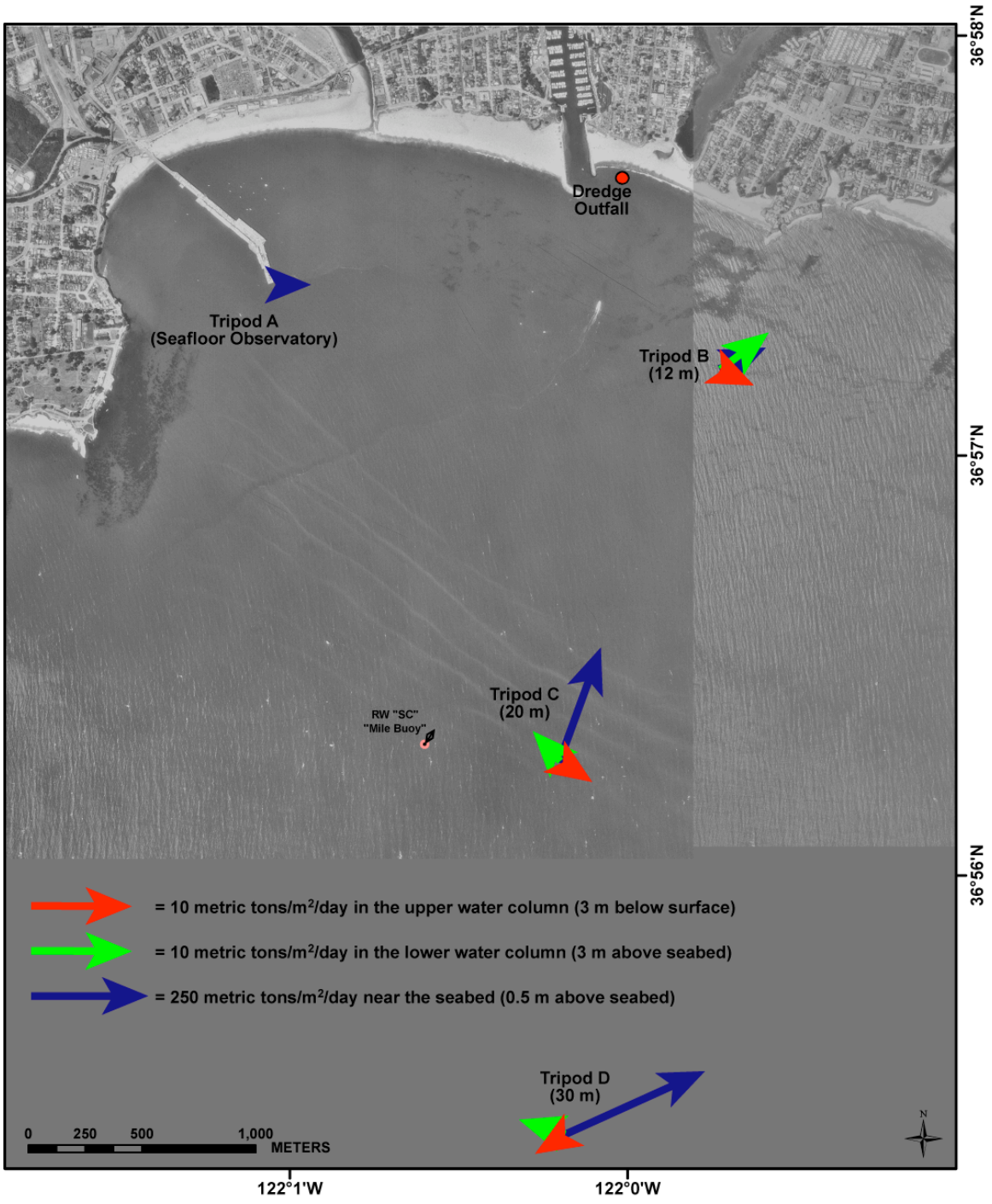

After Dredging

FIGURE 32. Map showing the daily mean suspended-sediment fluxes, in metric tons per square meter per day, after the dredging (2009 YD 325-339). Data from close to the seabed, the lower water column, and close to the surface are shown in blue, green, and red, respectively. Note the difference in scale of the vectors.

surface was low in magnitude and oriented primarily offshore. During the dredge operations (2009 YD 302-324; fig. 31), there was both vertical and horizontal shear in sediment flux, with

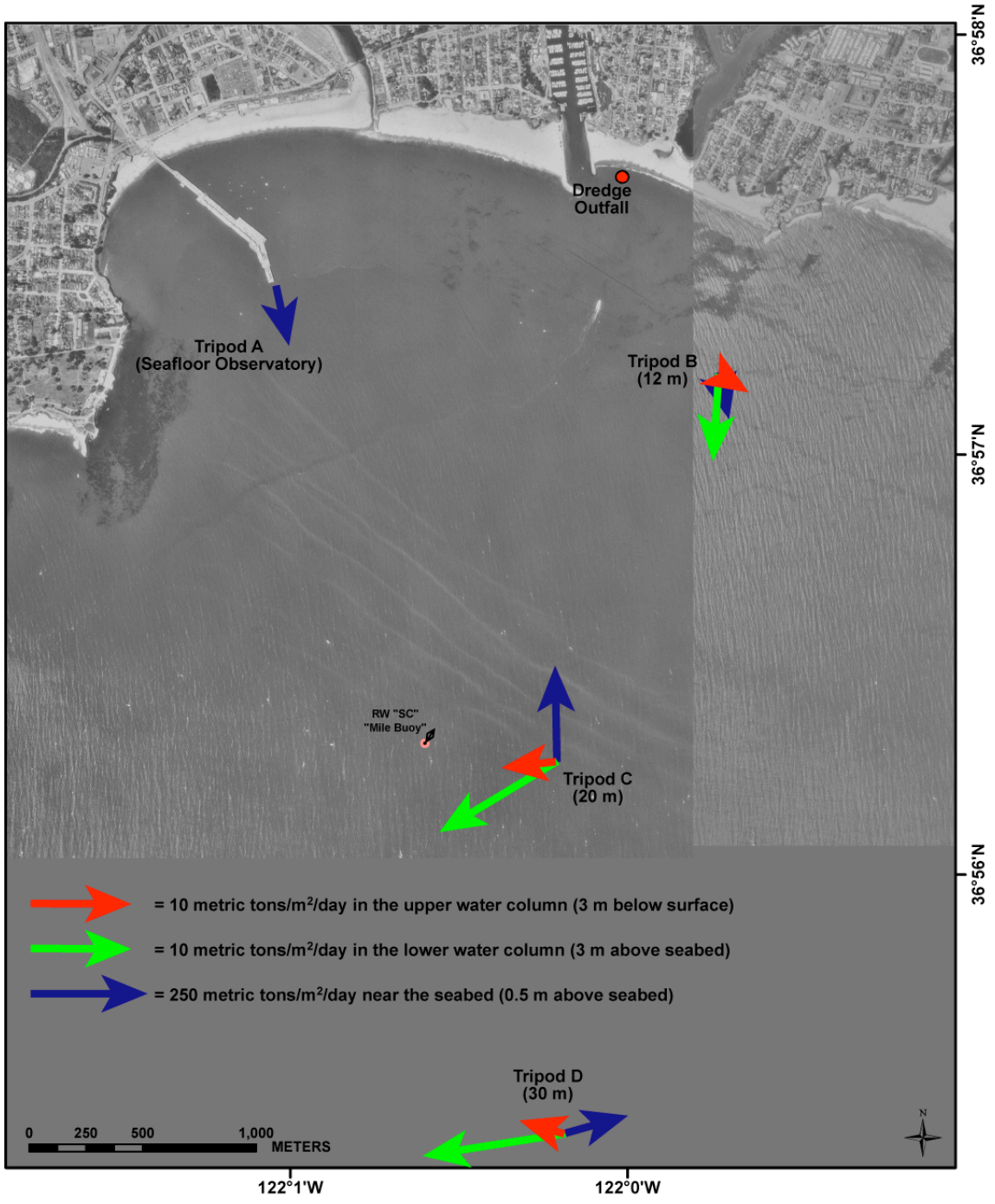

Storm and Flood

FIGURE 33. Map showing the daily mean suspended-sediment fluxes, in metric tons per square meter per day, during the storm and flood after the dredging (2009 YD 340-345). Data from close to the seabed, the lower water column, and close to the surface are shown in blue, green, and red, respectively. Note the difference in scale of the vectors.

the sediment flux near the seabed at all sites oriented obliquely onshore to the northeast and higher in magnitude offshore. The sediment flux in the entire water column off Black Point was oriented obliquely offshore to the southeast, while offshore along the 20 m and 30 m isobaths the sediment flux in water column was offshore to the southwest.

After the cessation of dredging (2009 YD 325-339; fig. 32), the sediment flux in the lower water column and near the surface off Black Point was oriented alongshore to the east, while offshore along the 30 m isobath the sediment flux in the lower water column and near the surface was weakly offshore to the southwest. Similar to the period of dredge operations (fig. 31), there was both vertical and horizontal shear in sediment flux during the storm and flood after the dredging (2009 YD 340-345; fig. 33). The sediment flux off Black Point was oriented obliquely alongshore to the southeast. Offshore, the sediment flux close to the seabed was onshore to the north along the 20 m isobath and to the east along the 30 m isobath, but it was to the west in the mid water column and near the surface. Overall, the net flux of what is assumed to be coarse-grained material near the seabed was primarily to the east into the bay. Fine-grain material higher up in the water column, presumably including the mud-sized sediment dredged from the Santa Cruz Harbor, was offshore to the southeast close to shore along the 12 m isobath and offshore to the southwest farther from shore along the 20 m and 30 m isobaths.The atmospheric (winds) and oceanographic (waves) forcing observed during the harbor dredge-disposal experiment was typical of the fall and winter months in the study area (Storlazzi and Wingfield, 2005), as was the fluvial discharge from the San Lorenzo River (NWIS, 2010), as shown in figure 34. This suggests that the resulting levels of near-bed shear stress (high enough to inhibit deposition of mud), turbidity levels, and sediment-flux patterns (onshore sand and offshore mud transport) observed during the dredge-disposal experiment likely are characteristic of the time period (October-November).

Summary of Findings

More than 400,000 measurements of oceanographic forcing and the resulting water-column and seabed properties were made in northern Monterey Bay, California, to understand the sediment dynamics and fate of fine-grain sediment dredged from the inner portion of Santa Cruz Harbor. These measurements were made in the 17-day period during which more than 7600 m^3 of sediment was dredged from Santa Cruz Harbor and discharged approximately 60 m offshore of the harbor at a depth of 2 m on the inner shelf. Key findings from these measurements and analyses include:

1) Waves and circulation generally were more vigorous to the east of the wharf and farther offshore. Flow was primarily to the east near the seabed close to shore and to the west and offshore higher up in the water column.

2) There did not appear to be significant net deposition of mud from either the San Lorenzo River or the Santa Cruz Harbor dredge-disposal operations because there was no shift to a finer grain-size class along the beach or on the inner shelf.

3) The difference between the grain size on the seabed and that captured in the sediment traps demonstrates that there was fine-grain, muddy sediment transported through the study area.

4) Chemical analysis of sediment, including C and N isotopic and elemental composition and short-lived radioisotope analyses, demonstrated that suspended sediment collected in sediment traps was not recent fluvial sediment from the San Lorenzo River or material discharged from

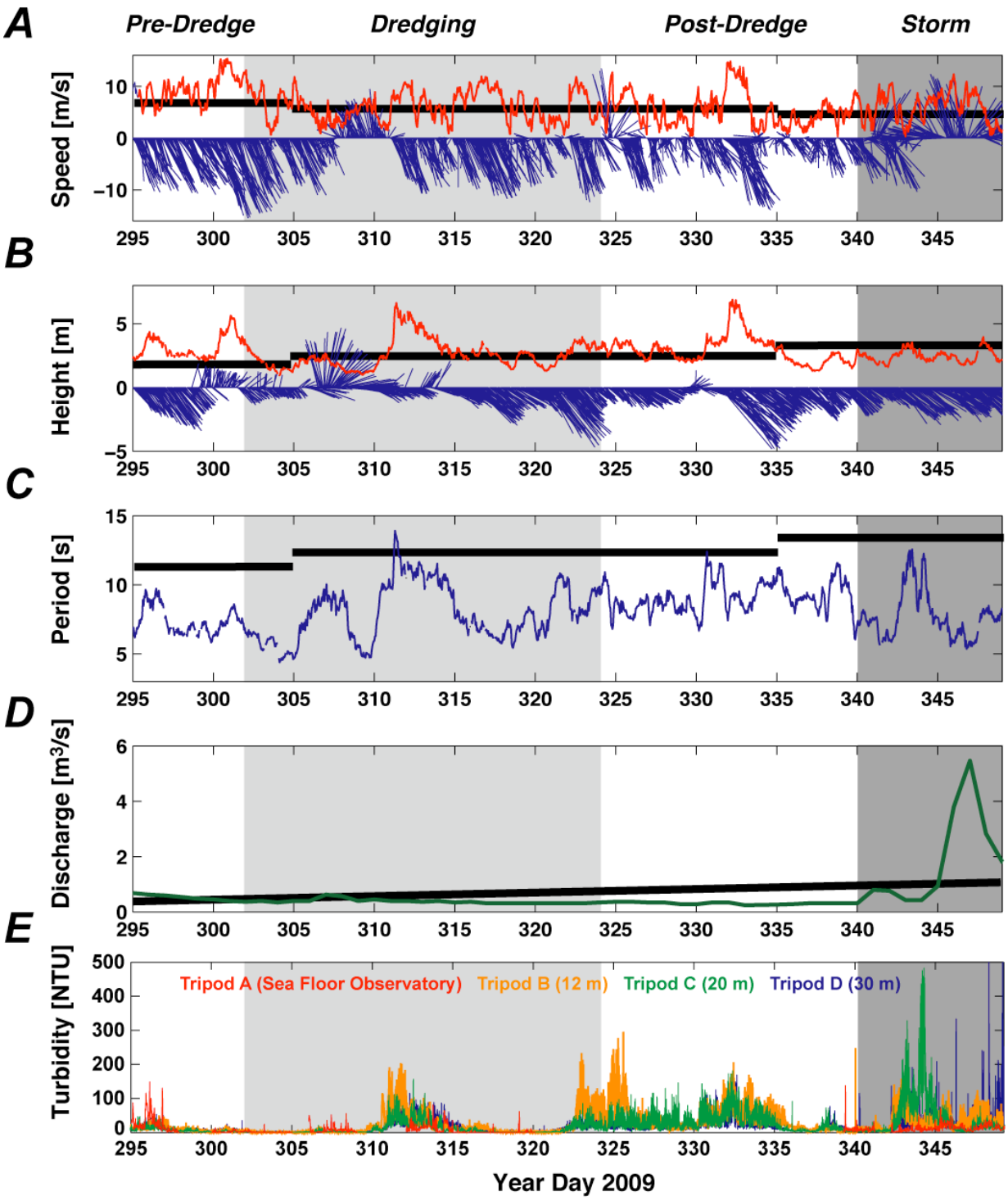

FIGURE 34. Time-series plot of regional meteorologic, oceanographic, fluvial, and resulting turbidity data during the study period. *A,* Red: wind speed, in meters per second; Blue: wind speed and direction, in meters per second from degrees true north. *B,* Red: wave height, in meters; Blue: wave height and direction, in meters from degrees true north. *C,* Wave period, in seconds. *D,* River discharge, in meters cubed per second. *E,* Near-bed turbidity, in National Turbidity Units (NTU), at the four tripods in the study area. The period of dredge-disposal operations and the post-dredging storm and flood are denoted by the light grey (2009 Year Days 302-324) and dark grey boxes (2009 Year Days 340-349), respectively. The heavy black horizontal lines in parts *A-C* show the 15-year averages (Storlazzi and Wingfield, 2005) and the 29-year average in part *D* (NWIS, 2010).

the dredging of northern Santa Cruz Harbor. Based on the observed sediment fluxes and numerical modeling results, this suggests that Santa Cruz Harbor dredge material and San Lorenzo River sediment made up a small fraction of total suspended material in the study area.

5) Except off the end of the wharf, the current shear stresses were high enough to keep coarse silt from settling out of suspension and depositing on the seabed only intermittently under the conditions observed during the experiment. However, in conjunction with the wave-induced shear stresses, the combined (wave+current) shear stresses generally were sufficient to inhibit the deposition of coarse silt and often kept fine sand in motion in the study area during the experiment. This was true for all instrument locations except off the wharf, where the combined shear stresses were sufficient to inhibit the deposition of coarse silt only intermittently during the course of the experiment.

6) The net flux of what is assumed to be coarse-grained material near the seabed primarily was to the east into the bay under the oceanographic conditions observed during the course of the experiment. Transport of finer-grained material higher in the water column, including presumably the mud-sized sediment dredged from Santa Cruz Harbor, was offshore to the southeast along the 12 m isobath and offshore to the southwest farther along the 20 m and 30 m isobaths.

7) The numerical model results suggest that the dredge-disposal plume would be advected alongshore to the southwest during low wave-energy conditions. During larger wave-energy conditions, the dredge-disposal plume would be advected first to the east towards Capitola. These modeled patterns resulted in temporary (maximum residence time = 20 days), thin (maximum thickness = 0.0011 m) deposition of fine-grain sediment on the seabed offshore Capitola. In the model, the dredge material subsequently was eroded from this temporary depocenter offshore Capitola and advected offshore to the southwest in the direction of the mid-shelf mud belt before the end of the dredging period. Due to the small errors in modeled wave and current patterns, and low modeled suspended-sediment concentrations, the thin, temporary accumulation patterns predicted by the model are well within the error of the model and are not assumed to be real.

8) Together, oceanographic observations, model results, and laboratory analyses suggest that the predominantly mud-sized sediment dredged from Santa Cruz Harbor and discharged to the coastal ocean: (a) did not result in observable deposition of fine-grain sediment on the beach and inner continental shelf, (b) likely was advected alongshore to the east, then offshore to the southwest in the direction of the mid-shelf mud belt, and (c) resulted in turbidity values lower than those values observed during a large wave event or a small flood of the San Lorenzo River.

9) The atmospheric (winds) and oceanographic (waves) forcing observed during the Santa Cruz Harbor dredge-disposal experiment was typical of the fall and winter months in the study area, suggesting that the resulting levels of near-bed shear stress (high enough to inhibit deposition of mud) and sediment flux patterns (onshore sand transport, offshore mud transport) likely are characteristic of the time period (October-November).

These data provide information on the nature and controls on flow and water-column and seabed properties in northern Monterey Bay, California, during late summer through winter conditions. A number of interesting phenomena were observed that indicate the complexity of coastal circulation and sediment dynamics in the northern part of the bay and may help

researchers and regulators to better understand the implications of the processes on sediment dynamics.

Acknowledgements

This work was funded primarily by the U.S. Army Corps of Engineers' (USACE) San Francisco District, the USGS's Pacific Coastal and Marine Science Center (USGS-PCMSC), and the Santa Cruz Port District. The research was carried out as part of the USGS's Benthic Habitats (Pacific) and Applied Sediment Transport Projects; the ultimate goal is to better understand the importance of sediment dynamics on benthic habitats along the U.S. west coast. This scientific research was done under Monterey Bay National Marine Sanctuary (MBNMS) research permit MBNMS-2009-025. Peter Mull (USACE) coordinated the funding and contributed advice on project planning. Brian Foss and the Santa Cruz Port District staff helped with project planning and provided significant logistical help and facilities to support our field operations. Mike Torresan (USGS) and Angela Lam (USGS) processed the sediment-trap samples for grain-size distributions. Peter Swarzenski (USGS) provided the geochemical radionuclide data. Carbon and nitrogen elemental and isotopic composition were processed by Steve Silva (USGS) and Doug Choy (USGS); samples for trace element composition were processed by Monique Adams (USGS). The Santa Cruz Harbor samples were provided by Steve Krcik of Red Hill Environmental. Erica Burton (MBNMS) helped with the permitting for this project. Rachel "Charlie" McGillis provided logistical support for the small boat survey operations. We would also like to thank Renee Takesue (USGS) and Steve Watt (USGS) who contributed numerous excellent suggestions and a timely review of our work.

References Cited

Anima, R.J., Eittreim, S.L., Edwards, B.D., and Stevenson, A.J., 2002, Nearshore morphology and late Quaternary geologic framework of the northern Monterey Bay Marine Sanctuary, California. Marine Geology, v. 181, no. 1-3, p. 35-54.

Baker, E.T., Milburn, H.B., and Tennant D.A., 1988, Field assessment of sediment trap efficiency under varying flow conditions: Journal of Marine Research, v. 46, p. 573-592.

Best, T.C., and Griggs, G.B., 1991. A sediment budget for the Santa Cruz littoral cell, California, in, From shoreline to abyss: Society for Sedimentary Geology Special Publication 46, p. 35-50.

Booij, N., Ris, R.C., and Holthuijsen, L.H., 1999. A third-generation wave model for coastal regions, Part I - Model description and validation: Journal of Geophysical Research, v. 104, p. 7649-7666.

Bothner, M.H., Reynolds, R.L., Casso, M.A., Storlazzi, C.D. and Field, M.E., 2006. Quantity, composition and source of sediment collected in sediment traps along the fringing coral reef off Molokai, Hawaii. Marine Pollution Bulletin, v. 52, no. 9, p. 1034-1047.

Buscombe, D., and Messelink, G., 2009. Grain-size information from the statistical properties of digital images of sediment. Sedimentology, v. 56, p. 421-438.

Buscombe, D., Rubin, D.M., and Warrick, J.A., 2010. A universal approximation to grain size from images of non-cohesive sediment. Journal of Geophysical Research, v. 115, F02015

Chezar, H., and Rubin, D.M., 2004. Underwater microscope system. U.S. Patent and Trademark Office, patent number 6,680,795, January 20, 2004, 9 p.

Delft3D User Manual, 2006. Delft3D-FLOW, Simulation of multi-dimensional hydrodynamic flows and transport phenomena, including sediment. User Manual. Delft Hydraulics, the Netherlands.

Edwards, B.D., 2002. Variations in sediment texture on the northern Monterey Bay National Marine Sanctuary continental shelf. Marine Geology, v. 181, no. 1-3, p. 83-100.

Egbert, G.D., and Erofeeva, S.Y., 2002. Efficient inverse modeling of barotropic ocean tides. Journal of Atmospheric and Oceanic Technology, v. 19(2), p. 183-204.

Gardner, W.D., Richardson, M.J., Hinga, K.R. and Biscaye, P.E., 1983. Resuspension measured with sediment traps in a high-energy environment: Earth and Planetary Science Letters, v. 66, p. 262-278.

Gemmill, W.H., and Peters, C.A., 1997. High-resolution ocean surface wind analyses using satellite derived ocean surface winds: Analyses validation using synthetic satellite data. NOAA-National Center for Environmental Prediction (NCEP) Technical Note 1997-147, 19 p.

Griggs, G.B., Savoy, L., 1985. Living with the California Coast. Duke University Press, Durham, NC, 393 p.

Griggs, G.B., 1991. Investigation of the dispersal of dredge spoils from the Santa Cruz Small Craft Harbor – Final report. Prepared for the Santa Cruz Harbor Port Commission.

Halliwell, G. R., Jr., 1998. Simulation of North Atlantic decadal/multi-decadal winter SST anomalies driven by basin-scale atmospheric circulation anomalies. Journal of Physical Oceanography, v. 28, p. 5-21.

Holthuijsen, L.H., Booij, N., and Ris, R.C., 1993. A spectral wave model for the coastal zone: 2nd International Symposium on Ocean Wave Measurement and Analysis, New Orleans, p. 630-641.

Kendall, C, Silva, S.R., Kelly, V.J., 2001. Carbon and nitrogen isotopic compositions of particulate organic matter in four large river systems across the United States: Hydrological Processes, v. 15, p. 1301–1346.

Leendertse, J.J., 1987. A three-dimensional alternating direction implicit model with iterative Fourth order dissipative non-linear advection terms. Report WD-3333-NETH, Rijkswaterstaat.

Lesser, G.R., 2009. An approach to medium-term coastal morphological modeling. CRC press/Balkema, Leiden, the Netherlands, 228 p.

Madsen, O.S., 1999. Coastal Sediment Transport Processes. New York, American Society of Civil Engineers Short Course, Coastal Sediments ’99 Conference.

McLaren, P., 2000. Sediment Trend Analysis (STA) – A sediment trend analysis of Santa Cruz Harbor and its vicinity: Implications to dredge-disposal operations. Prepared for Santa Cruz Port District with sponsorship from the California Department of Boating and Waterways

National Data Buoy Center, 2010. Station 46042 – Monterey data: National Oceanic and Atmospheric Administration [http://www.ndbc.noaa.gov/station_page.php?station=46042]. (last accessed March, 15, 2010).

National Water Information System, 2010. Station 11161000 – San Lorenzo River at Santa Cruz data: U.S. Geological Survey [http://waterdata.usgs.gov/ca/nwis/uv/?site_no=11161000]. (last accessed March, 15, 2010).

National Geophysical Data Center, Coastal Relief Model, 2010. Western U.S. data. National Geophysical Data Center [http://www.ngdc.noaa.gov/mgg/coastal/startcrm.htm] (last accessed November 19, 2010).

Paduan, J.D., and Cook, M.S., 1997. Mapping surface currents in Monterey Bay with CDAR-type HF radar. Oceanography, v. 10, p. 49-52.

Ris, R.C., Booij, N., and Holthuijsen, L.H., 1999. A third-generation wave model for coastal regions, Part II: verification: Journal of Geophysical Research, v. 104(4), p. 7649-7666.

Rubin, D.M., Chezar, H., Harney, J.N., Topping, D.J., Melis, T.S., and Sherwood, C.R., 2007. Underwater microscope for measuring spatial and temporal changes in bed-sediment grain size. Sedimentary Geology, v. 202, no. 3, p. 402-408.

Sea Engineering, Inc., 2006. Fall 2005 inner Santa Cruz Harbor dredge disposal monitoring program. Report prepared for the Santa Cruz Port District, 146 p.

Stelling, G.S., 1984. On the construction of computational methods for shallow water flow problems: Rijkswaterstaat communication series No. 35, The Hague.

Storlazzi, C.D., and Jaffe, B.E., 2002. Flow and sediment suspension events on the inner shelf of central California. Marine Geology, v. 181, p. 195-213.

Storlazzi, C.D., McManus, M.A., and Figurski, J.D., 2003. Long-term high-frequency ADCP and temperature measurements along central California: Insights into upwelling and internal waves on the inner shelf. Continental Shelf Research, v. 23, p. 901-918.

Storlazzi, C.D. and Wingfield, D.K., 2005. The spatial and temporal variability in oceanographic and meteorologic forcing along Central California – 1980-2002: U.S. Geological Survey Scientific Investigations Report 2005-5085, 39 p. [http://pubs.usgs.gov/sir/2005/5085/]

Storlazzi, C.D., Reid, J.A., and Golden, N.E., 2007. Wave-Driven Spatial and Temporal Variability in Seafloor Sediment Mobility in the Monterey Bay, Cordell Bank, and Gulf of the Farallones National Marine Sanctuaries. U.S. Geological Survey Scientific Investigations Report 2007-5233, 84 p. [http://pubs.usgs.gov/sir/2007/5233/]

Storlazzi, C.D., Golden, N.E., and Finlayson, D.P., 2008. Views of the Seafloor in Northern Monterey Bay, California. U.S. Geological Survey Scientific Investigations Map 3007, 1 p. [http://pubs.usgs.gov/sim/3007/]

Van Rijn, L.C., 1993. Transport of fine sands by currents and waves. Journal of Waterway, Port, Coastal and Ocean Engineering, v. 119(2), 123-143.

Van Rijn, L.C., 2007a. Unified view of sediment transport by currents and waves. I: Initiation of motion, bed roughness, and bed-load transport. Journal of Hydraulic Engineering, v. 133(6), p. 649-667.

Van Rijn, L.C., 2007b. Unified view of sediment transport by currents and waves. II: Suspended transport. Journal of Hydraulic Engineering, v. 133(6), p. 668-689.

Van Rijn, L.C., 2007c. Unified view of sediment transport by currents and waves. III: Graded beds, v. 133(6), p. 761-775.

Van Rijn, L.C., Walstra, D.R., van Ormondt, M., 2007. Unified View of Sediment Transport by Currents and Waves. IIII: Application of Morphodynamic model. Journal of Hydraulic Engineering, v. 133(7), p. 776-793.

Verboom, G.K., and Slob, A., 1984. Weakly-reflective boundary conditions for two-dimensional shallow water flow problems. Advances in Water Resources, v. 7(4), p. 192-197.

Walstra, D.J., Roelvink, J.A., and Groeneweg, J., 2000. Calculation of wave-driven currents in a 3D mean flow model: Proceedings of 27th Conference on Coastal Engineering, p. 1050-1063.

Watt, S.G., 2003. Monitoring harbor dredging and sedimentary changes in coastal habitats of the Santa Cruz Bight, California. Thesis Presented to the Faculty of Cal State Monterey Bay through Moss Landing Marine Laboratories, in partial fulfillment of the requirements for the degree Master of Science in Marine Science.

Watt, S.G., and Greene, H.G., 2002. Monitoring dredged upper Santa Cruz Harbor mixed sand and mud sediment released into the nearshore area of Santa Cruz, California. Prepared for the Santa Cruz Harbor Port District and the California Department of Boating and Waterways.

Additional Digital Information

For additional information on the instrument deployments, please see:
Tripod and Sediment Trap Deployments
http://walrus.wr.usgs.gov/infobank/i/id209mb/html/i-d2-09-mb.meta.html
http://walrus.wr.usgs.gov/infobank/i/id309mb/html/i-d3-09-mb.meta.html
http://walrus.wr.usgs.gov/infobank/i/ir209mb/html/i-r2-09-mb.meta.html
http://walrus.wr.usgs.gov/infobank/i/ir309mb/html/i-r3-09-mb.meta.html
http://walrus.wr.usgs.gov/infobank/i/ir409mb/html/i-r4-09-mb.meta.html

Seabed (Flying Eyeball) Surveys
http://walrus.wr.usgs.gov/infobank/f/fe109mb/html/f-e1-09-mb.meta.html
http://walrus.wr.usgs.gov/infobank/f/fe209mb/html/f-e2-09-mb.meta.html
http://walrus.wr.usgs.gov/infobank/f/fe309mb/html/f-e3-09-mb.meta.html
http://walrus.wr.usgs.gov/infobank/f/fe409mb/html/f-e4-09-mb.meta.html
http://walrus.wr.usgs.gov/infobank/f/fe509mb/html/f-e5-09-mb.meta.html

Water Column (CTD Profiler) Surveys:
http://walrus.wr.usgs.gov/infobank/w/wc109mb/html/w-c1-09-mb.meta.html
http://walrus.wr.usgs.gov/infobank/w/wc209mb/html/w-c2-09-mb.meta.html
http://walrus.wr.usgs.gov/infobank/w/wc309mb/html/w-c3-09-mb.meta.html
http://walrus.wr.usgs.gov/infobank/w/wc409mb/html/w-c4-09-mb.meta.html
http://walrus.wr.usgs.gov/infobank/w/wc509mb/html/w-c5-09-mb.meta.html

For an online PDF version of this report, please see:
http://pubs.usgs.gov/of/2011/1045/.

For more information on the U.S. Geological Survey Western Region's Coastal and Marine Geology Team, please see:
http://walrus.wr.usgs.gov/.

Direct Contact Information

Project Information
Curt D. Storlazzi (Project Chief): cstorlazzi@usgs.gov

Table 1. Experiment personnel.

Person	Affiliation	Responsibilities
Curt Storlazzi	USGS	Chief Scientist, oceanographer, diver
Christopher Conaway	USGS	Co-chief Scientist, geochemist
Joshua Logan	USGS	Information specialist, diver, vessel captain
Kathy Presto	USGS	Oceanographer, instrument specialist
Katherine Cronin	Deltares	Numerical modeler
Maarten van Ormondt	Deltares	Numerical modeler
Lynne Harden	UCSC	Geologist
Jamie Lescinski	Deltares	Numerical modeler
Jessica Lacy	USGS	Oceanographer
Pieter Tonnon	Deltares	Numerical modeler
Pete dal Ferro	USGS	Mechanical technician, diver, vessel captain
Tim Elfers	USGS	Mechanical technician, vessel captain
George Tate	USGS	Supervisory marine technician
Thomas Reiss	USGS	Diver
Peter Harkins	USGS	Mechanical technician
Cordel Johnson	USGS	Mechanical technician
Kurt Rosenberger	USGS	Oceanographer
Andy Ritchie	USGS	Geographer
Jamie Grover	USGS	*R/V Parke Snavely* vessel captain
Jim Christman	-	*R/V Shana Rae* vessel captain
Andrew Reynaga	UCSC	*R/V Paragon* vessel captain

Table 2. Instrument package sensors.

Site Name	Height Above Bed [m]	Depth [m]	Sensors
Tripod A (9 m)	2.0 to surface	9	RD Instruments 1200 kHz Workhorse ADCM profiler
	0.5	9	Sontek 5000 kHz ADCM velocimeter
	0.5	9	D&A Instruments OBS-3
	0.3	9	D&A Instruments OBS-3
	1.0	9	Seabird SBE-37SI Microcat doivity-temperature sensor
Tripod B (12 m)	1.0 to surface	12	Nortek 600 kHz AWAC ADCM profiler
	0.5	12	Aquatec/Seapoint 210-TY optical backscatter sensor
	0.5	12	Seabird SBE-37SI Microcat doivity-temperature sensor
Tripod C (20 m)	2.0 to surface	20	RD Instruments 600 kHz Workhorse ADCM profiler
	1.0	20	Nortek 2000 kHz Aquadopp ADCM profiler
	2.0	20	Aquatec/Seapoint 210-TY optical backscatter sensor
	0.5	20	Aquatec/Seapoint 210-TY optical backscatter sensor
	1.3	20	Seabird SBE-37SI Microcat doivity-temperature sensor
Tripod D (30 m)	2.0 to surface	30	RD Instruments 600 kHz Workhorse ADCM profiler
	0.5	30	Nortek 2000 kHz Aquadopp ADCM profiler
	0.5	30	Aquatec/Seapoint 210-TY optical backscatter sensor
	1.3	30	Seabird SBE-37SI Microcat doivity-temperature sensor
Trap-10 m	5	10	Sediment trap
Trap-15 m	5	15	Sediment trap
Trap-20 m	5	20	Sediment trap
Trap-30 m	5	30	Sediment trap
Terrestial Imaging System (TIS)	-	[15]*	Harbortronics time-lapse digital camera package
NDBC buoy	-	[5]*	ARES payload

*Height, in meters

Table 3. Instrument package location information.

Site Name	Latitude [decimal degrees]	Longitude [decimal degrees]
Tripod A (9 m)	36.9569030	-122.0170036
Tripod B (12 m)	36.9533102	-121.9954277
Tripod C (20 m)	36.9384208	-122.0042870
Tripod D (30 m)	36.9237328	-122.0030674
Trap-10 m	36.9576419	-122.0028116
Trap-15 m	36.9506359	-122.0035570
Trap-20 m	36.9385923	-122.0046942
Trap-30 m	36.9243497	-122.0034216
Terrestial Imaging System (TIS)	36.960672	-122.002175
NDBC buoy	36.789	-122.404
NWIS stream gauge	36.990833	-122.030833
Harbor dredge outfall	36.9612436	-121.9997965

Table 4. Flying Eyeball sample location information.

[A minimum of three samples were taken as close to each location as possible.]

Site ID/number	Latitude [decimal degrees]	Longitude [decimal degrees]
FE 1	36.9596971	-122.02250
FE 2	36.9579024	-122.02108
FE 3	36.9542971	-122.02112
FE 4	36.9506918	-122.02117
FE 5	36.9470866	-122.02121
FE 6	36.9434813	-122.02126
FE 7	36.9615077	-122.02103
FE 8	36.9614705	-122.01654
FE 9	36.9578653	-122.01658
FE 10	36.954260	-122.01663
FE 11	36.9506547	-122.01668
FE 12	36.9470495	-122.01672
FE 13	36.9434442	-122.01677
FE 14	36.9614332	-122.01204
FE 15	36.9578280	-122.01209
FE 16	36.9542227	-122.01214
FE 17	36.9506174	-122.01218
FE 18	36.9470122	-122.01223
FE 19	36.9434069	-122.01228
FE 20	36.9613958	-122.00755
FE 21	36.9577905	-122.0076
FE 22	36.9541852	-122.00765
FE 23	36.9505800	-122.00769
FE 24	36.9469747	-122.00774
FE 25	36.9433695	-122.00779
FE 26	36.9606140	-122.00310
FE 27	36.9577529	-122.00311
FE 28	36.9541476	-122.00315
FE 29	36.9505424	-122.00320
FE 30	36.9469371	-122.00325
FE 31	36.9433319	-122.00329
FE 32	36.9598570	-121.99855
FE 33	36.9577151	-121.99861
FE 34	36.9541098	-121.99866
FE 35	36.9505046	-121.99871
FE 36	36.9468993	-121.99876
FE 37	36.9432941	-121.99880
FE 38	36.9571037	-121.99311

FE 39	36.9540719	-121.99417
FE 40	36.9504666	-121.99422
FE 41	36.9468614	-121.99426
FE 42	36.9432561	-121.99431
FE 43	36.9386683	-122.00379
FE 44	36.9339908	-122.00379
FE 45	36.9294030	-122.00357
FE 46	36.9239602	-122.00362

Table 5. Beach Ball sample location information.

[A minimum of three samples were taken in the middle of the swash zone, and three samples were taken at the wet/dry line as close to the location as possible.]

Site ID/Number	Latitude [decimal degrees]	Longitude [decimal degrees]
BB 1	36.9611924	-122.0237600
BB 2	36.9626055	-122.0206446
BB 3	36.9632251	-122.0164798
BB 4	36.9629243	-122.0117562
BB 5	36.9622105	-122.0072010
BB 6	36.9612606	-122.0031108
BB 7	36.9613768	-121.9987895
BB 8	36.9597686	-121.9942191

Table 6. Water Column Profiler cast location information.

Site ID/Number	Latitude [decimal degrees]	Longitude [decimal degrees]
WC 8	36.9614705	-122.01654
WC 9	36.9578653	-122.01658
WC 10	36.9542600	-122.01663
WC 14	36.9614332	-122.01204
WC 15	36.9578280	-122.01209
WC 16	36.9542227	-122.01214
WC 20	36.9613958	-122.00755
WC 21	36.9577905	-122.00760
WC 22	36.9541852	-122.00765
WC 26	36.9606140	-122.00310
WC 27	36.9577529	-122.00311
WC 28	36.9541476	-122.00315
WC 29	36.9505424	-122.00320
WC 30	36.9469371	-122.00325
WC 32	36.9598570	-121.99855
WC 33	36.9577151	-121.99861
WC 34	36.9541098	-121.99866
WC 38	36.9571037	-121.99311
WC 39	36.9540719	-121.99417
WC 43	36.9386683	-122.00379
WC 46	36.9239602	-122.00362

Table 7. Sediment sample location and depth information.

USGS Sample Identifier	Sample Type	Latitude [decimal degrees]	Longitude [decimal degrees]	Water Depth [m]	Sample Depth [m]
Trap-10 m	Sediment trap	36.9576419	-122.0028116	10	5
Trap-15 m	Sediment trap	36.9506359	-122.0035570	15	10
Trap-20 m	Sediment trap	36.9385923	-122.0046942	20	15
Trap-30 m	Sediment trap	36.9243497	-122.0034216	30	25
Seabed-10 m	Sea floor	36.9576419	-122.0028116	10	10
Seabed-15 m	Sea floor	36.9506359	-122.0035570	15	15
Seabed-20 m	Sea floor	36.9385923	-122.0046942	20	20
Seabed-30 m	Sea floor	36.9243497	-122.0034216	30	30
Tripod D (30 m)	Tripod	36.9237328	-122.0030674	30	28

Table 8. Sediment settling velocities.

[Assumes a sediment bulk density of 2650 kg/m^3 in 12ºC water.]

Grain Class	Grain Diameter [mm]	Settling Velocity [m/s]
Coarse sand	1.000	0.1125524
Fine sand	0.200	0.0173889
Coarse silt	0.040	0.0096930
Fine silt	0.010	0.0006241
Clay	0.003	0.0000564

Table 9. Harbor Daily Dredge Volumes.

[N.D., No dredging occurred.]

2009 Year Day	Mud-sized (<63 μm) material [m^3]	Sand-sized (>63 μm) material [m^3]	Total [m^3]
302	372	71	443
303	372	164	536
304	N.D.	N.D.	N.D.
305	N.D.	N.D.	N.D.
306	392	44	436
307	20	57	76
308	412	47	459
309	341	202	543
310	346	82	428
311	N.D.	N.D.	N.D.
312	N.D.	N.D.	N.D.
313	413	31	443
314	205	101	306
315	359	177	535
316	134	57	191
317	38	38	76
318	N.D.	N.D.	N.D.
319	N.D.	N.D.	N.D.
320	403	95	498
321	398	99	497
322	417	83	501
323	417	111	528
324	381	772	1153

Table 10. Meteorologic, oceanographic, and river discharge statistics.

[All statistics were calculated for 2009 Year Days 295-349; wind and wave direction is “From”.]

Site Name	Mean ± 1 std deviation	Minimum	Maximum
Sea level barometric pressure [mb]	1017.1±3.5	1004.1	1024.4
Water temperature [^{o}C]	12.77±0.79	11.62	15.26
Wind speed [m/s]	6.32±3.18	0.34	15.39
Wind direction [^{o}True]	264.1±109.9	0.0	359.9
Wave height [m]	2.72±1.03	0.95	6.88
Wave period [s]	13.22±3.08	4.55	23.53
Wave direction [^{o}True]	299.5±18.0	182.3	333.4
River discharge [m^3/s]	0.63±0.89	0.25	5.47

Table 11. Wave statistics.

[All statistics were calculated for 2009 Year Days 295-349; wave direction is “From”.]

Site Name	Parameter	Mean ± 1 Std Deviation	Minimum	Maximum
Tripod A (9 m)	Height [m]	0.50±0.26	0.18	1.61
	Period [s]	14.9±2.9	4.2	22.3
	Direction [^{o}True]	212.0±63.7	180.8	359.1
Tripod B (12 m)	Height [m]	0.85 ±0.36	0.30	2.55
	Period [s]	10.9±2.1	3.2	15.3
	Direction [^{o}True]	218.5±7.3	192.9	238.1
Tripod C (20 m)	Height [m]	1.00±0.35	0.40	2.46
	Period [s]	12.2±5.5	2.0	25.6
	Direction [^{o}True]	230.7±11.4	176.9	267.4
Tripod D (30 m)	Height [m]	1.18±0.38	0.52	2.72
	Period [s]	11.7±5.4	2.1	25.6
	Direction [^{o}True]	251.5±14.6	190.3	291.4

Table 12. Current statistics.

[All statistics were calculated for 2009 Year Days 295-349; current direction is “Going to”.]
[N.S., Near-surface observation.]
[N.B., Near-seabed observation.]

Site Name	Parameter	Depth [m]	Mean ± 1 Std Deviation	Minimum	Maximum
Tripod A (9 m)	Speed [m/s]	8.5 (N.B.)	0.02±0.02	0.00	0.28
	Direction [°True]	8.5 (N.B.)	198.65±101.10	0.15	356.79
Tripod B (12 m)	Speed [m/s]	1.0 (N.S.)	0.052±0.03	0.00	0.21
	Direction [°True]	1.0 (N.S.)	155.8±93.7	0.0	359.9
	Speed [m/s]	11.0 (N.B.)	0.045±0.02	0.00	0.15
	Direction [°True]	11.0 (N.B.)	159.9±100.2	0.0	359.9
Tripod C (20 m)	Speed [m/s]	1.0 (N.S.)	0.08±0.05	0.00	0.30
	Direction [°True]	1.0 (N.S.)	187.9±84.1	14.3	359.5
	Speed [m/s]	17.5 (N.B.)	0.03±0.02	0.00	0.13
	Direction [°True]	17.5 (N.B.)	184.9±81.4	14.2	358.7
Tripod D (30 m)	Speed [m/s]	1.0 (N.S.)	0.09±0.05	0.00	0.31
	Direction [°True]	1.0 (N.S.)	164.6±80.6	0.8	358.6
	Speed [m/s]	26.5 (N.B.)	0.05±0.03	0.00	0.17
	Direction [°True]	26.5 (N.B.)	159.9±100.2	0.0	359.9

Table 13. Turbidity statistics.

[All statistics were calculated for 2009 Year Days 295-349.]

Site Name	Time Period [2009 Year Days]	Depth [m]	Mean ± 1 Std Deviation [NTU]	Minimum [NTU]	Maximum [NTU]
Tripod A (9 m)	Experiment [295-349]	8.5	39±41	1	118
	Pre-Dredging [295-301]	8.5	45±47	1	118
	Dredging [302-324]	8.5	36±39	1	79
	Post-Dredging [325-339]	8.5	36±33	3	36
	Storm and Flood [340-349]	8.5	41±38	1	74
Tripod B (12 m)	Experiment [295-349]	11	29±35	0	311
	Pre-Dredging [295-301]	11	11±7	1	53
	Dredging [302-324]	11	20±33	0	245
	Post-Dredging [325-339]	11	43±39	2	311
	Storm and Flood [340-349]	11	37±31	2	261
Tripod C (20 m)	Experiment [295-349]	18	6±6	1	61
	Pre-Dredging [295-301]	18	5±0	1	23
	Dredging [302-324]	18	5±36	1	32
	Post-Dredging [325-339]	18	8±7	2	42
	Storm and Flood [340-349]	18	11±16	1	61
	Experiment [295-349]	19.5	22±36	0	490
	Pre-Dredging [295-301]	19.5	8±7	1	48
	Dredging [302-324]	19.5	11±16	0	159
	Post-Dredging [325-339]	19.5	31±26	1	184
	Storm and Flood [340-349]	19.5	47±70	1	490
Tripod D (30 m)	Experiment [295-349]	29.5	17±20	2	693
	Pre-Dredging [295-301]	29.5	11±6	4	52
	Dredging [302-324]	29.5	14±16	3	132
	Post-Dredging [325-339]	29.5	22±19	4	169
	Storm and Flood [340-349]	29.5	23±32	2	693

Table 14. Temperature statistics.

[All statistics were calculated for 2009 Year Days 295-349.]

Site Name	Depth [m]	Mean ± 1 Std Deviation [^{o}C]	Minimum [^{o}C]	Maximum [^{o}C]
Tripod B (12 m)	11	12.12±0.79	10.89	14.31
Tripod C (20 m)	20	11.85±0.66	10.82	13.79
Tripod D (30 m)	30	11.58±0.56	10.56	13.59

Table 15. Salinity statistics.

[All statistics were calculated for 2009 Year Days 295-349.]

Site Name	Depth [m]	Mean ± 1 Std Deviation [PSU]	Minimum [PSU]	Maximum [PSU]
Tripod B (12 m)*	12	31.06±0.1.87	23.41	33.23
Tripod C (20 m)	19	33.43±0.06	33.14	33.59
Tripod D (30 m)	29	33.35±0.11	33.10	33.61

*Statistics are low due to biofouling of the sensor's doivity cell.

Table 16. Sediment sample grain-size information.

[N.D., No data.]

USGS Sample Identifier	Average Trap Collection Rate [mg/cm^2/day]	Gravel [percent]	Sand [percent]	Silt [percent]	Clay [percent]	Mud [percent]	Mean Size [mm]
Trap-10 m	0.676	0.00	16.34	62.51	21.15	86.91	0.0260
Trap-15 m	0.827	0.00	13.42	65.03	21.55	86.58	0.0249
Trap-20 m	0.824	0.00	16.63	63.22	20.15	87.80	0.0267
Trap-30 m	0.754	0.00	9.79	69.60	20.60	86.81	0.0227
Seabed-10 m	N.D.	0.04	69.15	23.92	6.89	88.36	0.0822
Seabed-15 m	N.D.	0.00	97.04	2.04	0.93	95.08	0.3702
Seabed-20 m	N.D.	0.17	83.55	13.04	3.23	97.76	0.1279
Seabed-30 m	N.D.	4.33	81.84	10.89	2.93	75.72	0.1232
Tripod D (30 m)	N.D.	0.00	47.06	41.78	11.16	67.24	0.0552

Table 17. Carbon and Nitrogen Signatures of Sediment Samples.

USGS sample identifier	Time frame [2009 Year Days]	C [percent]	N [percent]	$\delta^{15}N$	$\delta^{13}C$	C/N [molar ratio]
Trap-10 m	292-313	1.95	0.275	7.77	-21.65	8.3
Trap-15 m*	292-313	2.06	0.277	6.01	-21.26	8.7
Trap-20 m	292-313	1.83	0.236	7.19	-21.98	9.1
Trap-30 m	292-313	1.20	0.153	6.03	-22.56	9.2
Trap-10 m	313-336	2.60	0.343	6.74	-22.17	8.8
Trap-20 m	313-336	2.27	0.295	5.54	-21.98	9.0
Trap-30 m	313-336	2.00	0.219	6.43	-23.32	10.7
Trap-10 m	336-349	1.19	0.159	6.28	-21.86	8.7
Trap-20 m	336-349	1.18	0.147	5.89	-21.77	9.3
Trap-30 m	336-349	1.19	0.154	2.61	-22.09	9.0
Tripod D (30 m)	After 350	1.05	0.129	5.11	-20.91	9.5
Seabed-10 m	After 350	0.28	0.043	3.33	-24.02	7.6
Seabed-15 m	After 350	0.34	0.041	1.85	-22.73	9.7
Seabed-20 m	After 350	0.26	0.033	2.38	-22.17	9.2
Seabed-30 m	After 350	0.33	0.041	0.74	-23.79	9.3
A1 - harbor	Before 302	2.48	0.21	5.18	-25.58	14.1
A2 - harbor	Before 302	3.33	0.25	4.75	-25.70	15.4
A2A - harbor	Before 302	2.05	0.15	3.74	-25.05	15.6
A3 - harbor	Before 302	3.99	0.32	5.80	-25.50	14.5
A4 - harbor	Before 302	1.93	0.17	4.00	-24.87	13.6

*Data is available only for the Mooring-15 m's first sampling period because it was destroyed sometime after 2009 Year Day 313.

Table 18. Short-lived Radionuclide Activity in Sediment Samples.

[Radionuclide activity in disintegrations per minute per gram [dpm/g] in sediment. Excess ^{210}Pb ($^{210}Pb_{xs}$) is calculated as the difference between total ^{210}Pb activity and ^{226}Ra activity.]

USGS sample identifier	Time frame [2009 Year Days]	^{7}Be [dpm/g]	^{210}Pb [dpm/g]	Mean ^{226}Ra [dpm/g]	$^{210}Pb_{xs}$ [dpm/g]	^{137}Cs [dpm/g]	^{234}Th [dpm/g]	$^{234}Th/^{226}Ra$	$^{7}Be:^{210}Pb_{xs}$
Trap-10 m	292-313	0.66±0.40	4.2±0.4	1.0±0.1	3.3±0.4	0.04±0.01	7.4±0.39	7.65	0.20
Trap-15 m*	292-313	1.14±0.40	8.7±0.4	2.3±0.1	6.4±0.4	0.14±0.08	15.5±0.45	6.87	0.18
Trap-20 m	292-313	0.87±0.97	10.5±0.8	2.7±0.1	7.8±0.8	0.11±0.05	4.5±0.60	1.65	0.11
Trap-30 m	292-313	0.00±0.00	10.6±1.3	2.7±0.1	8.0±1.3	0.18±0.07	5.2±0.70	1.97	0.00
Trap-10 m	313-336	0.00±0.00	10.0±0.9	2.5±0.2	7.5±0.9	0.22±0.06	10.3±0.70	4.18	0.00
Trap-20 m	313-336	0.00±0.00	15.1±1.0	1.8±0.2	13.4±1.0	0.41±0.18	17.1±0.87	9.77	0.00
Trap-30 m	313-336	0.31±0.25	10.1±0.9	2.4±0.2	7.7±0.9	0.26±0.09	13.5±0.89	5.52	0.04
Trap-10 m	336-349	1.82±0.78	4.6±0.5	2.3±0.1	2.2±0.6	0.08±0.02	4.2±0.41	1.79	0.82
Trap-20 m	336-349	1.88±0.73	6.0±0.5	2.3±0.1	3.7±0.5	0.10±0.03	37.1±2.89	15.87	0.52
Trap-30 m	336-349	0.92±0.58	7.0±0.7	1.9±0.1	5.1±0.7	0.11±0.03	7.2±0.52	3.82	0.18
Tripod D (30 m)	After 350	0.19±0.75	5.7±0.6	1.9±0.1	3.7±0.6	0.08±0.02	3.1±0.39	1.59	0.05
Seabed-10 m	After 350	0.08±0.51	4.1±0.4	2.7±0.1	1.4±0.4	0.00±0.00	3.3±0.44	1.20	0.06
Seabed-15 m	After 350	0.37±0.53	4.8±0.5	4.0±0.1	0.8±0.5	0.03±0.01	3.8±0.59	0.95	0.48
Seabed-20 m	After 350	0.28±0.49	5.7±0.6	5.6±0.1	0.1±0.6	0.03±0.02	6.1±0.47	1.08	2.01
Seabed-30 m	After 350	0.00±0.00	4.1±0.5	2.5±0.1	1.6±0.5	0.06±0.02	2.6±0.35	1.06	0.00
A1 - harbor	Before 302	3.05±2.69	3.0±0.5	1.8±0.1	1.2±0.5	0.15±0.04	1.6±0.46	0.90	2.57
A2 - harbor	Before 302	0.00±0.00	2.7±0.4	1.8±0.1	0.9±0.4	0.10±0.02	1.0±0.40	0.53	0.00
A2A - harbor	Before 302	3.54±2.70	1.8±0.3	2.5±0.1	-0.7±0.4	0.00±0.00	1.7±0.32	0.70	-5.29
A3 - harbor	Before 302	0.00±0.00	4.4±0.4	1.7±0.1	2.7±0.4	0.27±0.08	2.0±0.31	1.16	0.00
A4 - harbor	Before 302	0.00±0.00	2.2±0.4	2.8±0.1	-0.6±0.4	0.00±0.00	2.2±0.44	0.81	0.00

*Data is available only for the Mooring-15 m's first sampling period because it was destroyed sometime after 2009 Year Day 313.

Table 19. Elemental composition of harbor sediment samples.

[Elemental composition of sediment in parts per million (ppm) as determined by mass spectrometry. Sediment collected before 2009 Year Day 302. "<1" is below the analytical detection limit.]

Element	A1-harbor	A2-harbor	A2A-harbor	A3-harbor	A4-harbor
Ag	<1	<1	<1	<1	<1
Al	71200	78300	74900	78000	73300
As	7.4	9.9	5.8	12.6	5.7
Ba	674	638	725	583	758
Be	1.5	1.4	1.3	1.5	1.3
Ca	18100	14400	19900	13000	16700
Ce	36.6	40.6	34.9	43.8	31.6
Co	10.3	12.3	10.5	10.8	10.7
Cr	66.1	78.2	64.1	85.6	87.9
Cs	3.4	4.2	2.9	4.7	3.2
Cu	86.8	98.2	60.8	158	23.3
Fe	33300	39200	29800	41400	28900
Ga	16.7	17.9	16.2	18.1	15.6
K	14500	14200	15000	15400	16200
La	18.7	20.2	17.3	21.9	15.8
Li	30.5	33.7	25.8	41.5	30.1
Mg	9560	9820	9270	10600	8940
Mn	360	419	344	281	561
Mo	1.5	1.8	1.4	2.4	2.8
Na	23000	23100	25100	23100	19700
Nb	7.8	7.5	7.2	7.9	6.7
Ni	28.6	38.6	26.8	40.6	49.5
P	741	872	454	910	364
Pb	23	27.9	23	31.3	17.4
Rb	62.8	67.4	61.2	75.7	66.4
Sb	1.1	0.9	0.68	1	0.75
Sc	12.3	13.8	11.5	13.6	11.3
Sr	312	269	352	234	286
Th	5.81	6.66	4.93	7.65	4.95
Ti	3850	3770	3780	3720	3150
Tl	0.5	0.48	0.38	0.54	0.44
U	1.98	2.36	2.03	2.62	2.32
V	106	119	97	123	89.7
Y	14.2	16.4	13.7	17	13.1
Zn	140	174	111	230	67.7

Table 20. Elemental composition of trap sediment: First deployment.

[Elemental composition of sediment in parts per million (ppm) as determined by mass spectrometry. Sediment collected 2009 Year Days 292-313.]

Element	Trap-10 m	Trap-15 m	Trap-20 m	Trap-30 m
Ag	<1	<1	<1	<1
Al	56600	58000	56200	57000
As	6.8	5.9	6	5.2
Ba	788	812	753	786
Be	1.6	1.6	1.3	1.3
Ca	16000	12700	12100	10800
Ce	42.1	42.5	42.2	39.9
Co	5	5.4	6.4	6.3
Cr	54	55.4	63.7	61
Cs	3.6	3.6	3.8	3.7
Cu	21.1	18.7	18	15.8
Fe	19600	19800	21600	20300
Ga	13.2	13.8	13.1	13
K	16900	17700	16200	16800
La	21.8	21.3	21.4	20.3
Li	26.8	26.7	30.8	30
Mg	7460	7880	8970	8380
Mn	183	187	207	196
Mo	1.5	1.4	1.2	0.93
Na	21100	22400	22200	19400
Nb	9.3	9.2	9.2	8.6
Ni	26.4	29.3	38.4	38.1
P	933	926	838	616
Pb	16.7	15.7	14.8	13.1
Rb	82.9	85.7	81.9	83.9
Sb	0.88	0.51	0.53	0.42
Sc	7	6.8	7.5	7.2
Sr	298	278	262	263
Th	7.53	7.1	8.03	7.5
Ti	2510	2540	2690	2530
Tl	0.54	0.49	0.46	0.49
U	2.56	2.53	2.47	2.29
V	68	67.3	72	69.2
Y	13.2	12.6	13.1	12.2
Zn	64	62.2	61.9	54.7

Table 21. Elemental composition of trap sediment: Second deployment*.

[Elemental composition of sediment in parts per million (ppm) as determined by mass spectrometry. Sediment collected 2009 Year Days 313-336.]

Element	Trap-10 m	Trap-20 m	Trap-30 m
Ag	<1	<1	<1
Al	49800	54800	70600
As	7.5	8.2	6.8
Ba	673	656	634
Be	1.2	1.5	1.3
Ca	15100	12900	16600
Ce	39.3	45	35.4
Co	5.3	7.3	8.3
Cr	55.5	76.6	88.4
Cs	3.9	4.7	4.4
Cu	32	23.2	22.2
Fe	20900	25500	30900
Ga	12.3	13.7	15.5
K	14700	15200	20100
La	19.6	22.8	17.7
Li	29	36.5	37.7
Mg	8810	12400	15300
Mn	171	211	245
Mo	1.5	1.5	1.4
Na	29800	35500	33100
Nb	7.8	9	8.3
Ni	29.1	49.7	54.8
P	905	972	861
Pb	17.1	15.9	13.5
Rb	76.3	83.8	87.4
Sb	0.45	0.63	0.62
Sc	7.2	8.6	10.3
Sr	272	266	240
Th	6.84	9.03	6.78
Ti	2340	2720	3120
Tl	0.42	0.46	0.49
U	2.44	2.64	2.16
V	70.7	85.8	94.1
Y	12.4	13.4	12.7
Zn	72.3	74	79.3

*Trap-15 m was destroyed sometime during this deployment; no sample was recovered.

Table 22. Elemental composition of trap sediment: Third deployment*.

[Elemental composition of sediment in parts per million (ppm) as determined by mass spectrometry. Sediment collected 2009 Year Days 336-349.]

Element	Trap-10 m	Trap-20 m	Trap-30 m
Ag	<1	<1	<1
Al	66400	68900	68200
As	6	5.6	5.9
Ba	789	806	741
Be	1.2	1.2	1.4
Ca	22200	18600	16700
Ce	32.1	35	31.1
Co	4.3	5.4	6.5
Cr	43	52	67.3
Cs	2.7	2.9	3.3
Cu	16.6	13.2	15.7
Fe	17600	20000	23200
Ga	13.4	14.1	14.3
K	22300	22400	21200
La	16.3	17.7	15.6
Li	19.4	21.4	26
Mg	7920	9370	12400
Mn	194	232	219
Mo	1.1	0.9	0.9
Na	34100	33200	43100
Nb	7.8	8.5	7.7
Ni	18.6	27.2	39.4
P	814	769	774
Pb	13.4	13.1	12.2
Rb	79.7	81.5	80.5
Sb	0.5	0.64	0.51
Sc	6.4	7.3	8.2
Sr	308	290	269
Th	5.36	6.02	5.93
Ti	2530	2840	2720
Tl	0.43	0.42	0.44
U	1.89	1.87	1.78
V	59.9	67.7	73.3
Y	11.5	12.5	11.2
Zn	56	53.7	58.8

*Trap-15 m was destroyed during the previous deployment; no sample was recovered.

Table 23. Elemental composition of seabed and tripod sediment samples.

[Elemental composition of sediment in parts per million (ppm) as determined by mass spectrometry. Sediment collected after 2009 Year Day 350.]

Element	Seabed-10 m	Seabed-15 m	Seabed-20 m	Seabed-30 m	Tripod D (30 m)
Ag	<1	<1	<1	<1	<1
Al	64500	63900	74100	67300	66900
As	3.2	4.2	4.2	4.1	6
Ba	939	881	986	908	777
Be	1.2	1.2	1.4	1.3	1.2
Ca	19500	18800	24100	16200	18400
Ce	37.2	53.2	65.4	35.4	34.7
Co	3.1	3.7	5.6	4.1	5.8
Cr	28	36.5	47.6	34.2	59.1
Cs	1.7	1.8	1.8	2	3.1
Cu	6.2	7.9	9.3	6.9	14.6
Fe	12000	14800	20700	14200	22300
Ga	12.8	13.5	15.8	13.4	14.1
K	24100	23400	26200	24300	22200
La	17.9	25.9	30.5	17.2	17.4
Li	10.6	12.1	12.9	16.6	22.3
Mg	4550	5200	7150	5380	9270
Mn	245	338	530	216	224
Mo	0.65	0.78	0.78	0.53	0.99
Na	24700	24600	27300	24800	29700
Nb	10	14	19	8.6	7.7
Ni	7.9	10.2	12.3	15.4	28.5
P	564	794	882	524	705
Pb	12.3	12.7	13.7	11.8	14
Rb	80.8	78.9	83.9	81.8	82.2
Sb	0.38	0.81	0.62	0.39	0.47
Sc	5.4	6.4	8.7	5.9	7.7
Sr	301	285	330	292	284
Th	4.89	18	8.38	6.1	6.04
Ti	2940	4220	6140	2570	2700
Tl	0.4	0.51	0.45	0.48	0.47
U	1.86	3.29	2.79	1.74	2.13
V	43.2	52.5	74.3	46.5	67.9
Y	13.6	17.8	23.3	11.9	11.7
Zn	32.9	40.2	47.7	36.2	57.4

Table 24. Sediment-flux statistics.

[All statistics were calculated for 2009 Year Days 295-349. Direction is “Going to”.]

Site name	Time period [2009 Year Days]	Depth [m]	Total sediment flux [metric tons/m^2]	Average daily sediment flux [metric tons/m^2]	Direction [^{o}True]
Tripod A (9 m)	Experiment [295-349]	8.5	163.98[1]	5.47[1]	140.5[1]
	Pre-Dredging [295-301]	8.5	53.10[2]	10.62[2]	257.5[2]
	Dredging [302-324]	8.5	179.54[3]	11.97[3]	122.1[3]
	Post-Dredging [325-339]	8.5	0.42[4]	0.42[4]	94.8[4]
	Storm and Flood [340-349]	8.5	42.85[5]	4.76[5]	167.6[5]
Tripod B (12 m)	Experiment [295-349]	3	2.16	0.04	139.4
	Pre-Dredging [295-301]	3	0.48	0.07	194.5
	Dredging [302-324]	3	0.85	0.04	128.8
	Post-Dredging [325-339]	3	0.79	0.05	113.2
	Storm and Flood [340-349]	3	0.24	0.02	120.1
	Experiment [295-349]	9	6.77	0.12	81.8
	Pre-Dredging [295-301]	9	6.67	0.95	31.2
	Dredging [302-324]	9	0.64	0.03	128.5
	Post-Dredging [325-339]	9	4.58	0.31	113.2
	Storm and Flood [340-349]	9	8.83	0.88	120.1
	Experiment [295-349]	10.5	7585.42	137.92	89.2
	Pre-Dredging [295-301]	10.5	105.46	15.07	26.1
	Dredging [302-324]	10.5	1505.45	65.45	80.8
	Post-Dredging [325-339]	10.5	990.65	66.04	63.5
	Storm and Flood [340-349]	10.5	442.63	44.26	166.1
Tripod C (20 m)	Experiment [295-349]	3	4.47	0.08	259.5
	Pre-Dredging [295-301]	3	0.73	0.10	82.7
	Dredging [302-324]	3	1.77	0.08	261.5
	Post-Dredging [325-339]	3	0.28	0.02	123.1
	Storm and Flood [340-349]	3	3.57	0.36	263.4
	Experiment [295-349]	16.5	21.75	0.40	237.1
	Pre-Dredging [295-301]	16.5	2.89	0.41	78.8
	Dredging [302-324]	16.5	8.65	0.38	232.9
	Post-Dredging [325-339]	16.5	1.18	0.08	317.9
	Storm and Flood [340-349]	16.5	15.97	1.60	238.9
	Experiment [295-349]	19.5	36172.52	657.68	17.1
	Pre-Dredging [295-301]	19.5	220.08	31.44	21.6
	Dredging [302-324]	19.5	3706.55	161.15	29.2
	Post-Dredging [325-339]	19.5	4650.62	310.04	21.7
	Storm and Flood [340-349]	19.5	1769.84	176.98	358.9
Tripod D (30 m)	Experiment [295-349]	3	3.15	0.06	273.4
	Pre-Dredging [295-301]	3	0.19	0.03	212.4
	Dredging [302-324]	3	0.58	0.03	268.4
	Post-Dredging [325-339]	3	0.36	0.02	239.9
	Storm and Flood [340-349]	3	2.24	0.22	286.6

	Experiment [295-349]	26.5	28.85	0.52	258.7
	Pre-Dredging [295-301]	26.5	1.84	0.26	132.5
	Dredging [302-324]	26.5	10.68	0.46	257.4
	Post-Dredging [325-339]	26.5	2.43	0.16	287.7
	Storm and Flood [340-349]	26.5	16.83	1.68	261.1
	Experiment [295-349]	29.5	55388.58	1007.07	60.1
	Pre-Dredging [295-301]	29.5	494.65	70.66	84.8
	Dredging [302-324]	29.5	10,843.21	471.44	47.0
	Post-Dredging [325-339]	29.5	6248.29	416.55	68.5
	Storm and Flood [340-349]	29.5	910.25	91.03	74.4

[1]Missing data from 2009 Year Days 298-299, 305, 309-311, 321-338, and 341.
[2]Missing data from 2009 Year Days 298-299.
[3]Missing data from 2009 Year Days 305, 309-311, and 321-324.
[4]Missing data from 2009 Year Days 325-338.
[5]Missing data from 2009 Year Day 341.

Appendix 1

Optical Backscatter Sensor (OBS) Suspended Sediment Concentration (SSC) Calibration Information

Sample	Sample volume [l]	Sediment mass [g]	Concentration [mg/l]	OBS [NTU]
SCH-1	10	0.004	7.86	2
SCH-2	10	0.049	92.28	14
SCH-3	10	0.640	1189.59	169

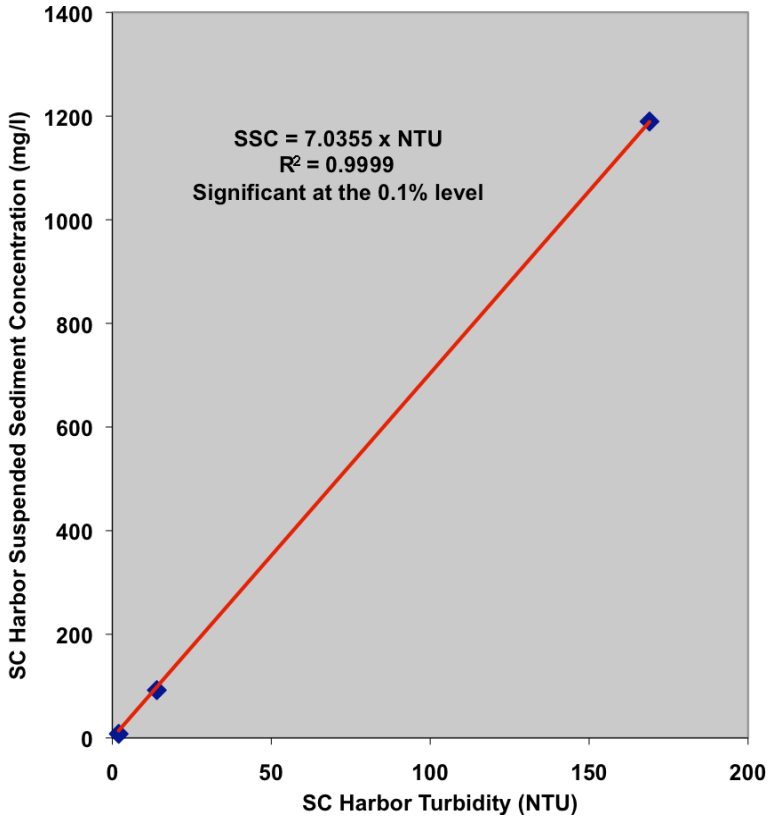

Sample	Sample volume [l]	Sediment mass [g]	Concentration [mg/l]	OBS [NTU]
SFO-1	50	2.632	52.64	0.0845
SFO-2	50	5.109	102.18	0.1103
SFO-3	50	10.106	202.12	0.1677
SFO-6	50	37.548	750.96	0.4953
SFO-10	50	125.230	2504.60	1.0833

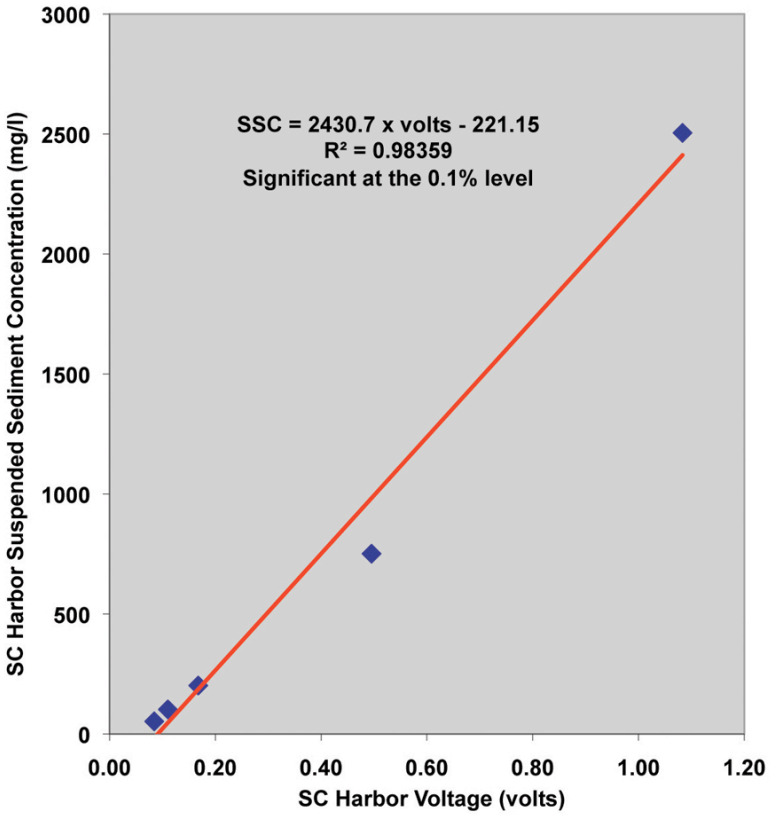

Appendix 2

Acoustic Doppler Current Meters (ADCM) Suspended Sediment Concentration (SSC) Calibration Information

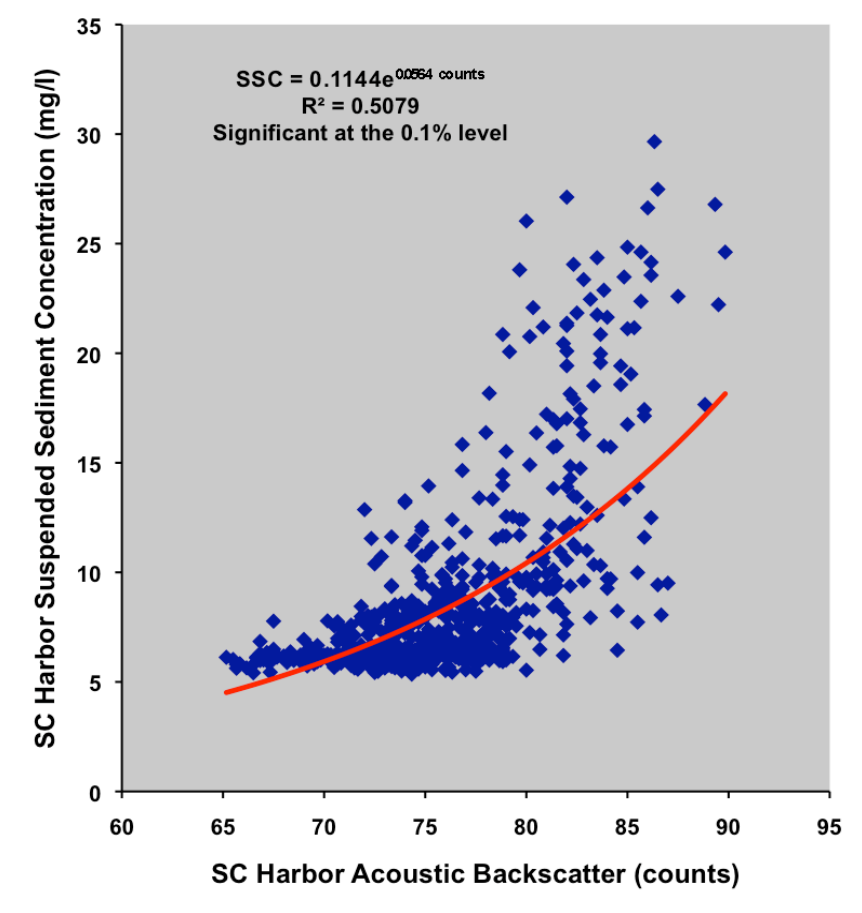

Appendix 3

Water Column Profiler (WCP) Optical Backscatter (OBS) Profiles

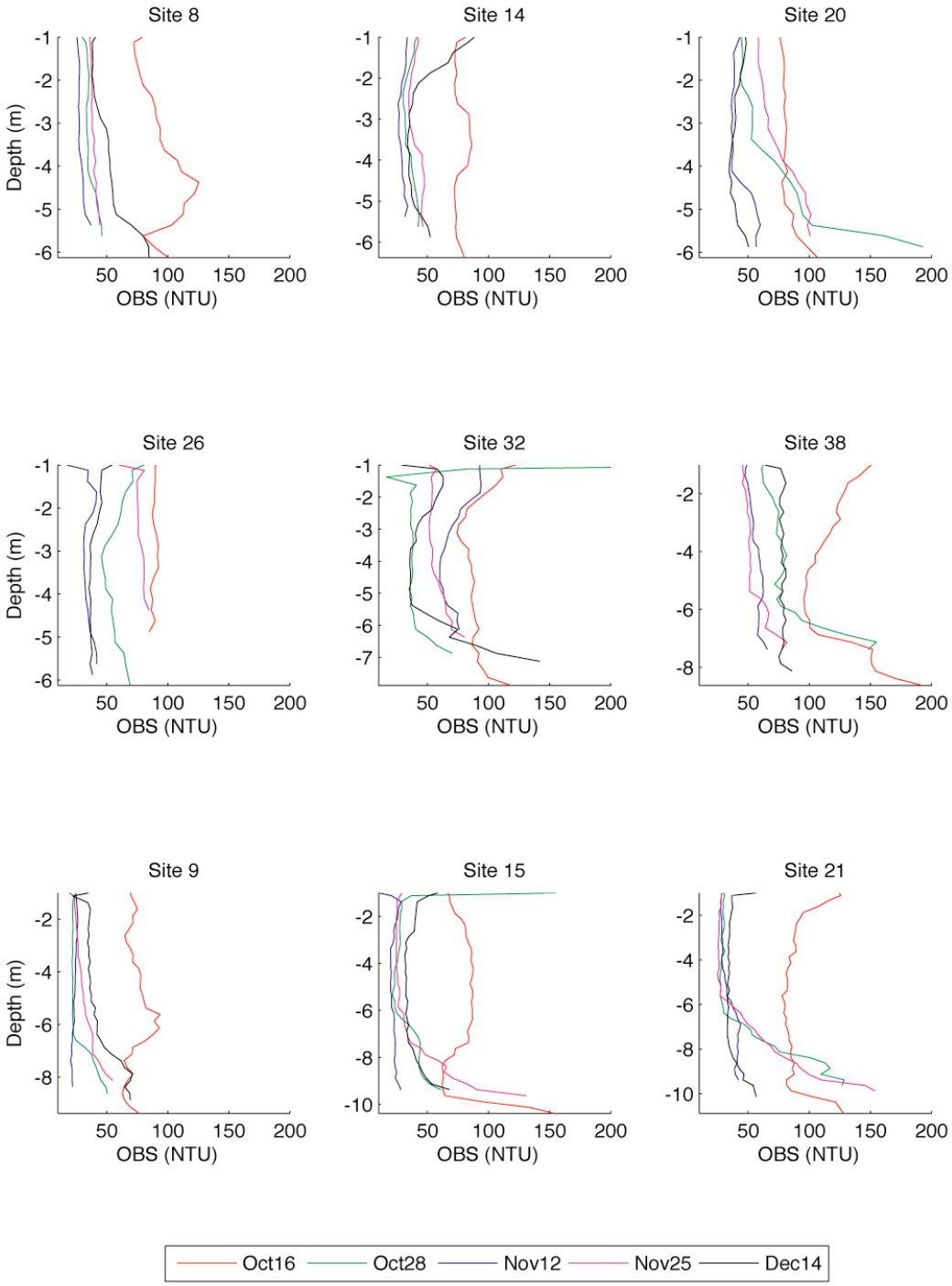

Appendix 3.1: Profiles of variation in turbidity, in National Turbidity Units, with depth for the 5 water-column surveys.

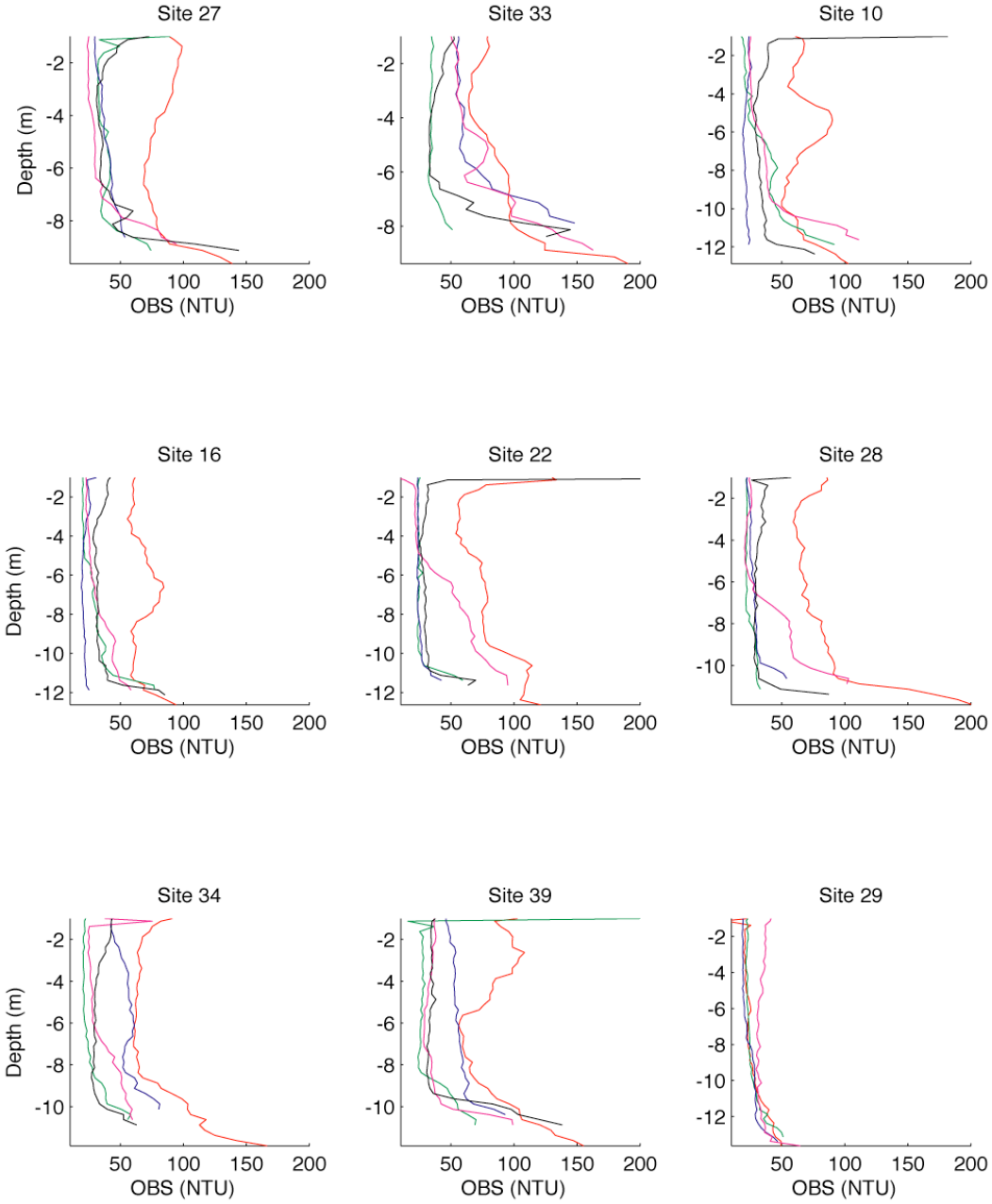

Appendix 3.2: Profiles of variation in turbidity, in National Turbidity Units, with depth for the 5 water-column surveys. Colors same as Appendix 3.1.

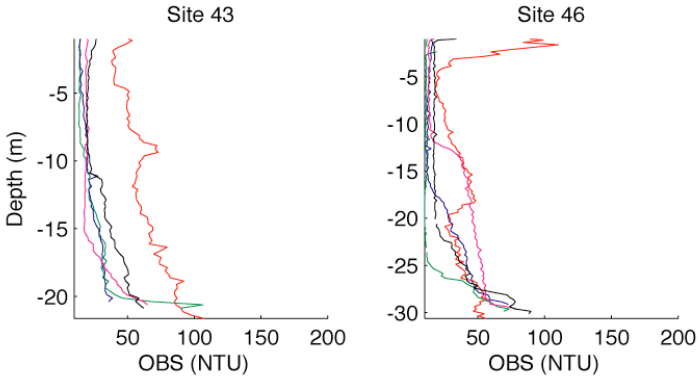

Appendix 3.3: Profiles of variation in turbidity, in National Turbidity Units, with depth for the 5 water-column surveys. Colors same as Appendix 3.1.

Appendix 4
Water Column Profiler (WCP) Light Transmission (Xmiss) Profiles

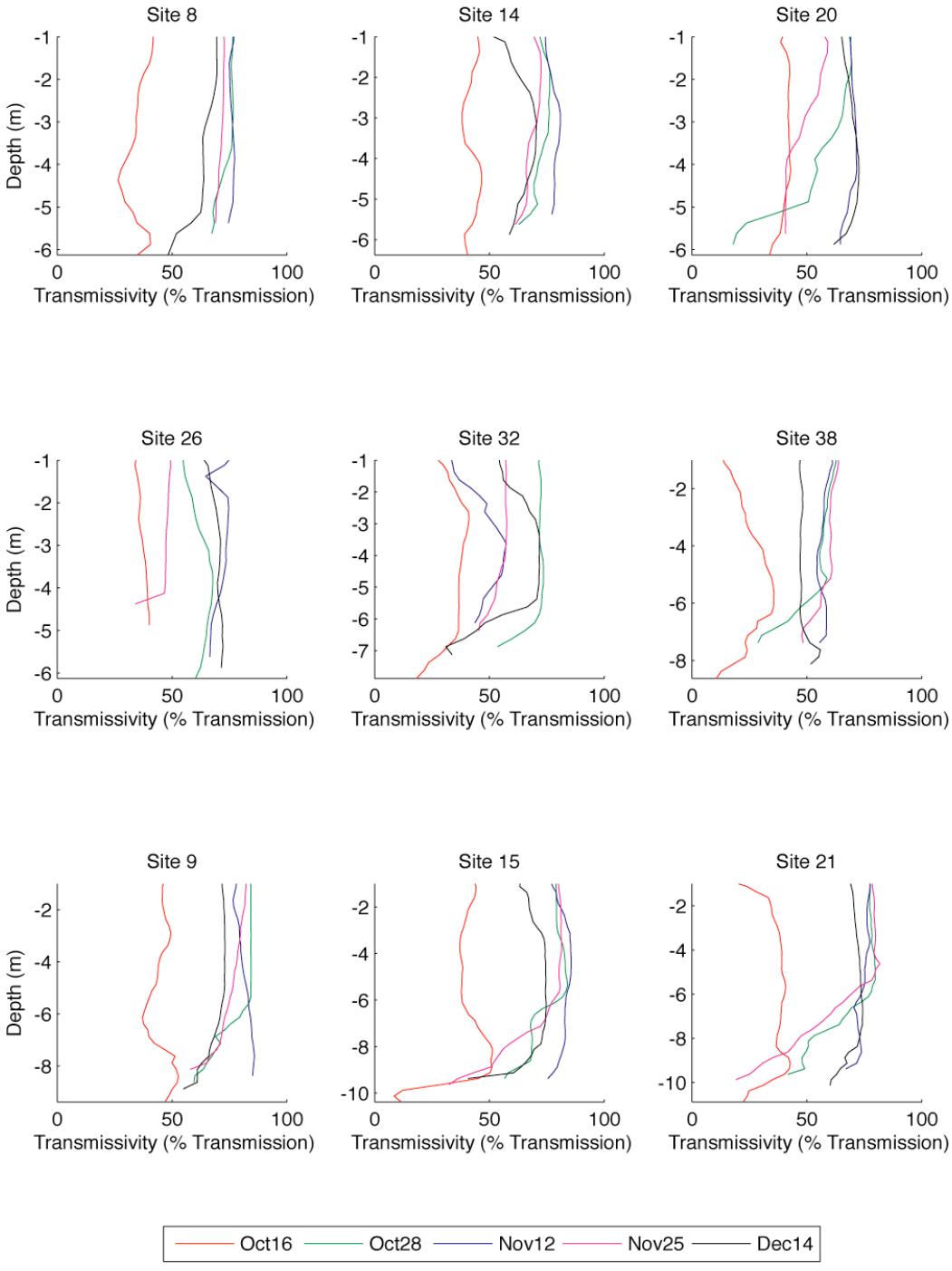

Appendix 4.1: Profiles of variation in light transmission, in precent, with depth for the 5 water-column surveys.

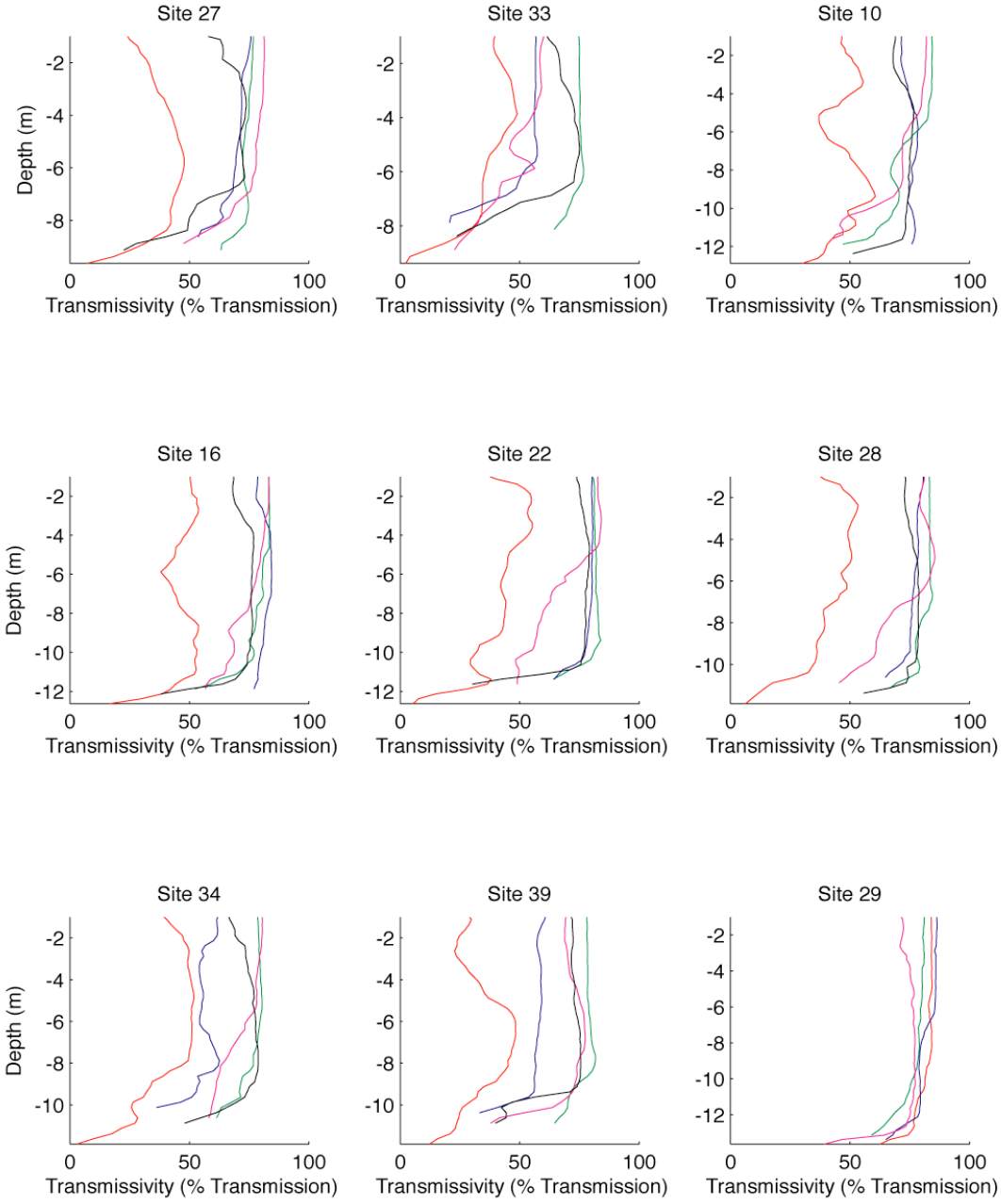

Appendix 4.2: Profiles of variation in light transmission, in precent, with depth for the 5 water-column surveys. Colors same as Appendix 4.1.

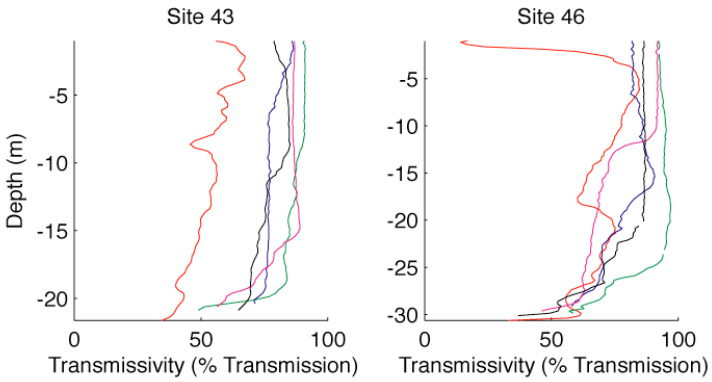

Appendix 4.3: Profiles of variation in light transmission, in precent, with depth for the 5 water-column surveys. Colors same as Appendix 4.1.

Appendix 5
Water Column Profiler (WCP) Chlorophyll (chl) Profiles

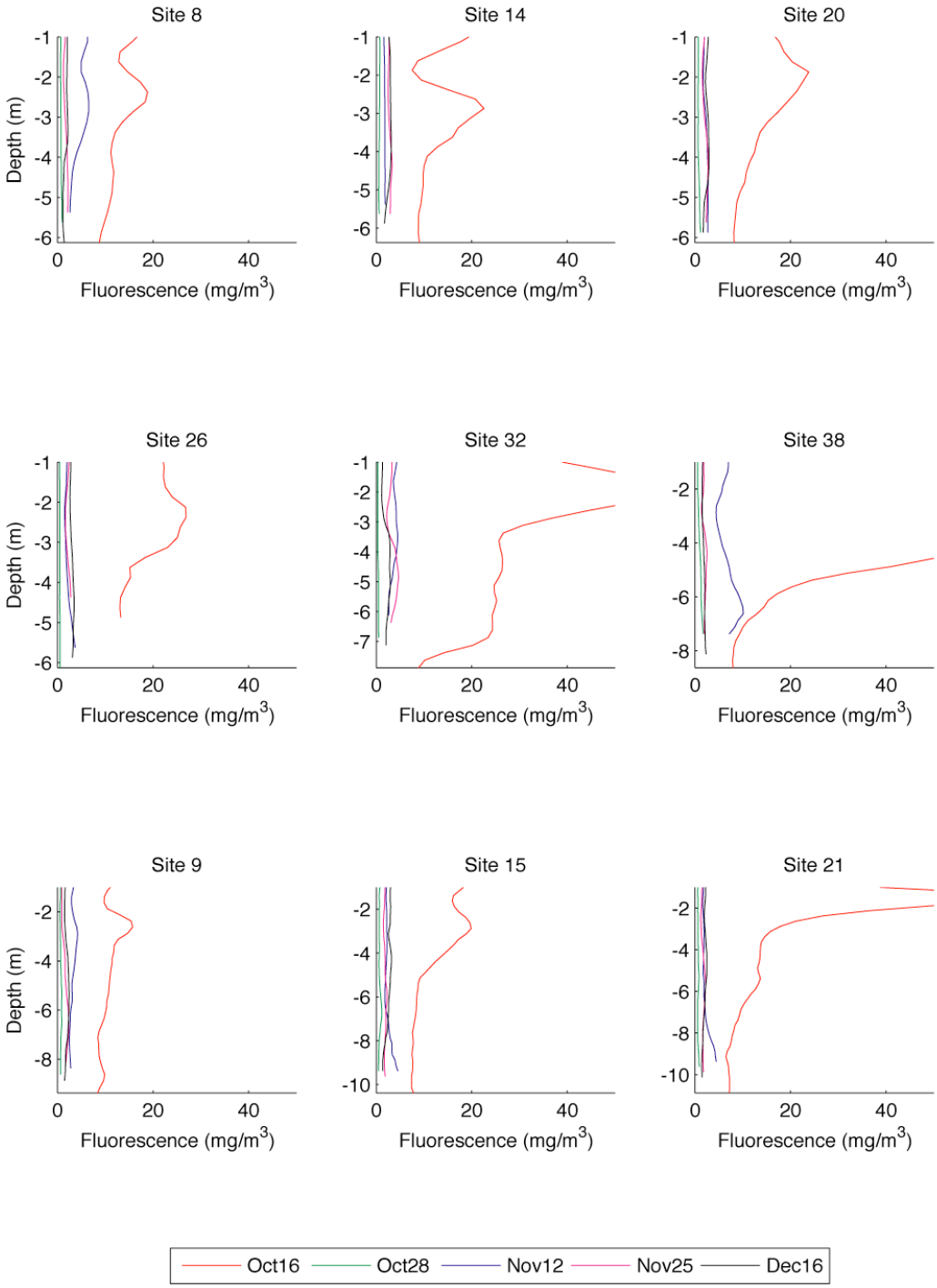

Appendix 5.1: Profiles of variation in chlorophyll, in milligrams per cubic meter, with depth for the 5 water-column surveys.

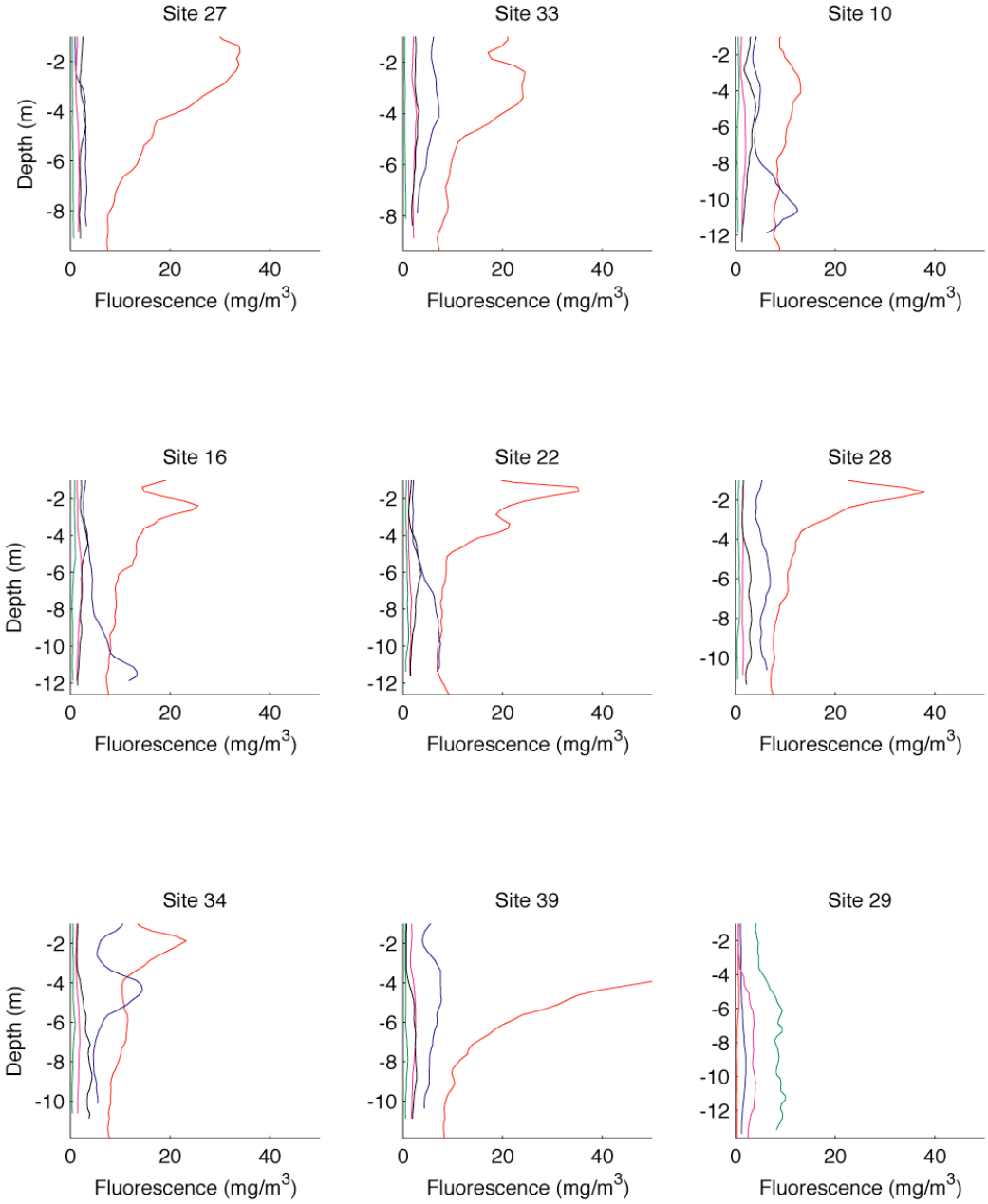

Appendix 5.2: Profiles of variation in chlorophyll, in milligrams per cubic meter, with depth for the 5 water-column surveys. Colors same as Appendix 5.1.

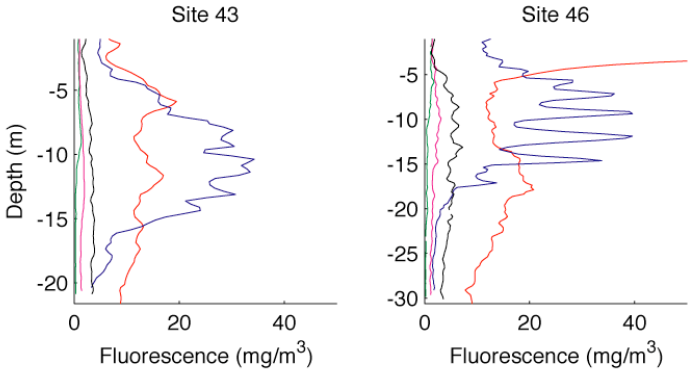

Appendix 5.3: Profiles of variation in chlorophyll, in milligrams per cubic meter, with depth for the 5 water-column surveys. Colors same as Appendix 5.1.

Appendix 6
Beach Ball (BB) and Flying Eyeball (FE) Surficial Grain-Size Measurements

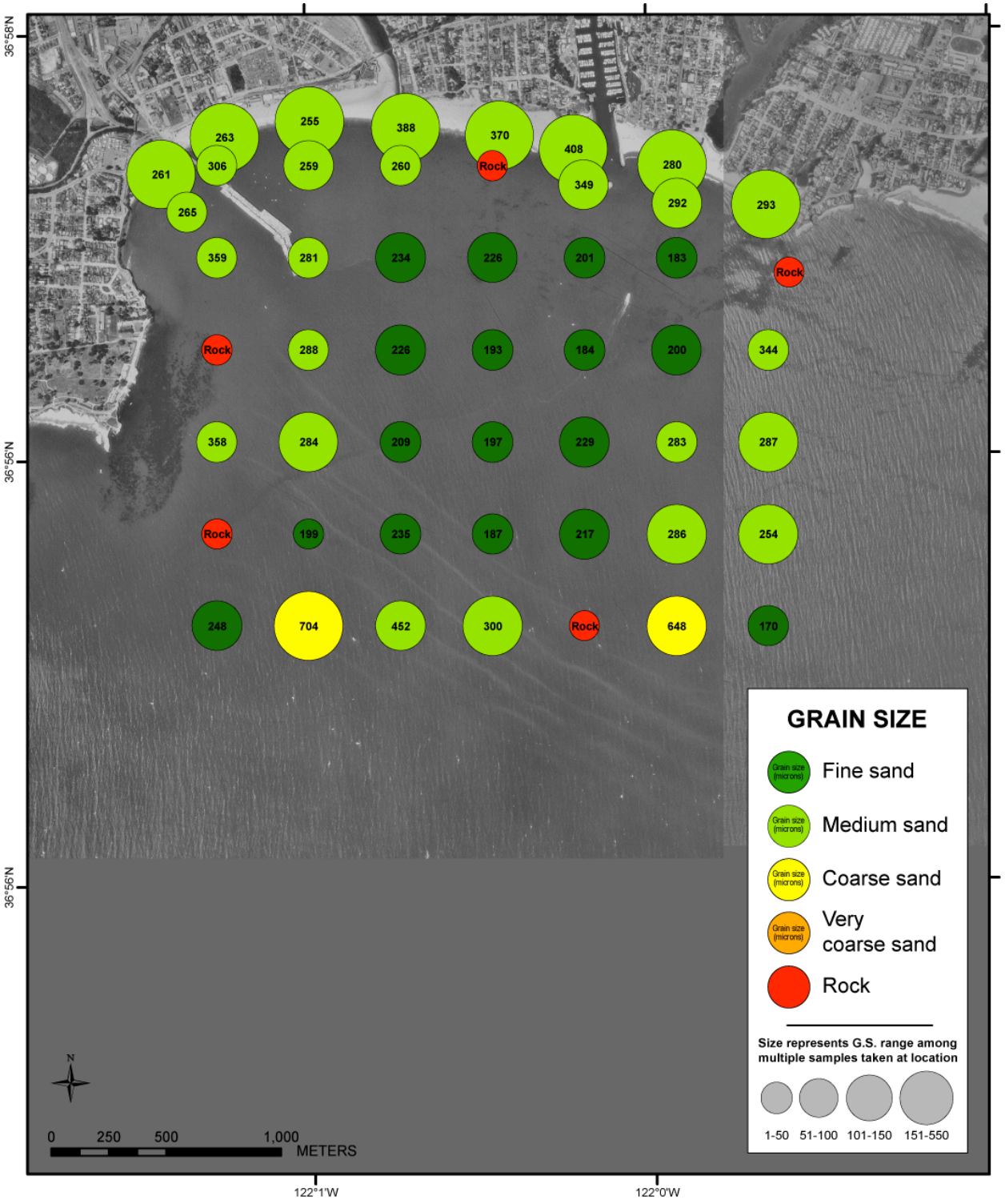

Appendix 6.1: Spatial variation in mean grain size and variability in grain size, in microns, for the grain-size surveys on 10/23/2009 (2009 Year Day 296).

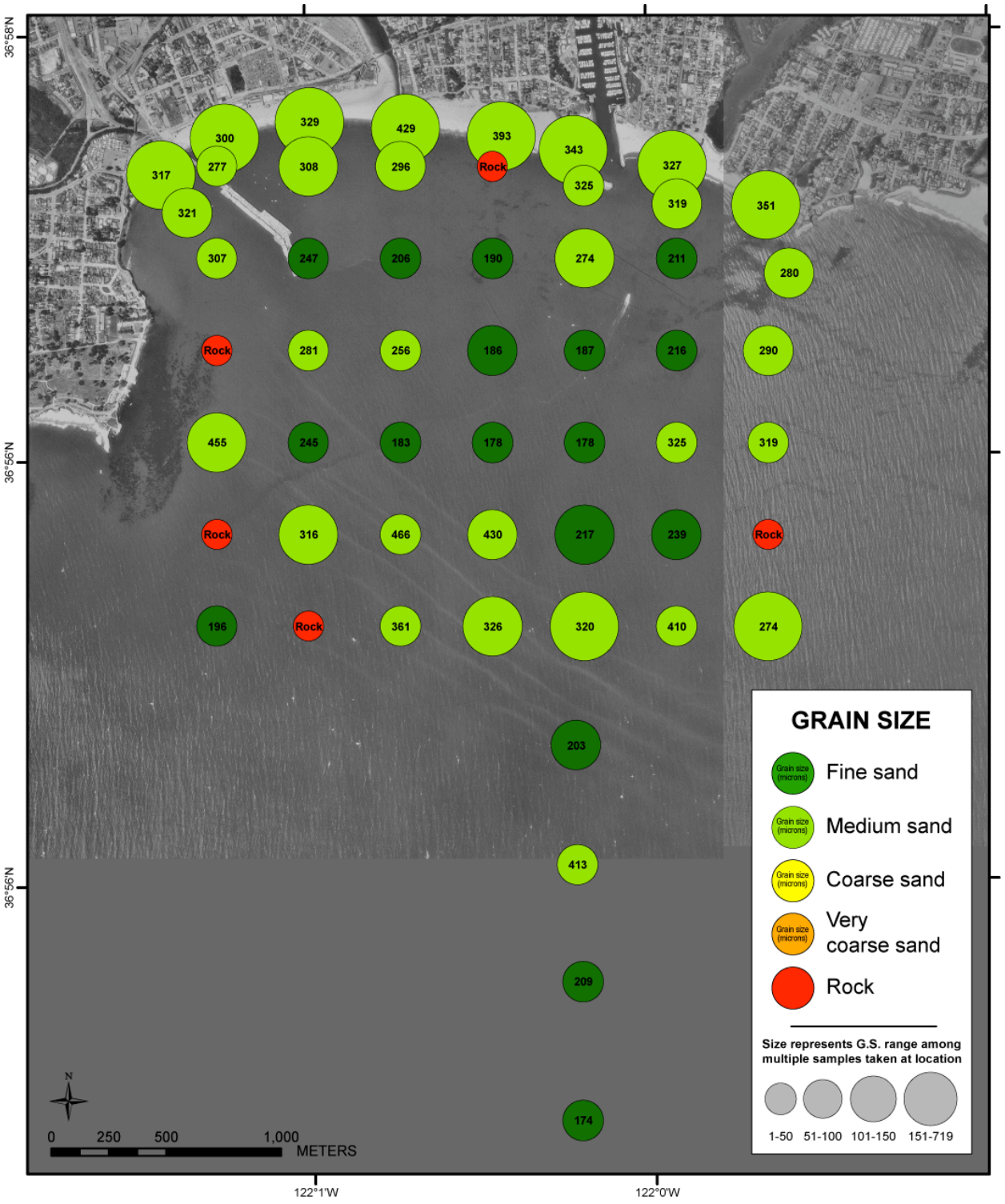

Appendix 6.2: Spatial variation in mean grain size and variability in grain size, in microns, for the grain-size surveys on 10/29/2009 (2009 Year Day 302).

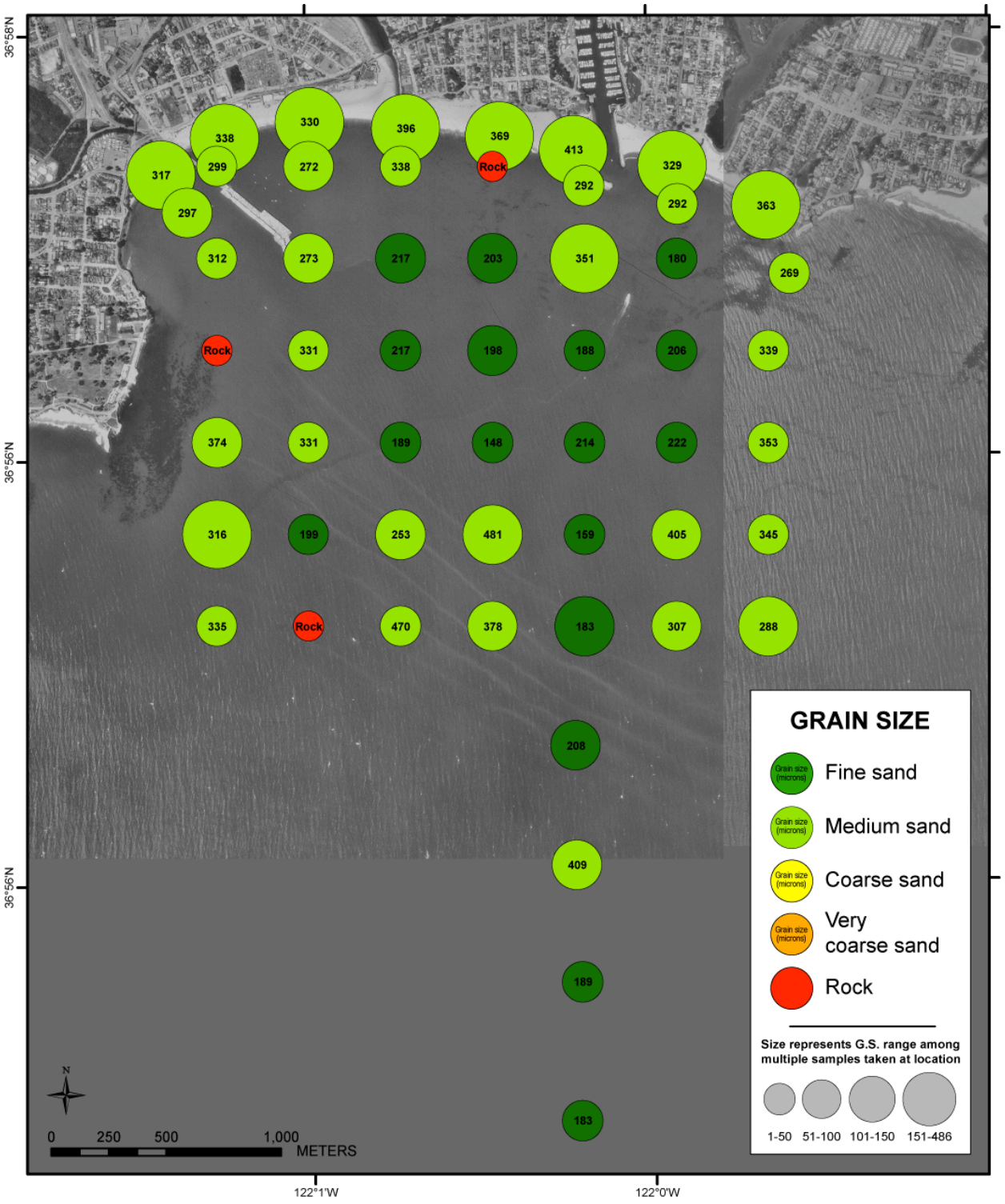

Appendix 6.3: Spatial variation in mean grain size and variability in grain size, in microns, for the grain-size surveys on 11/10/2009 (2009 Year Day 314).

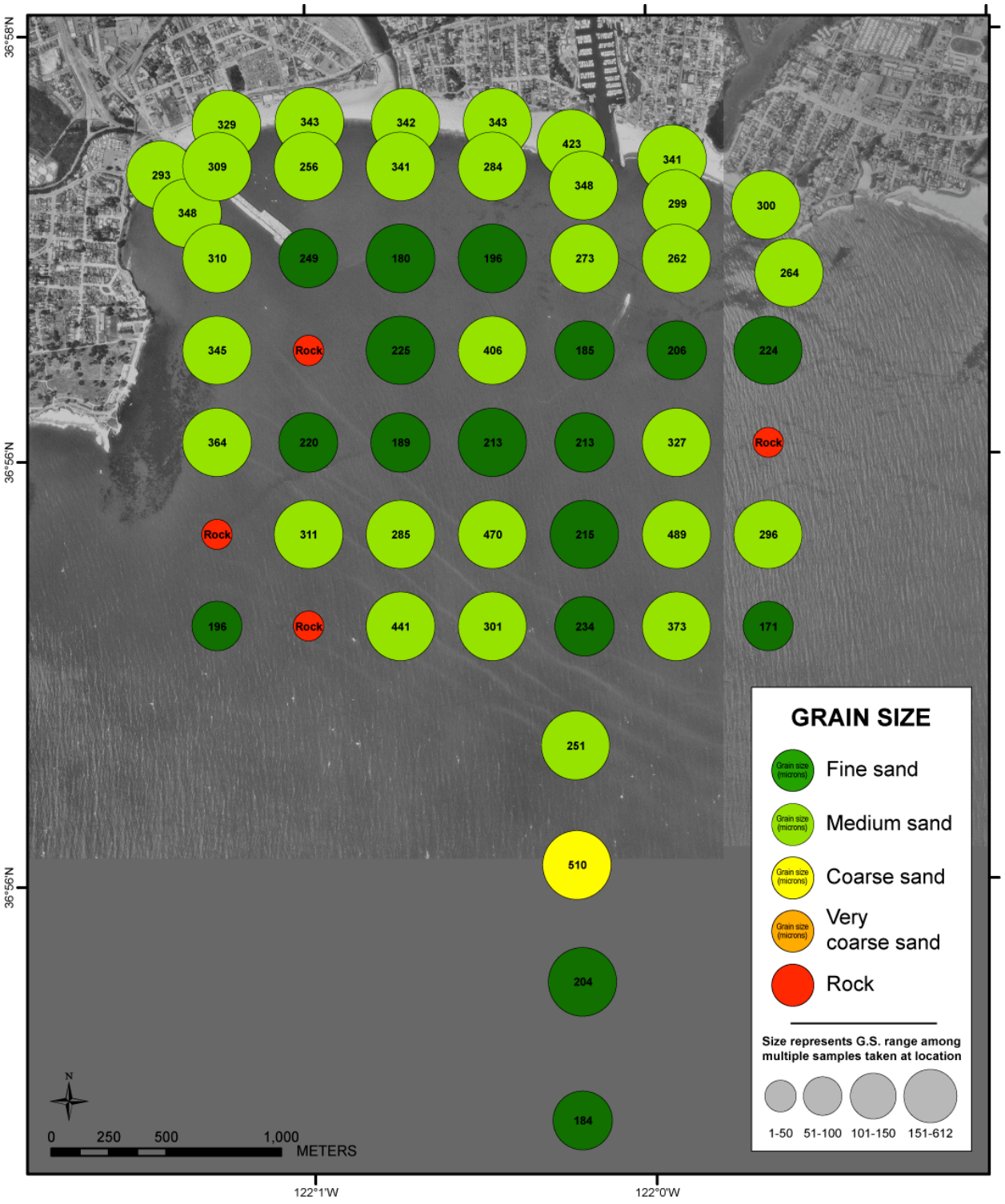

Appendix 6.4: Spatial variation in mean grain size and variability in grain size, in microns, for the grain-size surveys on 11/24/2009 (2009 Year Day 328).

Appendix 7
Numerical Model Calibration and Validation Information

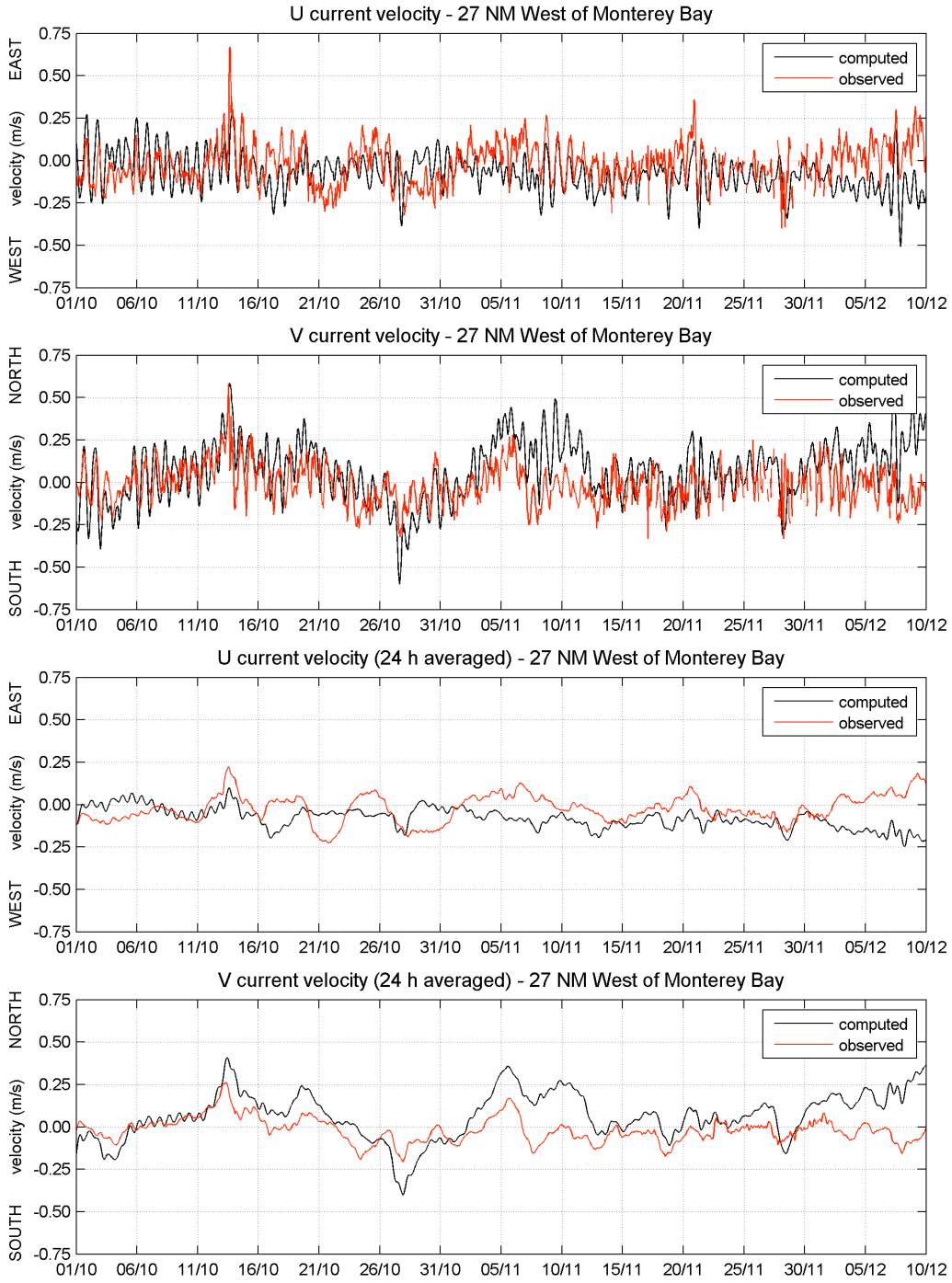

Appendix 7.1: Comparison of computed (MBY model) and observed (HF Radar) surface current velocities at Station 46042 – MONTEREY 27 NM West of Monterey Bay.

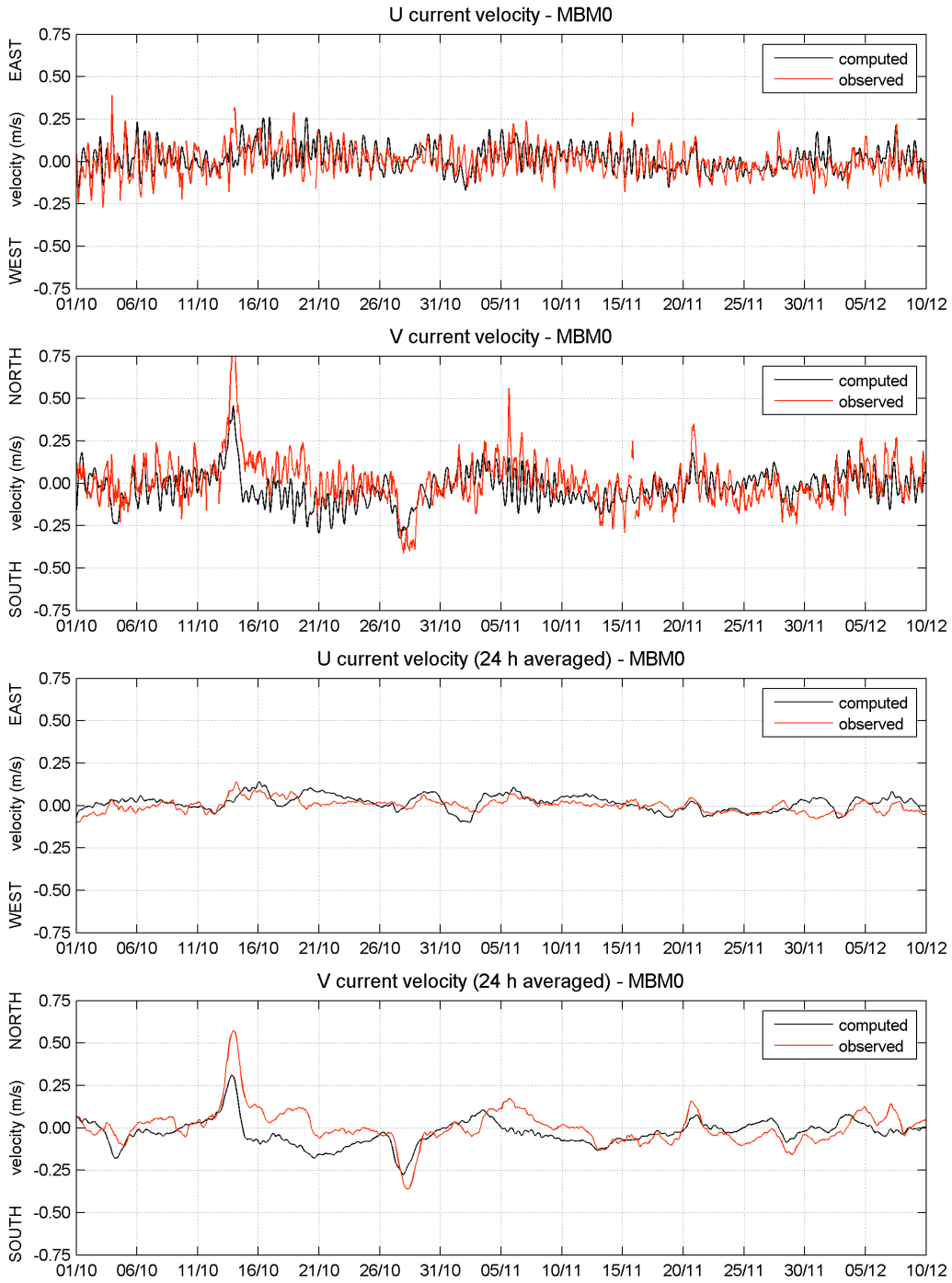

Appendix 7.2: Comparison of computed (MBY model) and observed (HF Radar) surface current velocities at Station 46091 – MBM0.

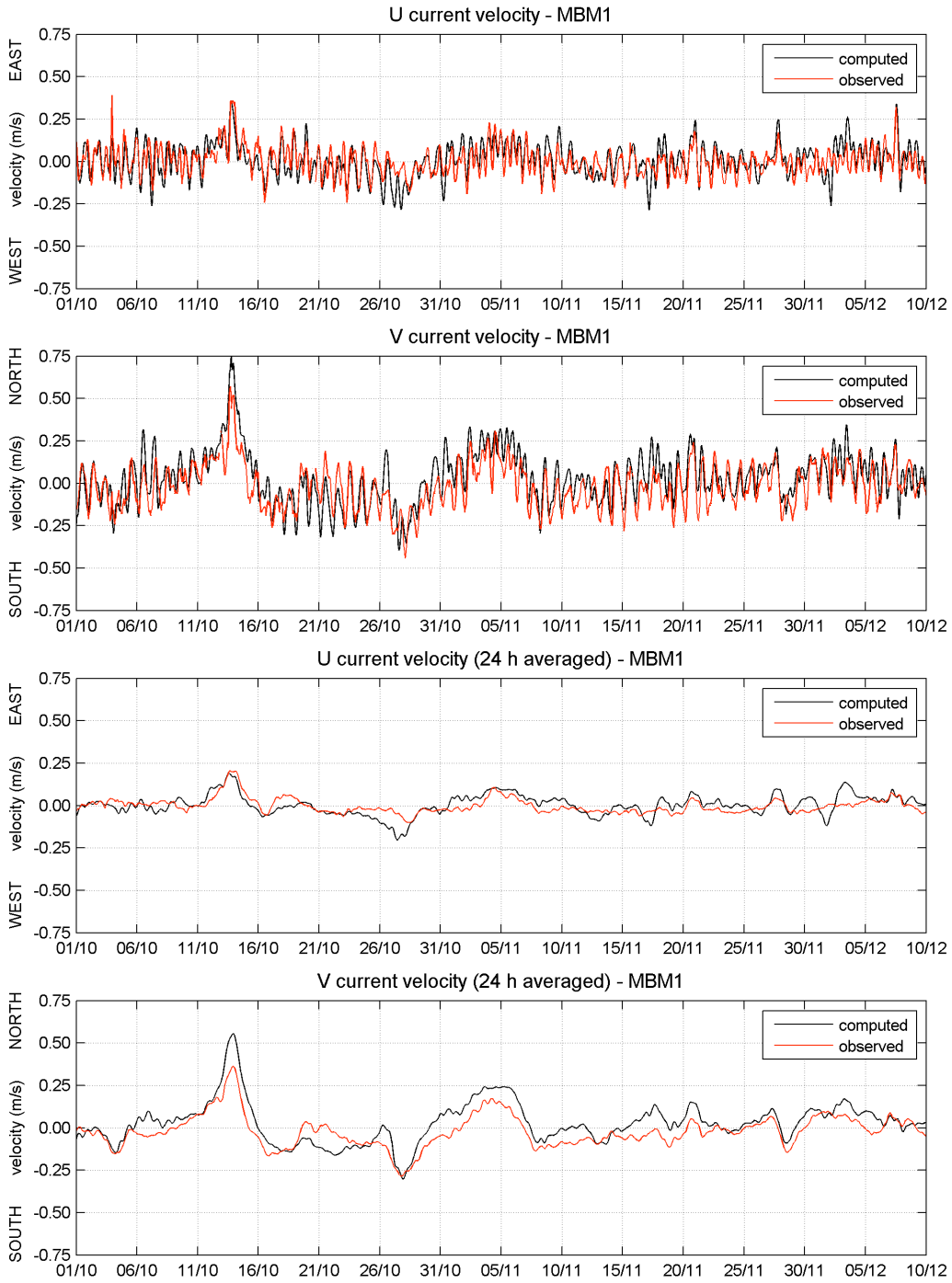

Appendix 7.3: Comparison of computed (MBY model) and observed (HF Radar) surface current velocities at Station 46092 – MBM1.

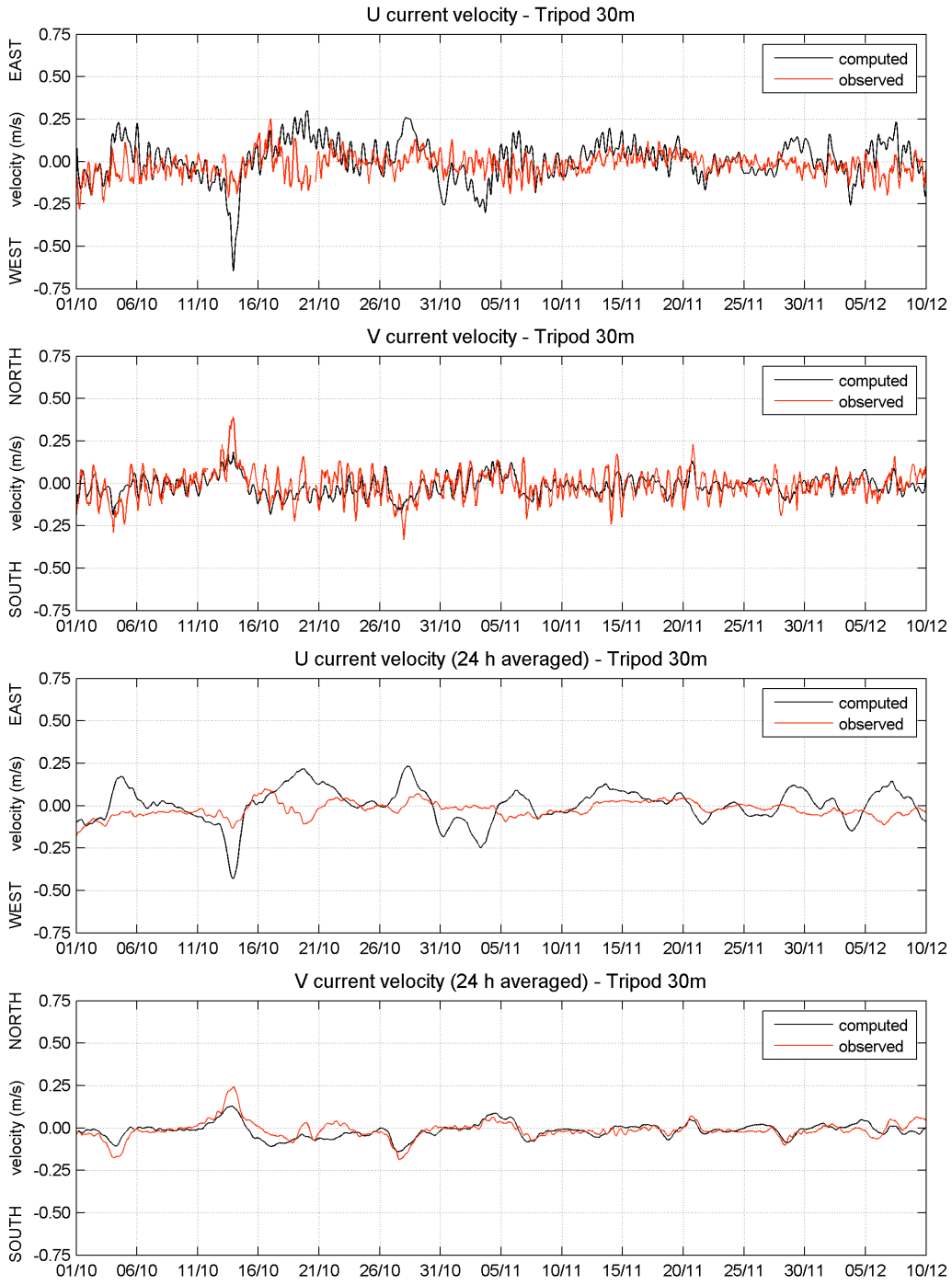

Appendix 7.4: Comparison of computed (MBY model) and observed (HF Radar) surface current velocities at Tripod D (30 m).

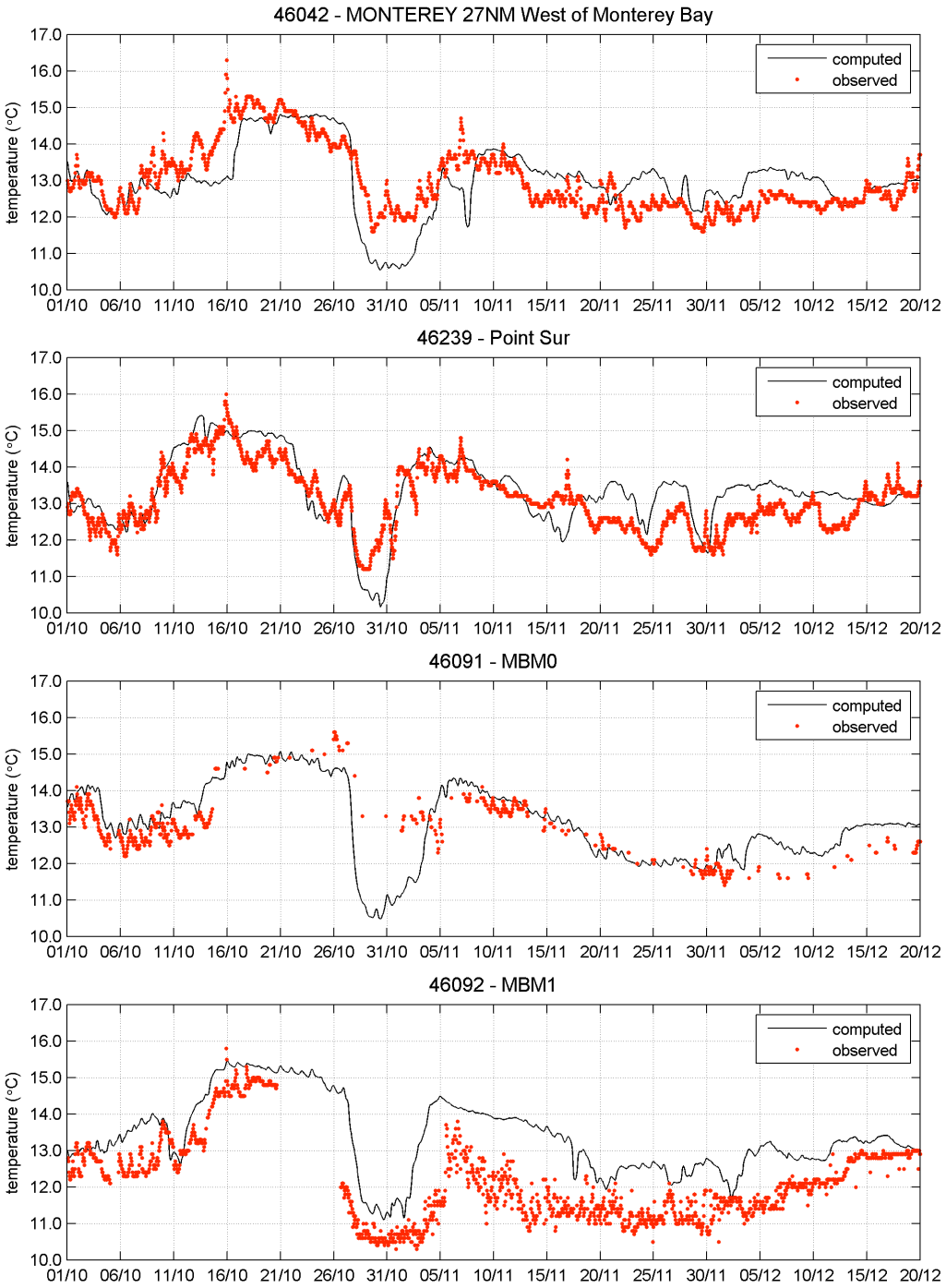

Appendix 7.5: Comparison of computed (MBY model) and observed surface water temperatures.

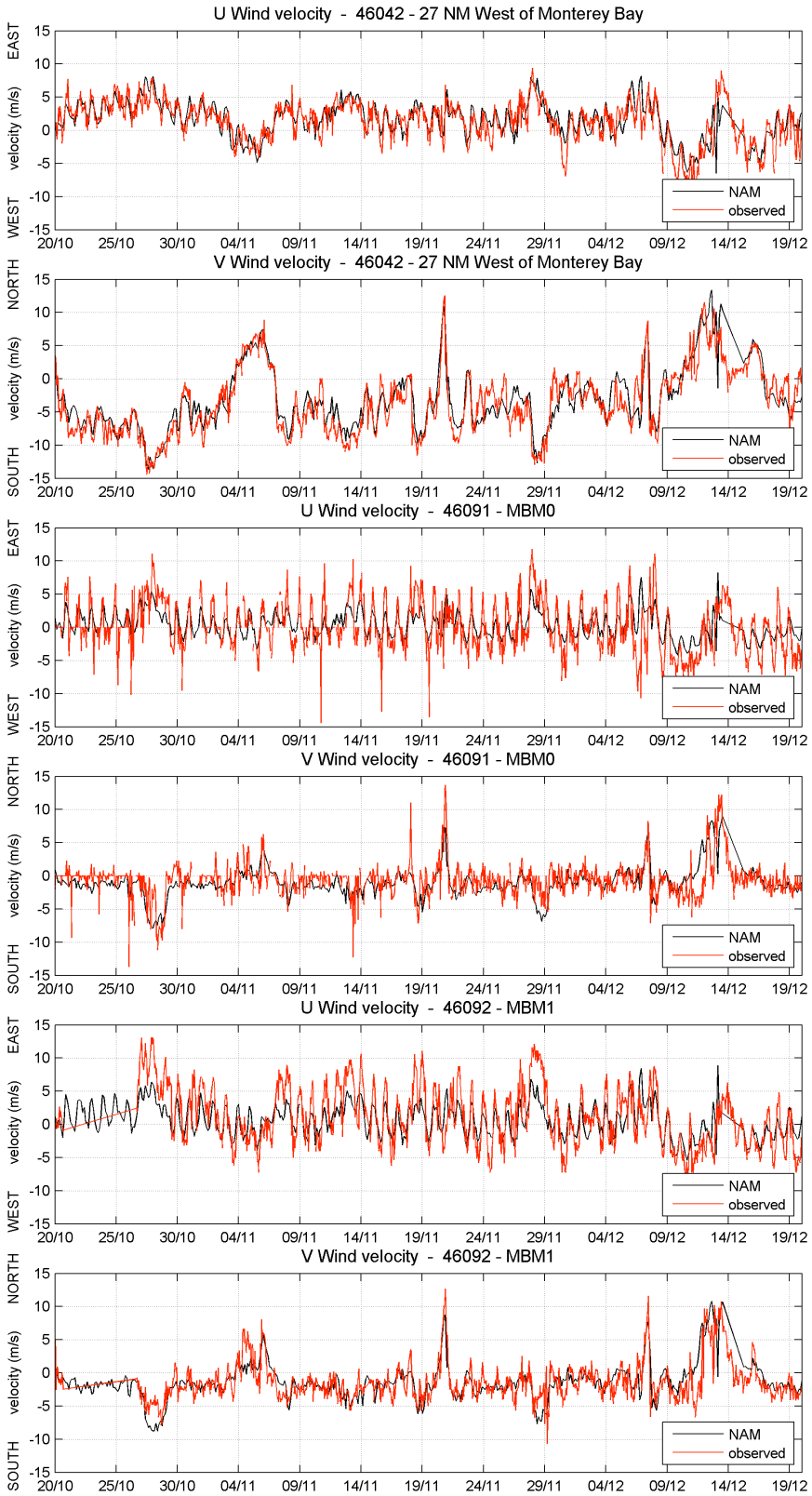

Appendix 7.6: Comparison of computed (NCEP-NAM model) and observed wind speeds.

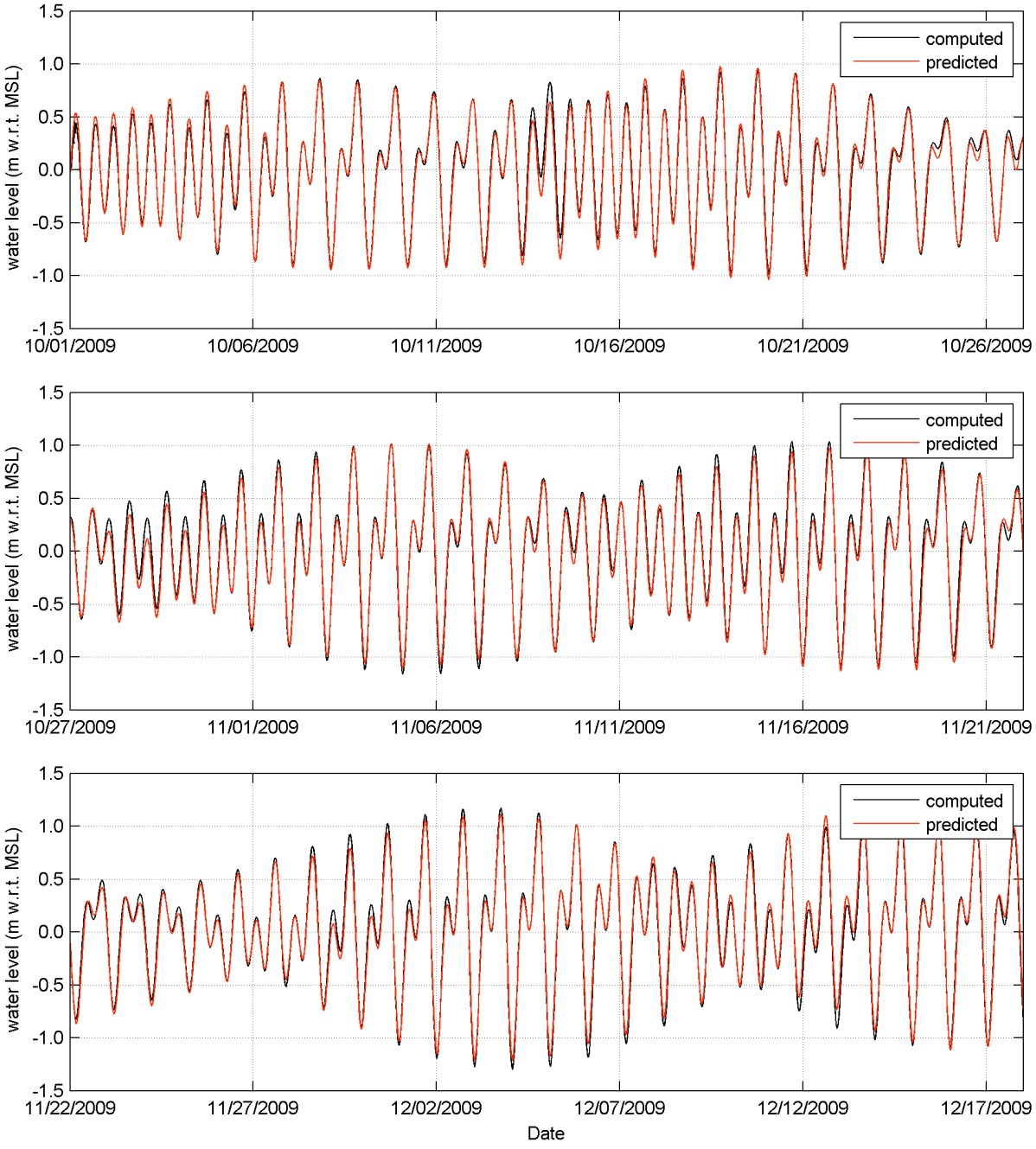

Appendix 7.7: Simulated versus NOAA predicted water levels at Santa Cruz Harbor.

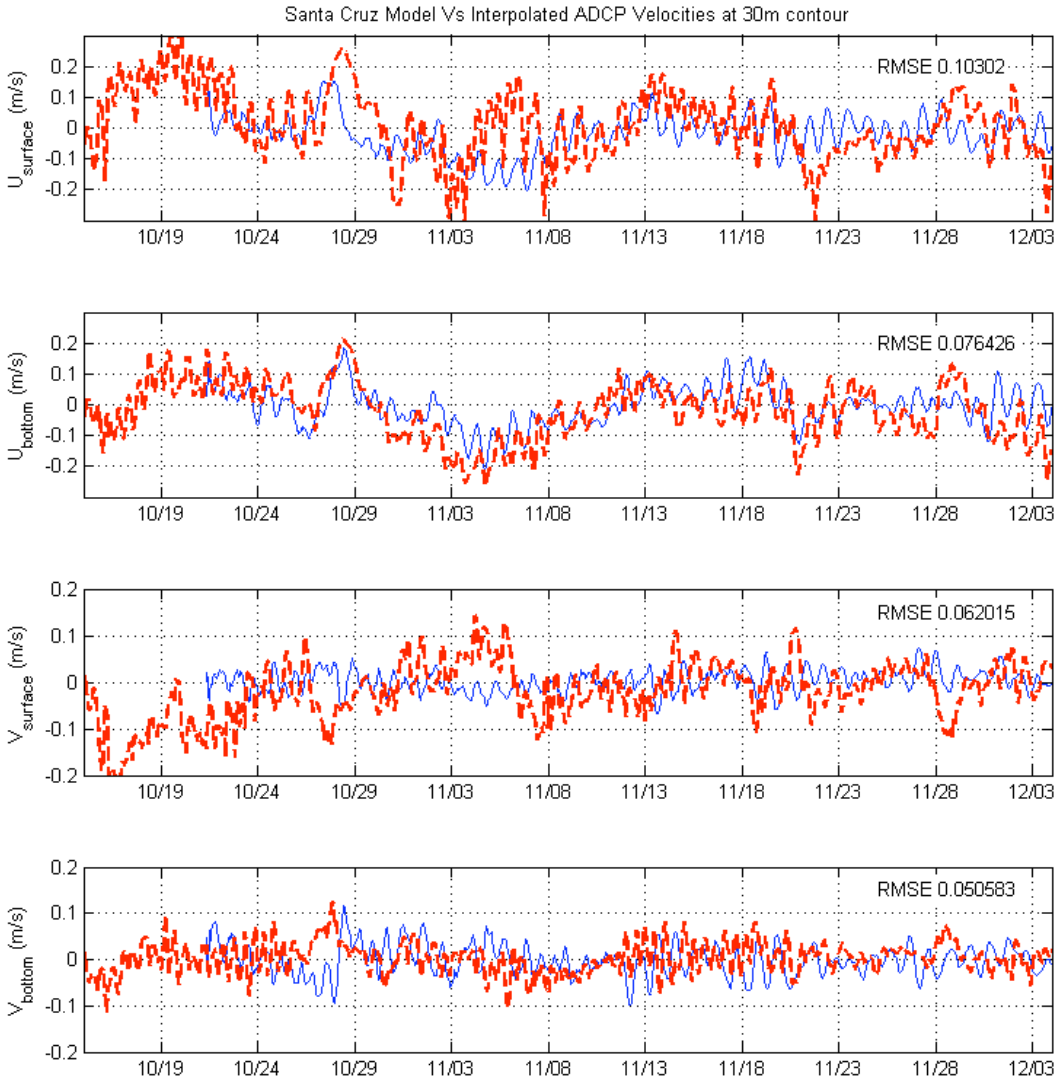

Appendix 7.8: Observed (blue) versus simulated (red) surface and bottom current velocities at Tripod D (30 m).

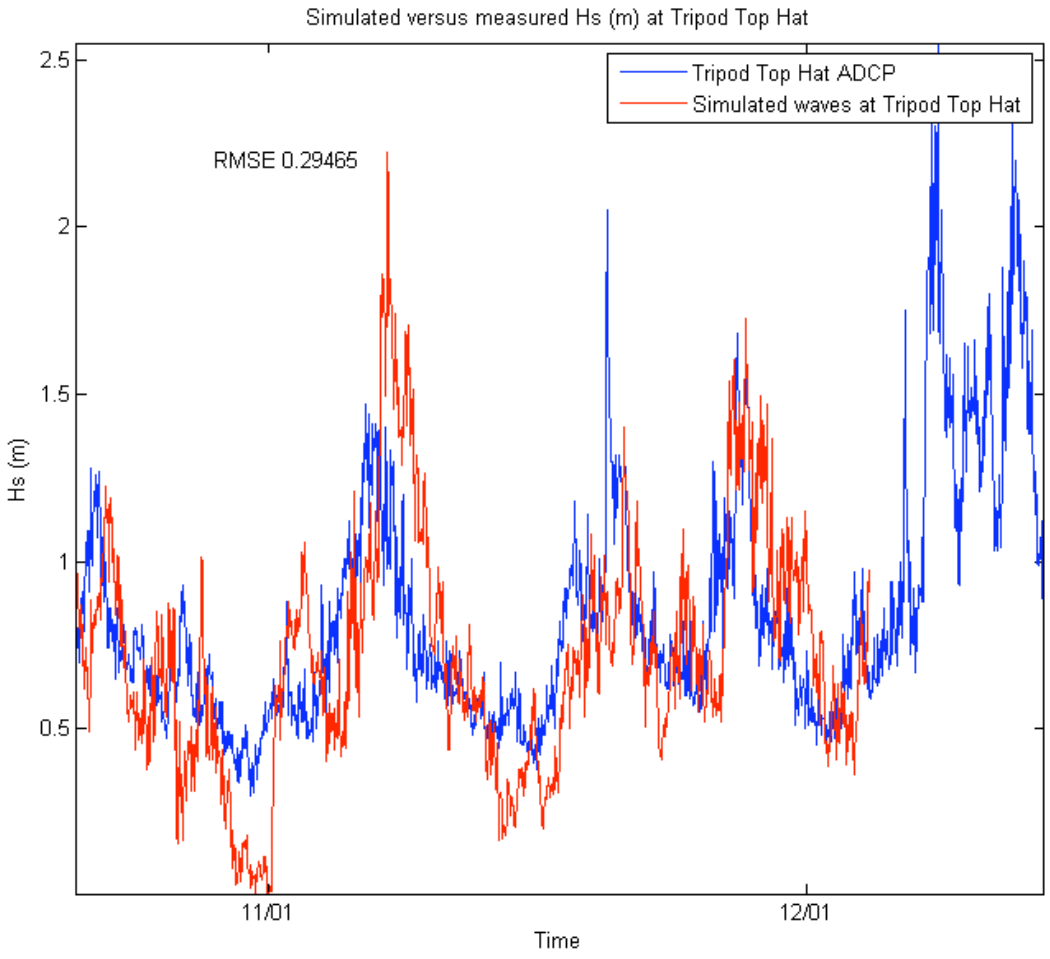

Appendix 7.9: Observed versus simulated wave heights at Tripod B (12 m).

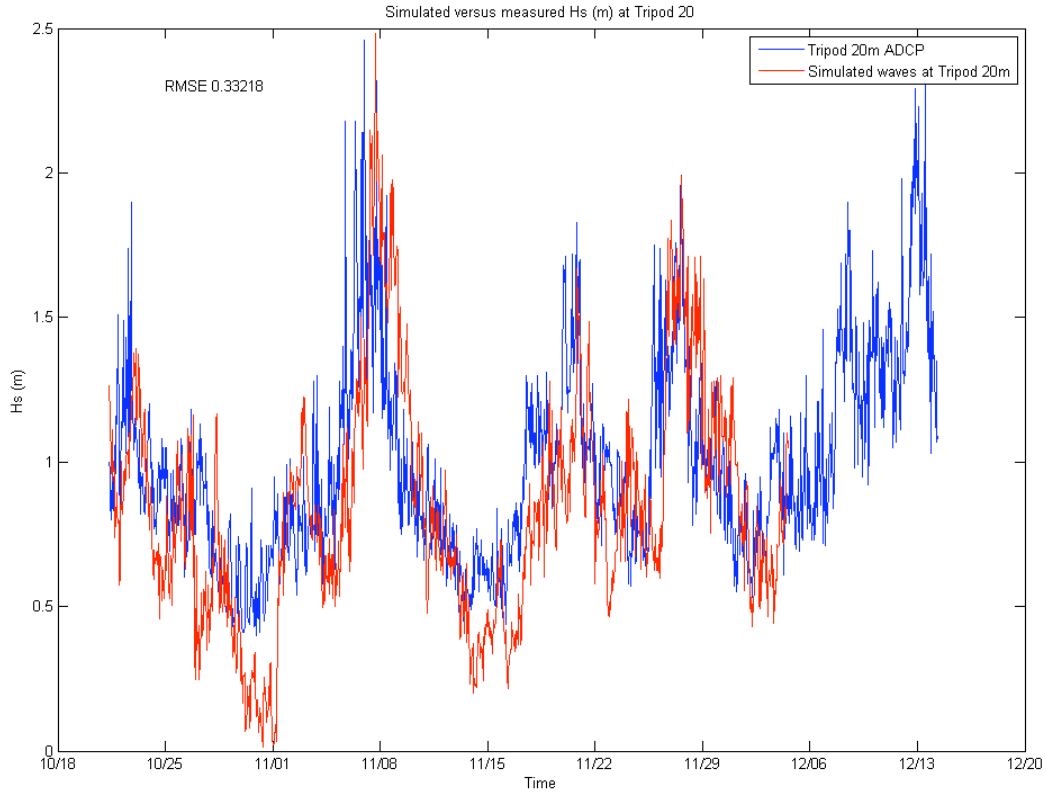

Appendix 7.10: Observed versus simulated wave heights at Tripod C (20 m).

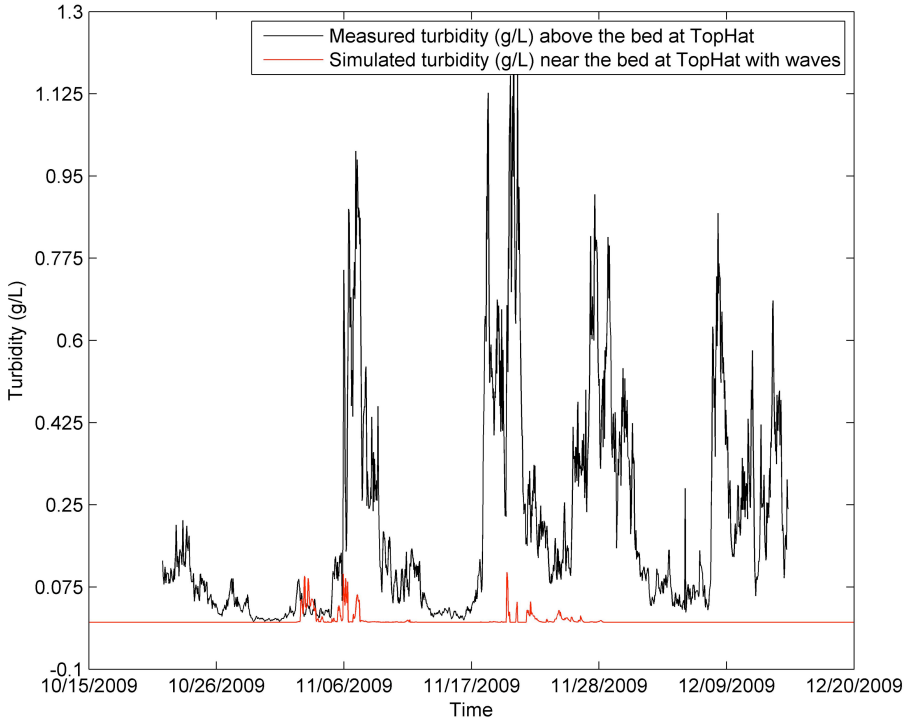

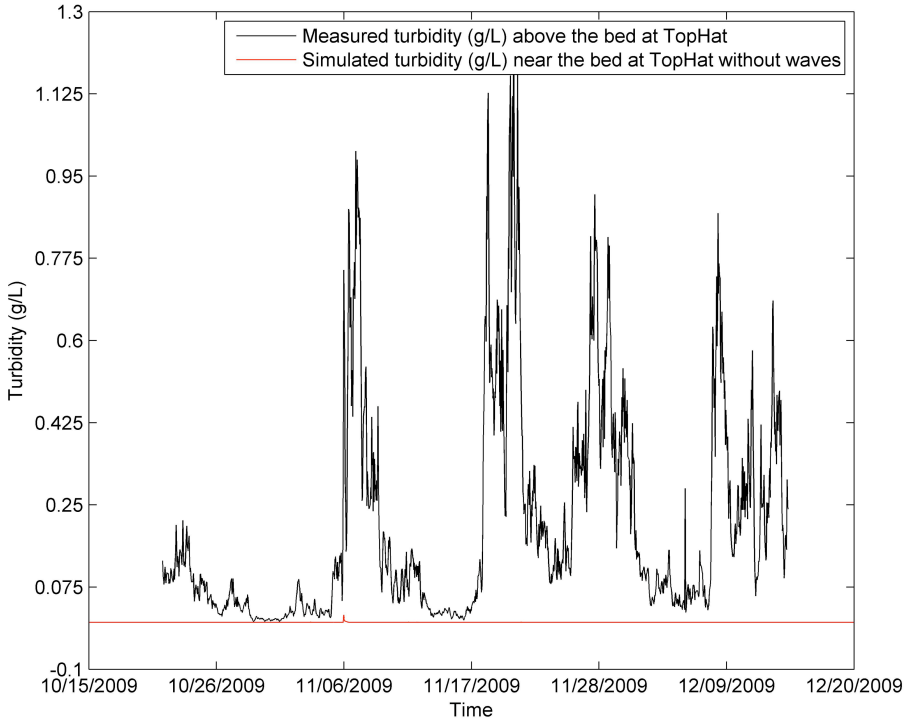

Appendix 7.11: Sediment concentration near the bed at Tripod B (12 m) with (upper panel) and without (lower panel) waves.

Appendix 8

2009 Year Day to Calendar Day Conversion Table

2009 Year Day	Calendar Day	2009 Year Day	Calendar Day
244	1-Sep	305	1-Nov
245	2-Sep	306	2-Nov
246	3-Sep	307	3-Nov
247	4-Sep	308	4-Nov
248	5-Sep	309	5-Nov
249	6-Sep	310	6-Nov
250	7-Sep	311	7-Nov
251	8-Sep	312	8-Nov
252	9-Sep	313	9-Nov
253	10-Sep	314	10-Nov
254	11-Sep	315	11-Nov
255	12-Sep	316	12-Nov
256	13-Sep	317	13-Nov
257	14-Sep	318	14-Nov
258	15-Sep	319	15-Nov
259	16-Sep	320	16-Nov
260	17-Sep	321	17-Nov
261	18-Sep	322	18-Nov
262	19-Sep	323	19-Nov
263	20-Sep	324	20-Nov
264	21-Sep	325	21-Nov
265	22-Sep	326	22-Nov
266	23-Sep	327	23-Nov
267	24-Sep	328	24-Nov
268	25-Sep	329	25-Nov
269	26-Sep	330	26-Nov
270	27-Sep	331	27-Nov
271	28-Sep	332	28-Nov
272	29-Sep	333	29-Nov
273	30-Sep	334	30-Nov
274	1-Oct	335	1-Dec
275	2-Oct	336	2-Dec
276	3-Oct	337	3-Dec
277	4-Oct	338	4-Dec
278	5-Oct	339	5-Dec
279	6-Oct	340	6-Dec
280	7-Oct	341	7-Dec
281	8-Oct	342	8-Dec
282	9-Oct	343	9-Dec
283	10-Oct	344	10-Dec
284	11-Oct	345	11-Dec
285	12-Oct	346	12-Dec
286	13-Oct	347	13-Dec
287	14-Oct	348	14-Dec
288	15-Oct	349	15-Dec
289	16-Oct	350	16-Dec
290	17-Oct	351	17-Dec
291	18-Oct	352	18-Dec
292	19-Oct	353	19-Dec
293	20-Oct	354	20-Dec
294	21-Oct	355	21-Dec
295	22-Oct	356	22-Dec
296	23-Oct	357	23-Dec
297	24-Oct	358	24-Dec
298	25-Oct	359	25-Dec
299	26-Oct	360	26-Dec
300	27-Oct	361	27-Dec
301	28-Oct	362	28-Dec
302	29-Oct	363	29-Dec
303	30-Oct	364	30-Dec
304	31-Oct	365	31-Dec